Spring 2012

Investigation of drillstring vibration reduction tools

Mohammed Fayez Al Dushaishi

INVESTIGATION OF DRILLSTRING VIBRATION REDUCTION TOOLS

by

MOHAMMED FAYEZ AL DUSHAISHI

A THESIS

Presented to the Faculty of the Graduate School of the

MISSOURI UNIVERSITY OF SCIENCE AND TECHNOLOGY

In Partial Fulfillment of the Requirements for the Degree

MASTER OF SCIENCE IN PETROLEUM ENGINEERING

2012

Approved by
Dr. Runar Nygaard, Advisor
Dr. Baojun Bai
Dr. Mingzhen Wei

ABSTRACT

Drilling related problems such as drillstring vibration is an important cause of premature failure of drillstring components and drilling inefficiency. The vibration of drillstring interferes with measurement collected while drilling. In severe cases, drillstring vibration will lead to wellbore instability that will result in an increase in the operation cost. In the late 1980's, a lot of studies and techniques were developed to mitigate drillstring vibration and downhole vibration measurements were introduced to the industry in two forms; real time measurements and memory devices measurements.

A study of drillstring vibration of three different wells located in the Norwegian North Sea was analyzed. The bottom hole assembly (BHA) of two wells consisted of anti-vibration technology. The study involved a verification of anti stalling technology (AST) and V-stab vibration reduction tools. Part of the study illustrates the different in lateral vibration in different wells of matching lithology which include a statistical analysis of anti-vibration tools performance. Finally, a statistical analysis was conducted on downhole vibration measurement to investigate the sampling rate of the device.

Alternating lithology has a big impact on lateral vibration; however, lateral vibration is not the same for different wells in the same formations due to the difference in the BHA assemblies. The study showed that lateral vibration using the V-stab was lower than the one using the AST tool. Considering torsional vibration, the analysis reveled that V-stab has a lower stick/slip severity than the AST tool. The field study showed that the roller-cone bit generates less torsional vibration than the PDC bit due to different cutting actions. One of the important findings was that there was no correlation between drillstring vibration and mechanical specific Energy (MSE).

ACKNOWLEDGMENTS

I want to personally thank my advisor Dr. Runar Nygaard for believing in me and accepting me as one of his graduate students. He taught me so much during the past two years and has pushed me to position myself as a Petroleum Engineer. Lundin Petroleum Norway gave me the opportunity to learn how real time information can be used in this line of work. I wouldn't be where I am without their willingness to help me. I also want to thank my sponsorship Saudi Arabian Cultural Mission to the USA sponsored by King Abduaal who gave me the financial support to finish both of my Bachelor and Master degree. In addition, I want to thank my committee members, Dr. Baojun Bai and Dr. Mingzhen Wei from Missouri S&T petroleum program for being in my committee and for valuable feedbacks. I also want to thank my research group; especially Steven Hilgedick and Anuroop Pandey for their valuable help.

Finally, I want to thank my parents and family for believing in me and supporting me in every step of the way.

TABLE OF CONTENTS

LIST OF ILLUSTRATIONS

LIST OF TABLES

NOMENCLATURE

Symbol	Description
A_r	Area of the Cross Section of the Shaft
A_s	Cross Sectional Area
C	Axial Wave Velocity
C_a	Damping Coefficient in the Equation of Motion of the Axial Vibration Model
C_A	Coefficient of Axial Wave Equation General Solution
C_B	Coefficient of Axial Wave Equation General Solution
C_C	Coefficient of Axial Wave Equation General Solution
C_D	Coefficient of Axial Wave Equation General Solution
C_r	Damping Coefficient of Stick/Slip Model
c_w	Damping Coefficient for the Whirling Model
E	Young's Modulus
e_0	Eccentricity of Center of Mass in the Whirling Model
F_f	Friction Induced Force in the Stick/Slip Model
F_P	Drillstring Axial Force
F_s	Friction Parameter in the Stick/Slip Model
F_{ss}	Friction Parameter in the Stick/Slip Model
F_y	Tangential Force
G	Shear modulus
G_a	Forcing Term in the Equation of Motion of the Axial Vibration Model
G_T	Forcing term in the Equation of Motion of the Torsional Vibration Model

g_z	The Gravity Acceleration
I	Mass Moment of Inertia in the Stick/Slip Model
I_z	Cross Sectional Area Moment of Inertia in the FE Lateral Vibration Model
J	Cross Sectional Area Polar Moment of Inertia
k	Torsinal Stiffness in the Stick/Slip Model
k_w	Stiffness Coefficient for the Whirling Model
L	Axial Elevation in the Bit-Bounce Model
L_0	Maximum Axial Elevation in the Bit-Bounce Model
L_y	Displacement in the Whirling Model
L_z	Displacement in the Whirling Model
$L_\emptyset$	Angular Displacement for Continuous and Stick/Slip Model
m	Equivalent Mass of the Collar in Whirling Model
$m(x)$	Mass of String Segment Centralized at Position x in the Drillstring
N	Bit Rotational Speed Per Minute
P	Density
r	Dimensionless Polar Coordinate in the Whirling Model
r_b	Radius of the Borehole
t	Time
T	Torque at any Point of the Drillstring
u	Lateral Displacement in the Continuous Lateral Vibration Model
V_0	Velocity Parameter in the Stick/Slip Model
v_w	The Velocity of Propagation of Torsional Wave Along the x-axis
Δ	Increment

Δt	Compressive Travel time
ε	Equation of Motion Term in the Whirling Model
$\varepsilon(x,t)$	Undamped Axial Motion
ξ	Damping Ratio Used in the Stick/Slip Model
ω_0	Natural Frequency of the Stick/Slip Model
ω_n	N-th Axial Natural Frequency
Ω	Rotary Table Speed of the Stick/Slip Model

ABBREVIATIONS

Abbreviation	Description
AST	Anti Stall Technology
AVD	Active Vibration Damper
BHA	Bottom Hole Assembly
DDR	Downhole Dynamic Recorder
DDS	Drillstring Dynamics Sensor
DMM	Drilling Mechanics Module
DSD	Drill String Dynamics
DVMCS	Downhole Vibration Monitoring and Control System
EM	Electromagnetic
FFR	Forced Frequency Response
ISS	Instrumented Surface Sub
MR	Magnetorheological
MVC	Multi-Axis Vibration Chassis
MWD	Measurement While Drilling
NB	Near Bit
PDC	Polycrystalline Diamond Compact
PWD	Pressure –While-Drilling
RMC	Root Mean Square
ROP	Rate of Penetration
SQRT	Square Root
STRS	Soft Torque Rotary System
TCR	Roller Cone
UB	Underbalanced Drilling
UCS	Unconfined Compressive Strength
Vib_x	Vibration in the x-Axis
Vib_y	Vibration in the y-Axis

Vib_z	Vibration in the z-Axis
WOB	Weight on Bit

1. INTRODUCTION

1.1. OVERVIEW

Drillstring vibrations are an important cause of premature failure of drillstring components and drilling inefficiency. Drillstring vibrations are extremely complex because of the random nature of a multitude of factors such as bit/formation interaction, drillstring/wellbore interaction, and hydraulics. They involve several phenomena that render the analysis quite challenging. Three primary modes of vibration are present while drilling; axial, torsional, and lateral. Each vibration mode has related phenomena that emphasize each mode. These phenomena including bit bounce for axial vibration mode, stick/slip for torsional mode and whirling for lateral mode.

The dynamical behavior of an active drilling assembly as used in the oil or gas industry is complex. As a result of such complicity, predicting the behavior of the drilling system is quite challenging. Understanding the complexity of drillstring vibration behavior is an important step to get a better control of drillstring vibration constructive and destructive behavior.

Service companies in the industry started using downhole mud motors and downhole measurement systems to improve drilling performance in vertical wells. Lately, the industry has been strongly interested in the drillstring vibration as a cause of drilling inefficiency. As a result, the industry started measuring the drillstring vibration either by using shock and vibration sensors installed in MWD or LWD tools or using some memory devices.

1.2. PROBLEMS CAUSED BY DRILLSTRING VIBRATIONS

Drillstring vibration is the main reason of drill bit and drillstring components failure. Drillstring vibrations interfere with measurement while drilling (MWD), which could lead to inaccurate measurement of sensitive parameters. Drillstring vibration leads to bit damage, wellbore instability and energy waste. Some studies show that the most harmful vibration is subjected to the drill collars and adjacent drill pipe. Each vibration model has its own effect on the drilling operation.

The problems of drillstring vibration for each mode can be summarized in Table 1.1.

Table 1.1. Negative Effects on Drilling Performance Caused by Drillstring Vibration

Vibration Mode	Type	Effect
Axial	Bit Bounce	Broken or rapidly worn bits, BHA failures Reduced ROP Impact inducing other vibration modes
Torsional	Stick/Slip	Damage or fatigue failure of bit cutting elements through variable RPM and cutter load Reduced ROP Connection fatigue and premature failure of drillstring, BHA and downhole tools Washouts, twist-offs Fishing trips and replacements Easily generated with PDC bits Increased costs
Lateral	Whirl	Reduced ROP Premature bit wear Uneven string stabilizer wear BHA washouts and twist offs Borehole enlargements Lateral impacts inducing other vibrations

1.3. CAUSES AND MODELS OF DRILLSTRING VIBRATIONS

Drillstring vibration first occurs when bit contacts the formation to start penetration. Drillstring vibration is a function of formation, bit, BHA and other factors that make it complex. The common areas where the three different vibration mode could occur can be summarized in Table 1.2.

Three different vibration models have been introduced. The most important vibration phenomena include torsional vibration oscillations induced by non-linear frictional torques between the drill-bit at the rock surface (*torsional "slip-stick"*), axial

vibrations that induce the drill-bit to intermittently lose contact with the rock surface (*"bit-bounce"*), whirling motion of the drillstring and the motion of the bit in the bore-hole (bit and BHA-whirl), which they are illustrated in Figure 1.1 and Table 1.1.

Table 1.2. Common Situations Where Vibration Modes Occur

Vibration Mode	Common Situations
Axial	Hard drilling regions Vertical wells Drilling with roller-cone bits
Torsional	Hard drilling regions Hard, abrasive lithologies High angle, deviated wells
Lateral	Alternating lithologies Vertical wells

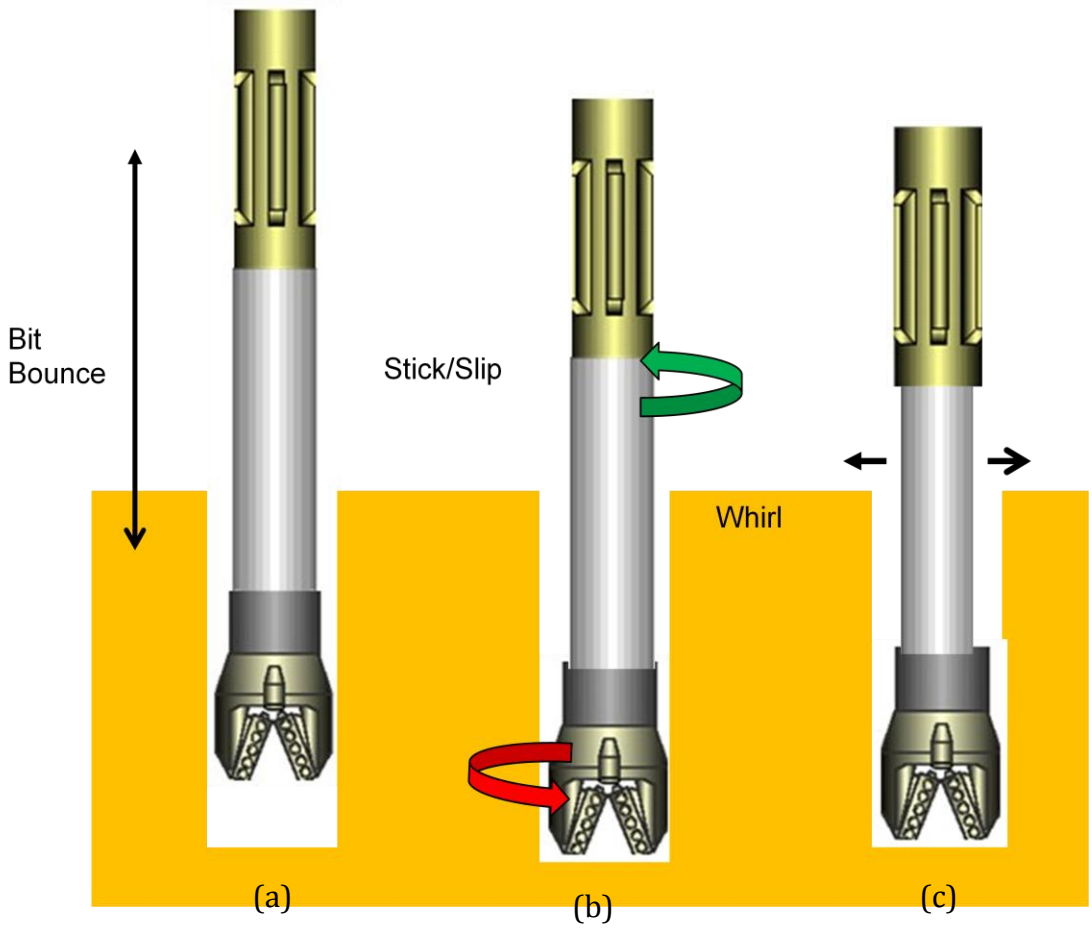

Figure 1.1 Drillstring Vibration Models

In addition to these violent excitations that can lead to rapid failure in the drilling operation, there are more subtle vibrations that are thought to contribute to fatigue and crack growth leading to ultimate failure of components. These include the transfer of energy between axial, lateral and torsional motion induced by the interactions of the drillstring and BHA with their environment. The nature of such inter-mode coupling can be dramatically influenced by drilling strategies and initial conditions.

Axial vibration appears during drilling operations in two forms:

- Vertical vibration while the bit is still in contact with the formation
- Bit bounce when contact is repeatedly lost as the bit bounce on and off the bottom

There are several factors that could reduce or increase the axial vibration:

- Lithology hardness
- Bit type
- Hole angle
- BHA length
- Fluid viscosity

These kinds of vibrations are present during all phases of the drilling operation. The drillstring axial vibration is produced by the initial impact of the bit with the formation on bottom. The initial bit bounce is triggered by an excessive impact speed when lowering the bit to the bottom. This model was long recognized in the field because they can travel from the bottom of the well to the surface, while lateral vibration model is usually trapped below the neutral point.

Strong axial vibration often occurs when using roller-cone bits. Axial vibration can be really helpful to drilling because they affect WOB which then will affect ROP. Axial vibrations are most common in hard drilling regions in vertical wells where propagation of energy is easier and when drilling with roller-cone bits.

Torsional vibration occurs when the rotation of the drillstring is slowed down or stopped at the bottom and released when the torque overcomes the friction resisting string rotation. There are several factors that could reduce or increase the torsional vibration:

- Bit type (PDC generates high levels of friction to initiate the stick phase)
- Hole angle (more pronounced oscillations in higher hole angles)
- BHA weight and stability

- Mud lubricity

Downhole measurement show that the application of a constant rotary speed at the surface does not necessarily translate into a steady rotational motion of the drill bit. The drill bit might come to a standstill because of the sudden WOB increase or combined effects of significant drag, a tight hole, sever doglegs, and keyseatings. Drillstring torsional vibration remained undetected for a long time and that because of the large inertia of the rotary table.

In stick/slip mode, assuming a constant rotary speed, the longer the drilling assembly is the more severe the torsional vibrations are. As the rotary speed approaches the critical speed, the stick/slip frequency approaches the torsional natural frequency of the drillstring.

Stick/slip may result in extensive bit wear, backward rotation, sever shock loading of the drillstring, fatigue, and eventually failure of drilling equipment (Dufeyte and Henneuse 1991; Smit 1995).The mean reason of the stick/slip behavior of the bit is the irregularity of the relationship between the frictions and the angular velocity at the bit (Jansen and van den Stenn 1995). Stick/slip behavior occurs frequently during drilling operations. Stick/slip phenomena occurs because the friction force is greater than the rotational speed, so the bit will stick until the bit overcome the friction force. On the other hand, stick/slip will not occur if the drillstring length was below the critical length (Lin and Wang 1991; Narasimhan 1987) where the critical length of the assembly is a function of the rotary speed of the string, the dry friction, and the system's viscous damping (Lin and Wang 1990). The stick/slip phenomenon at the surface is characterized by a groaning noise and sawtooth-like variations, of a large amplitude on the applied torque (van den Steen 1997; Dufeyte and Henneuse 1991; Kyllingstad and Halsey 1988).

Possible solutions include greater drillstring stiffness, higher BHA inertia, increase rotational speed, and reduced difference between static and dynamic frictions (van den Steen 1997; Dawson et al. 1987). MWD tools made it possible to detect the stick/slip phenomenon and identify its severity while drilling. Controlling the rotational behavior of a drilling assembly can be achieved by varying the rotary speed or the WOB. Modifying mud properties (to minimize downhole friction), and changing the type of drill bit or the configuration of the BHA (Smit; 1995).

Lateral vibration is defined as non-central rotation of the bit and/or BHA, causing lateral impacts with the sides of the wellbore. The rotation of the drillstring generates and maintains this motion. The result of this motion causes a dynamic imbalance, which generates torsional, axial, and lateral vibration. It can take three forms:

- Bit whirl: describes an off-center bit rotation, which is especially common with PDC bits.
- Forward BHA whirl: describes off center BHA rotation with its center line rotation in the same direction as the drillstring rotation.
- Backward BHA whirl: occurs where the borehole wall friction causes the center like rotation to become opposite to the rotation of the drillstring.

There are several factors that could reduce or increase the lateral vibration:

- Bit type
- BHA stability and centralization
- Lithology
- Bit profiling when commencing with a new bit

The effects of the lateral vibration stay unrecognized for a period of time since the lateral mode does not travel to the surface (Chin 1994). However, with the new technology of MWD it had been recognized faster than before. Lateral vibration can cause severe damage to the borehole wall (Mason and Sprawls 1998) and affect the drilling direction (Millheim and Apostal 1981).

A very important phenomenon related to lateral vibration is whirling of the BHA. Whirling is a condition where the instantaneous center of rotation moves about the bit face as the bit rotates (Warren et al. 1990; Vandiver et al. 1990; Brett et al. 1990), and it can be forward, backward, or chaotic. The amplitude of vibration resulting from bit whirl increase with the formation strength for both PDC and RC bits.

Most of the BHA operates in compression which makes it a region where buckling and whirling are likely to occur. Strong whirling can be observed on the rig floor by the lateral motion of the traveling black and the whipping of the drawworks. The most known kind of lateral vibration is the backward whirl. Backward whirl can originate from the friction between the stabilizers and the wellbore if this exceeds structural and hydrodynamic damping forces (Shyu 1989). Backward whirl is a significant threat to

drilling assemblies because it superimposed on the forward rotary speed by inducing fluctuating bending moments with periodic changes of sign (Jansen1991). The mathematical equations of drillstring vibration are provided in APPENDIX. A.

1.4. DRILLSTRING VIBRATION MEASUREMENT

The first attempt to record and process the surface and downhole vibration was in the early 1960 (Dubinsky et al. 1992). The drilling vibration can be detected at the surface through torque and standpipe pressure oscillations. Lately, downhole vibration is detected using MWD and LWD tools. With the technology improvements, some real time vibration modes have been introduced. These models predict critical rotary speeds that stimulate lateral vibration which should be avoided. The main purpose of real time vibration modeling is to help BHA design and recommends operating parameters (Heisig and Neubert 2000). However, downhole data proves that these models often have limitations for practice applications.

Surface vibration measurement is another technique to measure the vibration level. Surface torque and its oscillations provide information about downhole vibration (Dubinksy et al. 1992; Macpherson et al. 1993). Every vibration mechanism has its own symptoms that help to identify the kind of vibration occurrence. Table 1.3 summarizes each drillstring vibration mode identifier (Bernt et al. 2009).

Downhole vibration measurements are categorized in two categories. First category is memory measurement device that measures and record vibration to be retrieved lateral for analysis. Second category is real time vibration measurements.

An example of memory measurement devices is BlackBox^{TM}. The BlackBox^{TM} (BlackBox) is a memory mode vibration logging tool that can be used anywhere in the BHA (Figure 1.2). This device is powered by lithium batteries which gives it a life of 220 hours. The device records three types of vibration. The three types consist of maximum lateral acceleration, RMS acceleration and stick/slip indicator. This device can be placed anywhere in the BHA to give the ability to analysis the dynamic behavior of the whole system. More than one device could be installed in the BHA to get a better understanding of the dynamic behavior around the whole drillstring.

Downhole Dynamic Recorder (DDR) is a MWD tool that consists of an accelerometer that measures lateral acceleration (Lesso et al. 2011). The DDR device is powered by batteries and has the capability to sample lateral acceleration at 400Hz and record data every 2.6 seconds. The DDR is usually installed with MWD and LWD tools.

One of the real time vibration measurements is Multi-axis Vibration Chassis (MVC) is a 4 axis shock measurement tool. The first axis of the device refers to the strain gauges used for torsional measurement. The other 3 axis refer to a system consisting of the vibration acquisition board and three of board accelerometers. The system is mounted on a special chassis in the MWD tool. The vib_x sensor measures axial shocks, vib_y and vib_z sensors measure lateral shocks. Also, the vibration acquisition system measures the root mean square (RMS) value of the tool acceleration.

Table 1.3 Identity of Drillstring Vibration Mode

Vibration Mode	Surface	Downhole	Tool Damage
Stick/Slip	Surface Torque, RPM Fluctuations, Top Drive Stalling, Reduction of ROP	Low Frequency Torsional Vibration	PDC Cutter Damaged, Drillstring twist off or washout
BHA Whirl	Reduction of ROP	High Frequency of Lateral and Torsional Vibration	Cutter and/or Stabilizers, Increased Torque
Bit Bounce	Large Surface RPM, Large WOB Fluctuations, Reduction of ROP	Large Axial Vibration	Bit Damaged and BHA Washout
Coupling	Large WOB Fluctuations and Reduction of ROP	Large Lateral, Torsional and Axial vibration	Drillstring Twist off/Washout

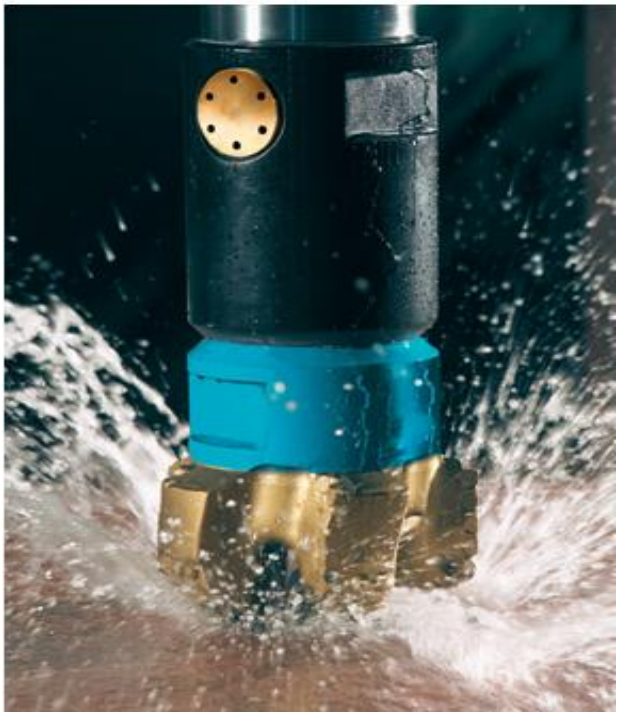

Figure 1.2. BlackBox (Murdock, 2011)

The TeleScope™ is a high speed MWD/LWD device (Schlumberger, 2007). The TelScope can transmit measured data from multiple tools; given comprehensive downhole information. These measured data include real time updates on downhole shocks, vibration and flow. The Tool can be combined with other MWD/LWD devices.

1.5. VIBRATION REDUCTION TOOLS

Lately, the industry has been taking into consideration the effect of the vibration. Two devices have been developed and used in the BHA to reduce the effect of vibration on the BHA. Anti Stall technology (AST) is one of anti-vibration tool that consists of a mechanical hydraulic converter placed in the lower part of the drillstring (Figure 1.3). Under normal conditions, the device will transfer torque and weight as a passive part of the BHA. However, if the transfer of energy to the bit becomes erratic, the tool is designed to actively control the bit tracking in order to improve the situation and provide the most stable conditions. The process of the AST device can be summarized as the following:

- The AST will contract when the bit speed drops and reactive torque builds fast (bit stall indication).
- When the bit is back to speed the AST will gradually release the accumulated torsion.

The AST works actively in the string to stabilize downhole forces. The purpose of the AST is to eliminate drillstring failures and overload while simultaneously increasing penetration rates through improving drilling efficiency. Figure 1.3 shows the AST device and its components.

Figure 1.3 above shows the AST device that consist of telescopic unit (1), compressible spring (3) and a helical spline (2). An excessive torsion force with magnitude will overcome the compressed spring, which will result in a rotation of both the lower telescopic unit and the external helical spline. As a result, the AST becomes shorter in overall length and the push in the drill bit is released. However, when the bit is back is at speed, the accumulation of the force in the spring will be released. The helical threaded convert excessive torsion into a linear force. The AST device is supported with an effective shock absorber designed to eliminate the risk of the BHA entering into axial oscillations.

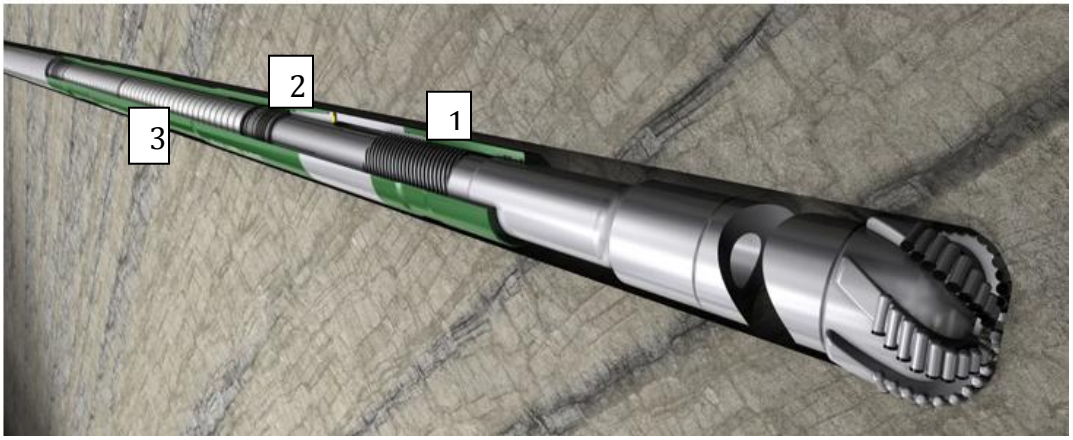

Figure 1.3. AST Tool (www.tomax.no, 2012)

The V-Stab is dampening tools that minimize both the magnitude and frequency of drilling shocks (Figure 1.4). Reducing drilling shocks, will reduce the damage to the BHA moreover, will increase overall bit performance and the ROP. The V-Stab tool lowers the risk on the field because it has no moving parts and it is an integral blade design.

This device has this ability to minimize the vibration (shocks) because of its unique geometry. V-Stab reduces vibration because its asymmetric cross-sectional geometry provides variable freedom of movement of the drillstring, and an eccentric mass that applies centripetal forces to the string (Figure 1.4).

V-Stab is designed using a bicenter geometry. The use of a bicenter geometry allows the stabilizer to pass through a smaller hole but stabilize the string in a large hole. When string vibration occurs, the undersized stabilizer can move in all directions, but it does help reduce how far the string can move in any direction. On the other hand, drillstring vibration will be worse if the stabilizer was undersized then nearly the same size as the hole stabilizer. The V-Stab has two blades that are the full hole diameter, the string is not allowed to move in the opposite direction. The third blade from the V-Stab is missing to allow the string movement in one side of the hole.

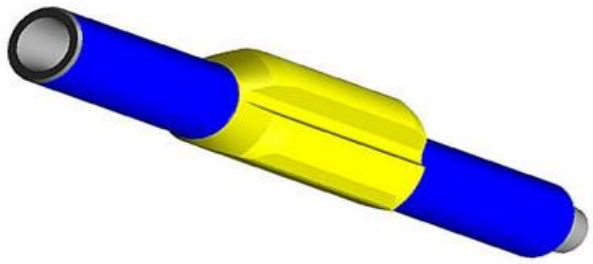

Figure 1.4. V-Stab Tool (www.nov.com, 2012))

1.6. SCOPE OF WORK

An investigation of lateral acceleration measured by blackbox data recorder will be analyzed. The investigation will cover three different wells, each well consist of

several sections. Each well has a different BHA design, some of the BHA's consist of vibration reduction tool and some does not.

Analysis of lateral vibration for each formation will be conducted. A comparison between the lateral acceleration for each formation will be analyzed and compared within the same well. The measured lateral acceleration from three different blackboxes within the same wells will be analyzed and compared.

The possibility of have matching ranges of lateral vibration at a matching lithology of Well A and Well B will be investigated. A statistical approach will be used to compare the lateral vibration of matching lithology.

Near bit lateral acceleration will be analyzed according to the strength of the rock. This section will cover the analysis of measured lateral acceleration and a possible signature of lateral acceleration for either rock strength.

Drilling data analysis for the three different wells are going to be analyzed by studying the drilling parameters. The drilling parameters consist of WOB, torque, surface and downhole RPMs.

Statistical study of the effect of multiple parameters on lateral vibration will take place. The study will cover a statistical study of the different between the three different wells and a statistical study of the effect of multiple parameters on lateral and torsional vibration.

Lateral acceleration measured from each section will be compared with the anti vibration tool installed in the BHA. A comprehensive study of the effect of anti vibration tools on lateral acceleration will be analyzed and compared. Also a complacent between lateral acceleration generated with BHA with and without anti-vibration tools will be established during this investigation.

Torosinal vibration (Stick/Slip) will be identified for each well. Stick/Slip severity will be compared for each well to evaluate the anti-vibration tools in each well.

The BlackBox downhole recorder measures vibration every 2.5 seconds. A statistical comparison of the original measured lateral acceleration and every 10^{th} sample of the original data will be analyzed to see if the memory base system can be used in real time with mud pulses.

2. METHODOLOGY

The analysis of drillstring vibration will be performed on three different wells. For each well, three drilled sections will be included in the study. Table 2.1 gives an overview of the three wells.

Table 2.1. Wells Summary

Well	Section diameter (in)	Bit Run Length (m)	Vibration Tool	Bit Type	MWD (Sg)	WOB (tons)	RPM
A	12.25	585-1880	AST	PDC	1.30-1.35	1-12	120-152
	8.5	1880-1915	AST	PDC	1.31-1.34	4-18	60-150
	N/A	1915-1976	N/A	N/A	N/A	N/A	N/A
	8.5	1976-2150	AST	PDC	N/A	6-13	120-150
B	12.25	763-1803	V-Stab	PDC	1.3	2-6	138
	8.5	1803-1913	None	PDC	1.2	5-9	150
	N/A	1913-1961	N/A	N/A	N/A	N/A	N/A
	8.5	1961-2020	None	PDC	1.2	10-12	130
C	8.5	2000.7-2200	None	Tri Cone	1.31-1.34	12-15	128
	8.5	2200-2270	None	PDC	1.32-1.33	5-12	50-81
	8.5	2270-2303	None	PDC	1.33	4-12	40-120

The study of drillstring vibration and vibration reduction tools will consider the two type of drillstring vibration. Lateral and torsional drillstring vibration will be analyzed and evaluated for each well. For drillstring torsional vibration, stick/slip phenomena will be analyzed for the three different wells. The study will also include the

analysis of drillstring vibration measurements and sampling rate. The study of drillstring vibration can be summarized in Figure 2.1.

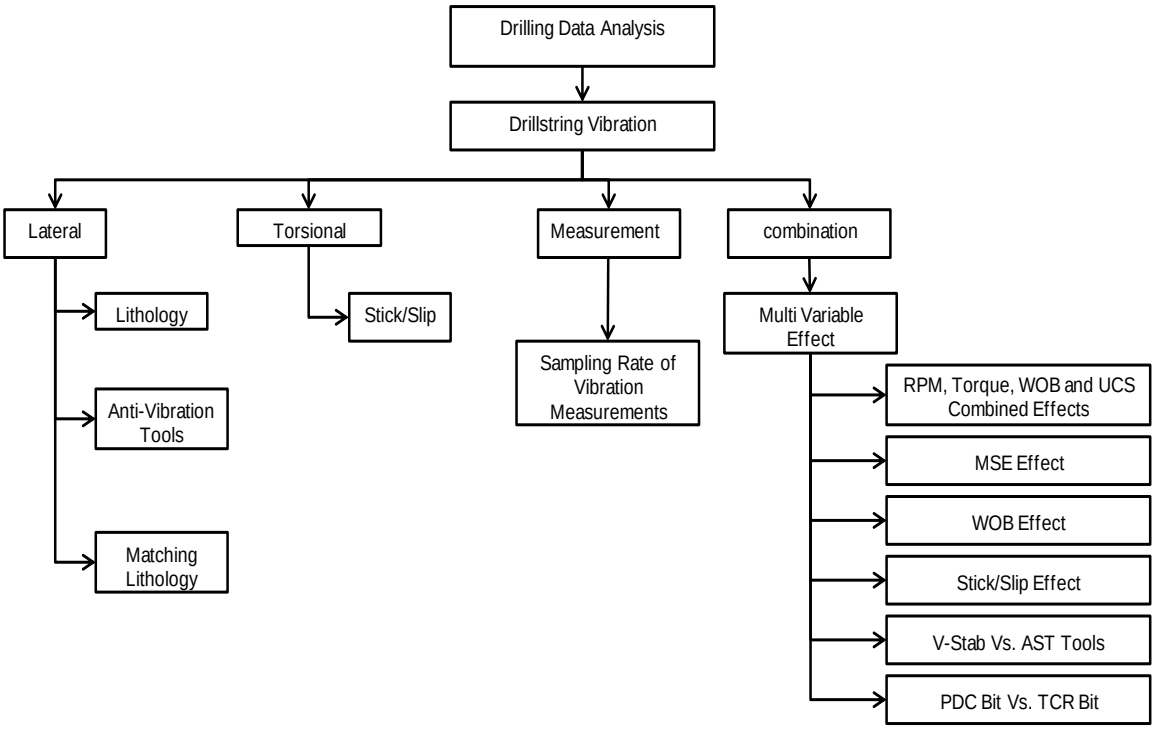

Figure 2.1. Summary of Study

2.1. FIELDS OF INVESTIGATIONS

The fields of study are offshore wells located in the Norwegian North Sea. Each well drilled consist of multiple sections. However, only three sections from each well are going to be covered in this study.

Well A was drilled vertically to TD. Figure 2.2 shows Well A schematic with the emphases in each whole and casing sizes. The first section subjected to the study of Well A is the 12 ¼'' than the 8 ½'' section before coring then finally 8 ½'' after coring to TD. The BHA for the 12 ¼'' section had three different blackboxes installed. Also, AST vibration reduction tool was installed in the BHA for the three different sections. More detailed information about the BHA's of the three different sections are available APPENDIX B.

Well B is vertical. Three different bit runs are going to be covered in this study. The well schematic can be seen in Figure 2.2. The first section is 12 ¼'' that consist of V-stab anti vibration tool. The other two sections are 8 ½'' in diameter, and the BHA assembly does not contain any anti vibration tools. More specifics on the BHA's of the three different bit runs can be seen in APPENDIX B.

Last well is Well C which is a vertical well. The 8 ½" hole section will be subjected to the study. This section was drilled with three different bit runs. On the first run, a roller cone bit was used. For the second and third run, a PDC bit was used. In this well only two blackboxes were installed, one near bit and the other one in the BHA below the drill collar and above the non-Magnetic drill collar. More specifics on the BHA's of the three different bit runs can be seen in APPENDIX B.

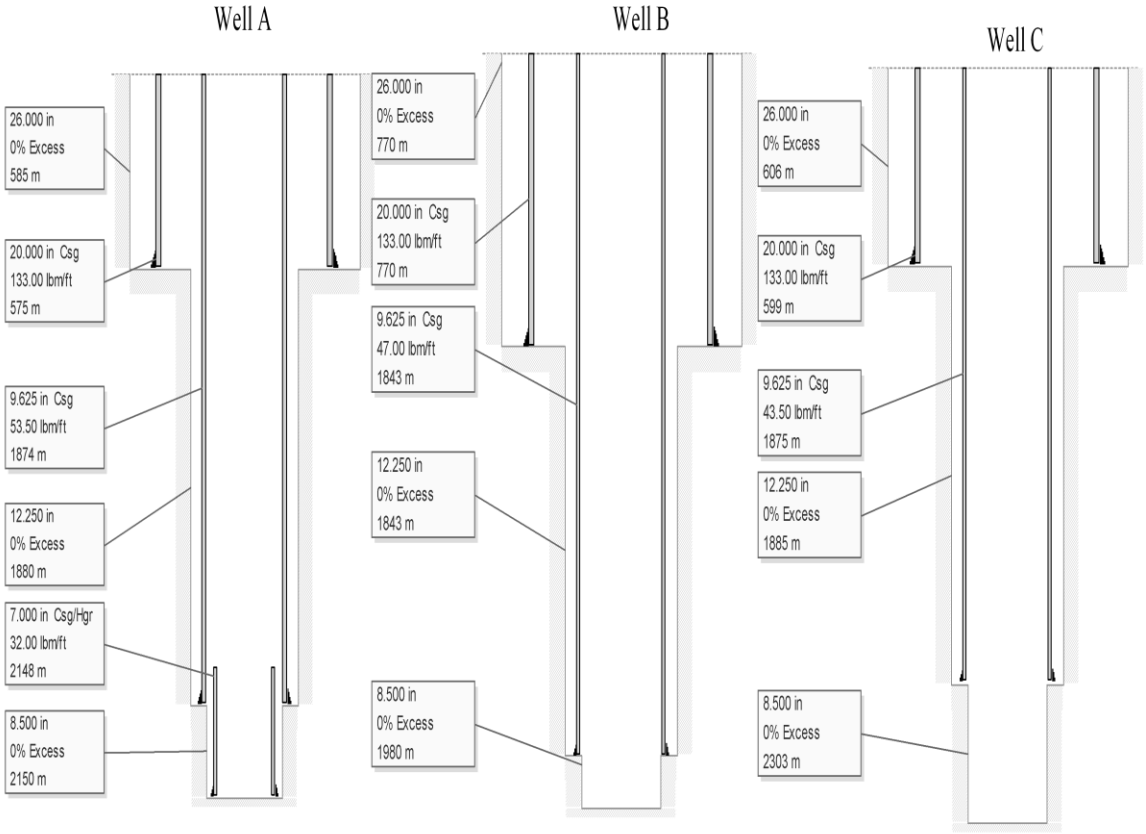

Figure 2.2 Schematics of Three Different Wells

2.2. DRILLING DATA ANALYSIS

The overall vibration of the drillstring is going to analyzed using the drilling parameters. The drilling parameters for Well A and Well B are measured by the blackbox measurement. However, for Well C, the measurement from both the blackbox and mud logging measurement will be combined for the analysis.

The data that was measured by downhole measurement will be used to analyze the overall vibration of each section. Log graphs will be created for the available drilling parameters for each well. When the log graphs are created, a study of the wells parameters will be initiated and compared with the overall lateral and torsional vibration measured by the blackbox.

For Well B, surface RPM was not provided with the blackbox data, however, the different between downhole RPM and surface RPM was recorded. Log graphs will be created for torque, WOB and the different between surface and downhole RPM. The different between the two RPM will be represented in percentage.

For Well C, the collected data from the blackbox measurement did not have the surface RPM; as a result, mud logging measurements are going to be included in this study. Log graphs are going to be created for the following parameters: near bit RPM, WOB, torque and surface RPM. Using the created log graph, vibrations are going to be identified through the whole section.

The rock strength for Well A and Well B will also be included with the drilling data log graphs. The measured near bit lateral acceleration will be collected and graphed in a log graph with the calculated rock strength for each well.

The calculated rock strength will be calculated based on the dynamic properties which will be derived from well logs measurements. The dynamic strength will be calculated from acoustic velocity and bulk density from logs and lithology measurements. Lithology will be derived from gamma ray logs. Based on this lithology, Equation.1 (Hilgedick et al. 2010)

$$UCS = \left(\frac{1}{k_1(\Delta t_c - k_2)}\right) + k_3 \quad (1)$$

Where UCS is unconfined compressive strength in MPa. k_1, k_2 and k_3 are constants based on lithology and Δt_c is compressive travel time in μ sec/ft.

Finally, near bit lateral acceleration and UCS (based on percentage of lithology) will be plotted against measured depth, and then a comparison between the two parameters will take place.

2.3. FORMATION TOPS VERSUS LATERAL VIBRATION

A statistical study of the effect of formations on lateral acceleration will be investigated. The study will cover Well A and Well B. Well C will not be included in this study since the collected vibration data was only for one formation.

By using statistical software, lateral and lateral RMS acceleration will be analysis. The analysis of lateral vibration and formation tops will be conducted by first initiating a box-plot. Box-plot is a graphical summary of the distribution of a sample that shows its shape, central tendency, and variability. Figure 2.3 gives a simple box plot of random data for more illustration.

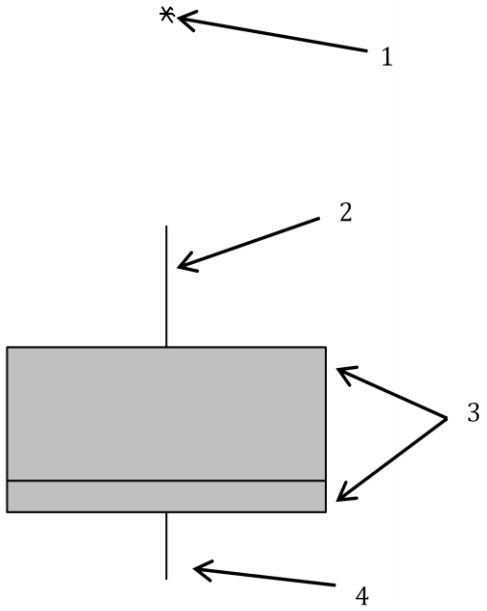

Figure 2.3 Description of Box-plot Median, outliers, Maximum and minimum Data Points

In figure 2.3, the upper start called an outlier which is represented by number 1. The outlier represents observation that is beyond upper or lower whisker. Upper whisker and lower whisker (donated with number 2 and 4 respectively in Figure 2.3) represent the maximum and minimum data points respectively. Finally, the box in the middle (number 3 in Figure 2.3) represents the median of the data.

Near bit lateral acceleration will be compared with the lithology by performing two box-plots for both lateral and RMS acceleration. The reason of taking both maximum near bit lateral acceleration and maximum near bit RMS lateral acceleration is when measuring vibration in acceleration, the device measures the wave from zero to the maximum point in the wave. However, for the RMS acceleration it measures from zero to the root mean square of the wave (Figure 2.4).

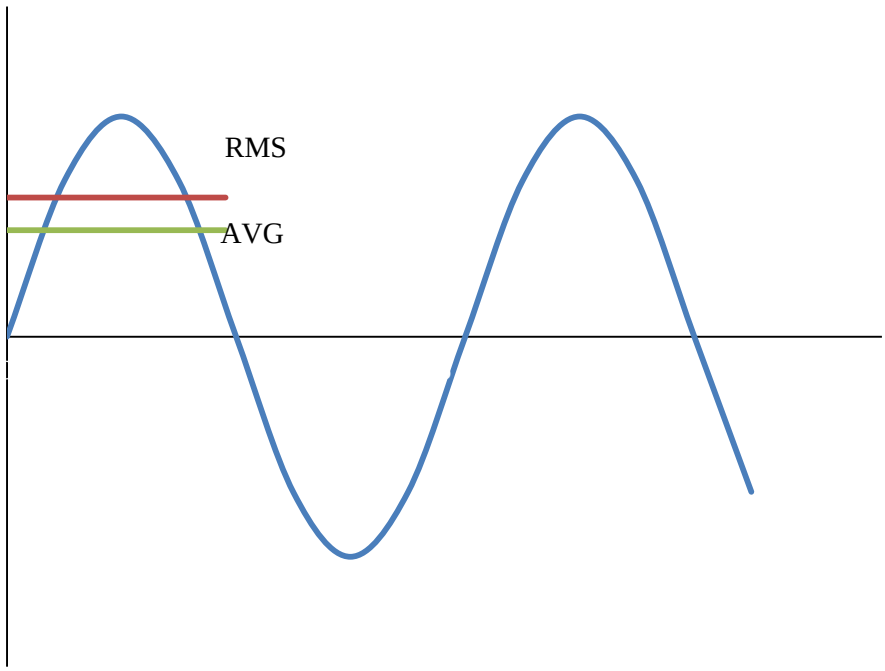

Figure 2.4 Different Between Lateral and Lateral RMS Illustration

To confirm the results from the previous statistical tests, a test for the equal variances will be performed on near bit lateral acceleration. Test of equal variances is used to test the equality of variances between populations. The test of equal variances has two hypotheses:

- H_0: all variances are equal
- H_1: Not all the variances are equal

The statistical software will use Bartlett's and Levene's tests to preforme the equal variances test. Bartlett's test calculates the weighted arithmetic average and weighted geometric average of each sample variance based on the degrees of freedom. Bartlett's test (X^2) is as follow: (Minitab user manual, 2011)

$$X^2 = \frac{(N-K)\ ln(S_p^2) - \sum_{i=1}^{K}(n_i - 1)\ ln(S_i^2)}{1 + \frac{1}{3(K-1)}\left(\sum_{i=1}^{K}\left(\frac{1}{n_i - 1}\right) - \frac{1}{N-K}\right)} \quad (2)$$

$$S_p^2 = \frac{1}{N-K}\sum_{i}(n_i - 1)\ S_i^2 \quad (3)$$

$$N = \sum_{i=1}^{K} n_i \quad (4)$$

Where k is the number of samples and n_i is the size of the sample. The sample variances is donated by S_i^2. Equation 3 and Equation 4 are the pooled estimate for the variance. The computational method for Levene's Test is a modification of Levene's procedure (Levene; 1960) developed by Brown and Forsythe (1974). This method considers the distances of the observations from their sample median rather than their sample mean. Using the sample median rather than the sample mean makes the test more robust for smaller samples and makes the procedure asymptotically distribution-free. If the p-value is smaller than the chosen confident level (α), reject the null hypothesis that the variances are equal.

$$W = \frac{(N-K)\sum N_i(Z_i - Z_{..})^2}{(K-1)\sum\sum\left(Z_{ij} - Z_i\right)^2} \quad (5)$$

$$Z_{ij} = \begin{cases} |Y_{ij} - \overline{Y_{\iota}}| \\ |Y_{ij} - \widetilde{Y}_{\iota}| \end{cases} \quad (6)$$

Where W is the statistical test of Levene's, K is the number of different groups which the sample belongs to, N is the total number of samples, N_i is the number of samples in the i^{th} group (first group), Y_{ij} is the value of the j^{th} sample from the i^{th} group, $\widetilde{Y}_{\iota}$ is the median of i^{th} group and $\overline{Y}_{\iota}$ is the mean of the i^{th} group.

2.4. VIBRATION REDUCTION TOOLS EVALUATION

A comparison was conducted between Well A and Well B who had anti-vibration tools installed in the BHA and Well C who did not have anti-vibration tool installed in the BHA. The analysis will cover three bit runs of Well A, B and C. Lateral acceleration and RMS lateral acceleration was collected and organized for the three different wells in one sheet to compare lateral vibration for each well. Then, three log graphs of lateral near bit acceleration versus measure depth for each well will be created. Also, another three log graphs will be created for lateral RMS acceleration.

Furthermore, for each of the lateral and lateral RMS acceleration for each well, the average, median and stander deviation will be calculated for each well. Then a bar graph will be created of the average, median, maximum and standard deviation for each well.

2.5. COMPARING LATERAL VIBRATION OF MATCHING FORMATIONS AND LITHOLOGY

Lateral acceleration from both Well A and Well B are going to be compared with matching lithology. Both wells have similar formation; however, they are at different depth. Lateral vibration of both wells will be arranged according to formation tops for each well. Formation tops of Well A and well B are listed in Table 2.2. The matching formations between Well A and Well B and the depth of each formation with each

formation thickness are summarized in Table 2.3. N/A in Table 2.3 represent that the listed formation does not existed.

A more detailed lithology description can be found in APPENDIX C.

A log graph of near bit lateral acceleration versus depth will be created for each well at each formation. Since the two wells are in different areas, the matching formations are at different depth. As a result, when creating the log graphs, the lateral acceleration and depth of one well will be created. To draw the next well acceleration of the same formation in the same plot, an additional y-axis (depth) will be created. Also, a bar graph will be created of lateral acceleration of both wells at each formation. The bar graph will represent the average maximum lateral acceleration for each well at each formation.

Statistical software will be used to analyze the lateral acceleration generated from each well at each formation. A box-plot of lateral acceleration generated from one formation will be created for both wells. Then an interval plot of the standard deviation of lateral acceleration from both wells will be created using the same statistical software and will be represented in the same graph with the box-plot. F-test and Levene's test will be used within the box and interval plot. The F-test will be used instead of Bartlett's test because the comparison is between two data sets. The F-test has the following hypotheses:

- H_0 : two data sets are equal
- H_1 : two data sets are not equal

If the P value is smaller than the α value, the hypotheses H_0 will be rejected. The F test uses the following: (Minitab user manual, 2011)

$$F = \frac{S_1^2}{S_2^2} \tag{6}$$

Where S_1^2 is the variance of the first sample and S_2^2 is the variance of the second sample.

Table 2.2 Well A and Well B Formation Tops

Formation Tops	Well A MD (m)	Well B MD (m)
Undif. Nordland	136	14.5
Utsira	773.5	800
Undif. Hordaland	869.5	877
Skade	994	940
Undif. Hordaland	1188.5	1007
Grid	1499.5	1276
Grid Sst Mbr	1552.5	N/A
Undif. Hordaland	1641.5	N/A
Balder	1767.5	1350
Sele	1778.5	1387.5
Lista	1800	1395.5
Vaale	1881	1465
Undif.Shetland	N/A	1485
Ekofisk	1892	N/A
Undif.C.knoll	1917	1780
Draupne,Shale	N/A	1915
Reservoir	1919	N/A
Draupne,Sand	N/A	1927
Granitic Basement	N/A	1941
TD	2150	2020

Table 2.3 Matching Formations of Well A and Well B

Matching Formations	From (m)		To (m)		Thickness	
	Well A	Well B	Well A	Well B	Well A	Well B
Utsira	773.5	800	869.5	877	96	77
Skade	994	940	1188.5	1007	194.5	67
Grid	1499.5	1276	1552.5	1350	53	74
Balder	1767.5	1350	1778.5	1387.5	11	37.5
Sele	1778.5	1387.5	1800	1395.5	21.5	8
Lista	1800	1395.5	1881	1465	81	69.5
Vale	1881	1465	1895	1485	14	20

2.6. EVALUATING STICK/SLIP

One of the most common phenomena of torosional vibration is stick/slip. Stick/slip will be identified for the three different wells. For the identification of Stick/slip, downhole RPM measurements tool will be used. From the measurement tool, the different between surface RPM and downhole RPM will be converted to percentage. Using the percentage as an indicator of stick/slip severity, the stick/slip severity will be calculated. The Stick/Slip severity will be compared between the three wells. Table 2.4 will be used to distinguish between the severity levels of stick/slip.

Table 2.4. Stick/Slip Interpretation

Stick/Slip %	Mode	Severity Level
0-40	Normal	Low
40-80	Torsional Oscillations	Medium
80-100	Stick/Slip	High
100+	Stick/Slip	Severe

2.7. STATISTICAL ANALYSIS OF SAMPLING RATE

The sampling rate of the measurement of lateral acceleration of blackbox will be statistically analyzed. The data collected by the Blackbox will be filtered; each 10^{th} sample of measurement will be collected. Then, a statistical analysis will be performed on the original data collected by the BlackBox and the filtered data.

A statistical software (Minitab) will be used to analyze the difference between the two set of data (Minitab user manual, 2011). First, a statistical and graphical summary will be produced for both set of data. The summary consist of three graphs; histogram of both data with an overlaid normal curve, boxplot and 95% confidence intervals for the median. The summary also includes the statistical summary of the data and Anderson-Darling Normality test. Anderson-Darling test is used to measures how well the data follow a particular distribution by calculating the P-Value and having the following hypotheses:

- H_0: The data follow a specific distribution

- H_1: The data do not follow a specific destitution

An α value, which the confident level, of 0.05 will be chosen to test both hypotheses.

Another statistical approach will take place to analyze the difference between the actual and the 10^{th} sampling data. Tow statistical tests will be performed using Minitab to test for the difference between the two data sets.

First test is Wilcoxon test. Performing a 1-sample Wilcoxon signed rank test of the median and estimate confidence interval. The Wilcoxon signed rank test hypotheses are

- H0: Median = hypothesized median
- H1: Median ≠ hypothesized median

Second test is a nonparametric distribution analysis (survival test), which consists of two tests. The two tests are Log-Rank and Wilcoxon. This test will calculate the P-Value using both tests, if the P-Value is less than the α value that will indicate that survival curves are significantly different.

The statistical analysis of sampling rate will be applied on the data collected from the three wells. The results from each well will be analyzed and compared with each other.

2.8. MULTI VARIABLES EFFECT ON DRILLSTRING VIBRATION

The study of the effect of more than one variable on lateral and torsional vibration will be investigated. With the use of statistical software, the effect of multi variables on lateral and torsional vibration will be analyzed. JMP statistical software will be used to conduct the analysis.

First, lateral vibration will be analysied as a function of WOB, torque, RPM and UCS. JMP statistical software will be used to study the hypotheses of having a correlation between lateral vibration and these parameters. The analysis will be applied to Well A, Well B, and Well C. Then a linear model of lateral vibration will be predicted to shows the effect of each parameter on lateral vibration.

The effect of Mechanical Specific energy (MSE) on lateral and torsional vibration will be analyzed. MSE is known as the work required to destroy a given volume of rock. MSE can be used to as a monitoring parameter to provide in formations about drilling

efficiency. The MSE mathematical equation as a function of drilling parameters is as follow: (Teale. 1965)

$$MSE = \frac{WOB}{A_B} + \frac{120\,\pi \times RPM \times T}{A_B \times ROP} \quad (7)$$

Where A_B is the area of the Bit, T is the applied torque and ROP is the rate of penetration.

The analysis will be run for different bits with a specific range of UCS and flow rate will be chosen to eliminate the effect of these parameters in the model. Table 2.5 summarizes the chosen ranges.

Table 2.5 Parameters Range of MSE Model

Well	Parameter		
	Bit Type	UCS (Mpa)	Flow Rate (L/Min)
A	PDC	58.16-59.92	2200-2276
C	Roller Cone	52-54	2200-2206
C	PDC	69-71	2200-2252

After sorting the data out, JMP statistical software will be used to investigate the possibility of having correlations between vibration (lateral and torsional) and MSE.

Another side of the study will be analyzing the effect of WOB on drillstring vibrations. Drilling parameters and UCS will be chosen at a constant range to analysis the effect of WOB. Table 2.6 summarizes the chosen ranges of drilling parameters and UCS.

A statistical cross plot will be plotted to study the effect of WOB on the drillstring lateral and torsional vibration.

A statistical analysis will be conducted to study effect of torsional vibration on lateral vibration. The analysis will take into consideration drilling parameters, a constant range of drilling parameters and UCS will be chosen to study the effect of stick/slip on lateral vibration. Table 2.7 summarizes the chosen ranges of drilling parameters and UCS.

Table 2.6 Parameters Range of WOB Model

Well	Parameter				
	UCS (Mpa)	Flow Rate (L/Min)	Torque (KNm)	RPM	WOB (tons)
A	6.8-8.8	2200-2276	1.5-10	120-150	4-5
B	N/A	3100-3200	3-4	N/A	3-4
C	52-71	2200-2252	2-6	51-87	1-13

Table 2.7 Parameters Range of Torsional Model

Well	Parameter				
	UCS (Mpa)	Flow Rate (L/Min)	Torque (KNm)	RPM	WOB (tons)
A	5-9	2200-2276	3-4.5	119-121	4-5.9
B	N/A	3127-3200	5-7	N/A	3.4-5.2
C	65-100	2233-2251	2-5	81-87	6-8

Vibration reduction tools used in Well A (AST) and Well B (V-stab), will be compared. The comparisons will take two forms of drillstring vibration (lateral and torsional). Before comparing the two tools, the data from the two wells will be arranged according to formation tops, then drillstring vibration from the two wells will be compared at each matching formation. A statistical graph of the vibration will be graphed to shows which tool has the less amount of vibration.

Drillstring vibration generated from PDC and roller cone bits will compared. Lateral and torsional vibration of the first 8 ½" bit run section used in Well C will be used to represent the roller cone bit. The next bit run of Well C using PDC bit will be chosen for the comparison Stick/Slip severity and lateral vibration generated from both bits will be statistical compared in an interval plot to analyze the different between the two types.

3. RESULTS

3.1. DRILLING DATA ANALYSIS

The drilling and logging parameters of Well A was plotted against depth in Figure 3.1. The drilling and logging parameters consisted of flow rate, SPP, sonic log, GR, WOB, surface RPM, downhole RPM, lateral acceleration, lateral RMS acceleration and calculated UCS.

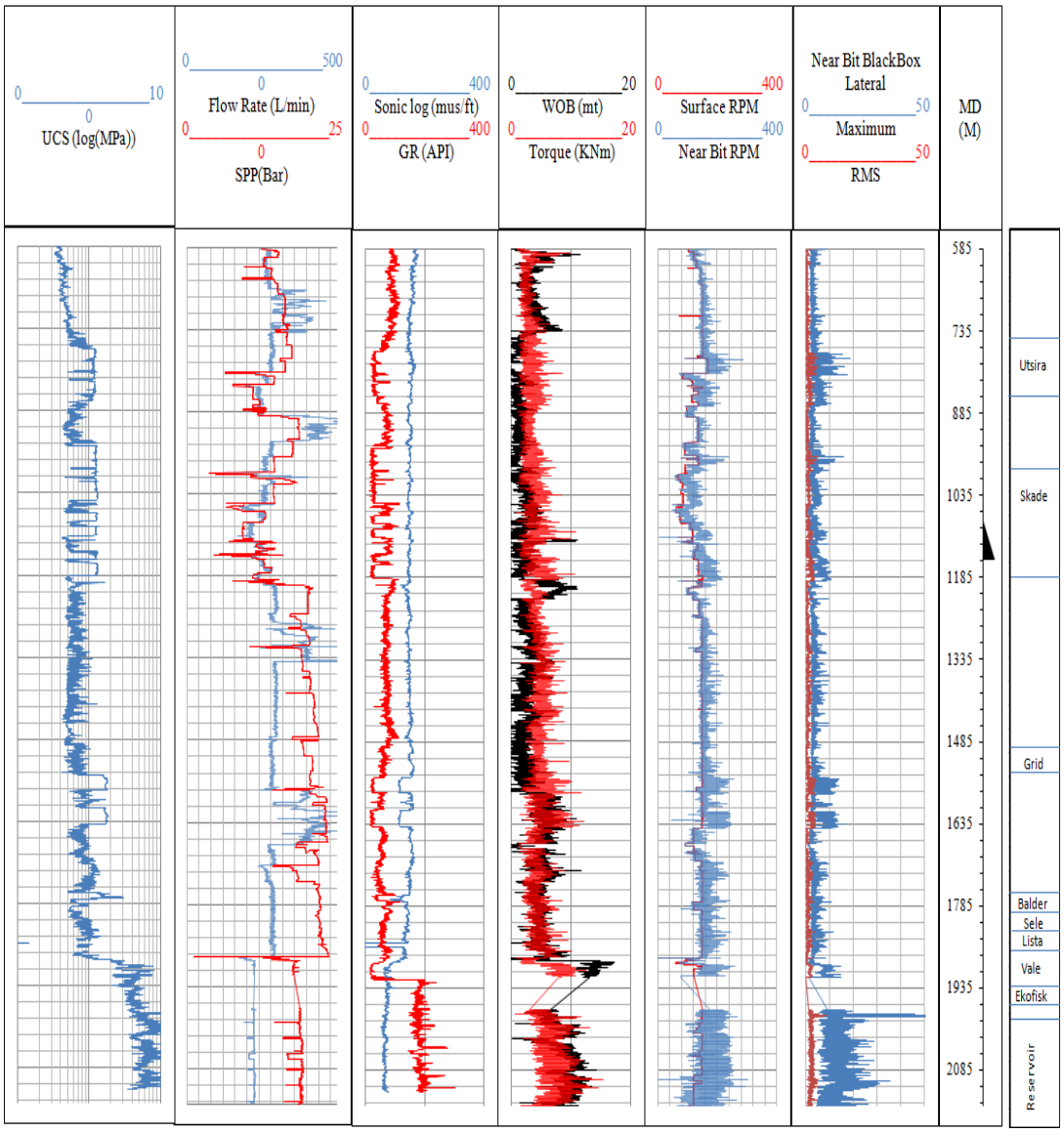

Figure 3.1. Drilling Data of Well A

Figure 3.1 shows that the downhole RPM is almost the same as the rotary RPM from 585-758m, and torque is lower than WOB on the same section, which indicate a smooth drilling. However, in the Utsira formation the downhole RPM start to spike and WOB drops, which indicate some torosional vibration. However, drilling the reservoir section, an erratic DH RPM can be noticed, which causes a high level of vibration

The UCS based on lithology percentage was calculated at different depth interval. Then the calculated UCS and maximum near bit lateral acceleration versus depth was plotted (Figure 3.1). The x-axis in the figure above was set to a log scale in order to notice the small changes between the USC and acceleration. It's clear that the UCS in this well follow the same pattern. When lateral acceleration increases, UCS tends to increase as well.

For Well B, the first section of this well was drilled using V-Stab anti vibration tool. The first section was drilled from 763m-1803m. In the next two sections, no anti vibration tool were used. Figure 3.2 shows log graph of the operating drilling parameters. Very low level of lateral acceleration and erratic RPM can be seen during drilling the first section. At 1528m, lateral acceleration started to increase. The increase in lateral acceleration is caused by the increase of torque over WOB. This increased also caused an increase of stick/slip severity. Overall, Well B did not face any severe lateral or torsional vibration. 1976-2150m section did face some abnormal condition of lateral and torsional vibration.

For Well C the WOB, Torque and Surface RPM data were measured by mud logging tools. Log graph of WOB, torque, near bit RPM and surface RPM of this well can be seen in Figure 3.3. Roller cone run bit shows a smooth drilling from 2025-2200 m, with a steady torque and surface RPM. In the next section, a different bit was used to drill from 2200-2270 m. During this section the bit faced a high frequency of erratic RPM indicated that the bit was in stick/slip mode. The last section was also drilled with a PDC bit from 2270-2303 m, also a high frequency erratic RPM can be noticed indicated stick/slip.

The calculated UCS based on lithology percentage and maximum near bit lateral acceleration versus depth can be seen in Figure 3.3. The UCS and maximum near bit lateral acceleration does not follow the same pattern in most cases. In some areas, the

UCS and lateral acceleration tend to have the same pattern but these areas are for a small interval. There are some spikes in near bit lateral acceleration while UCS decreasing. Since the x-axis was set to a log scale, a very small changes in acceleration will be noticed which could explain the inconsistency for these few spikes.

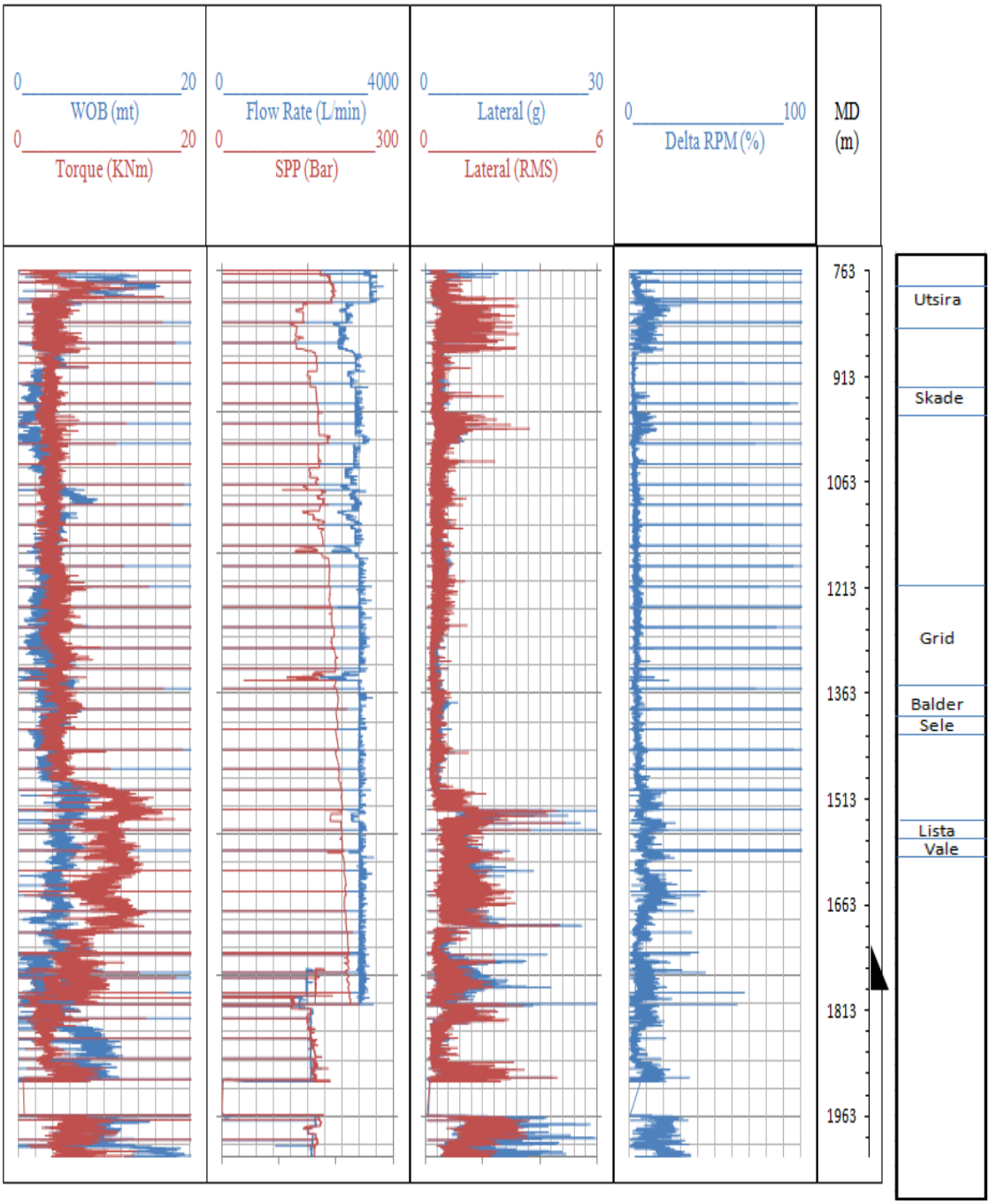

Figure 3.2 Drilling Data of Well B

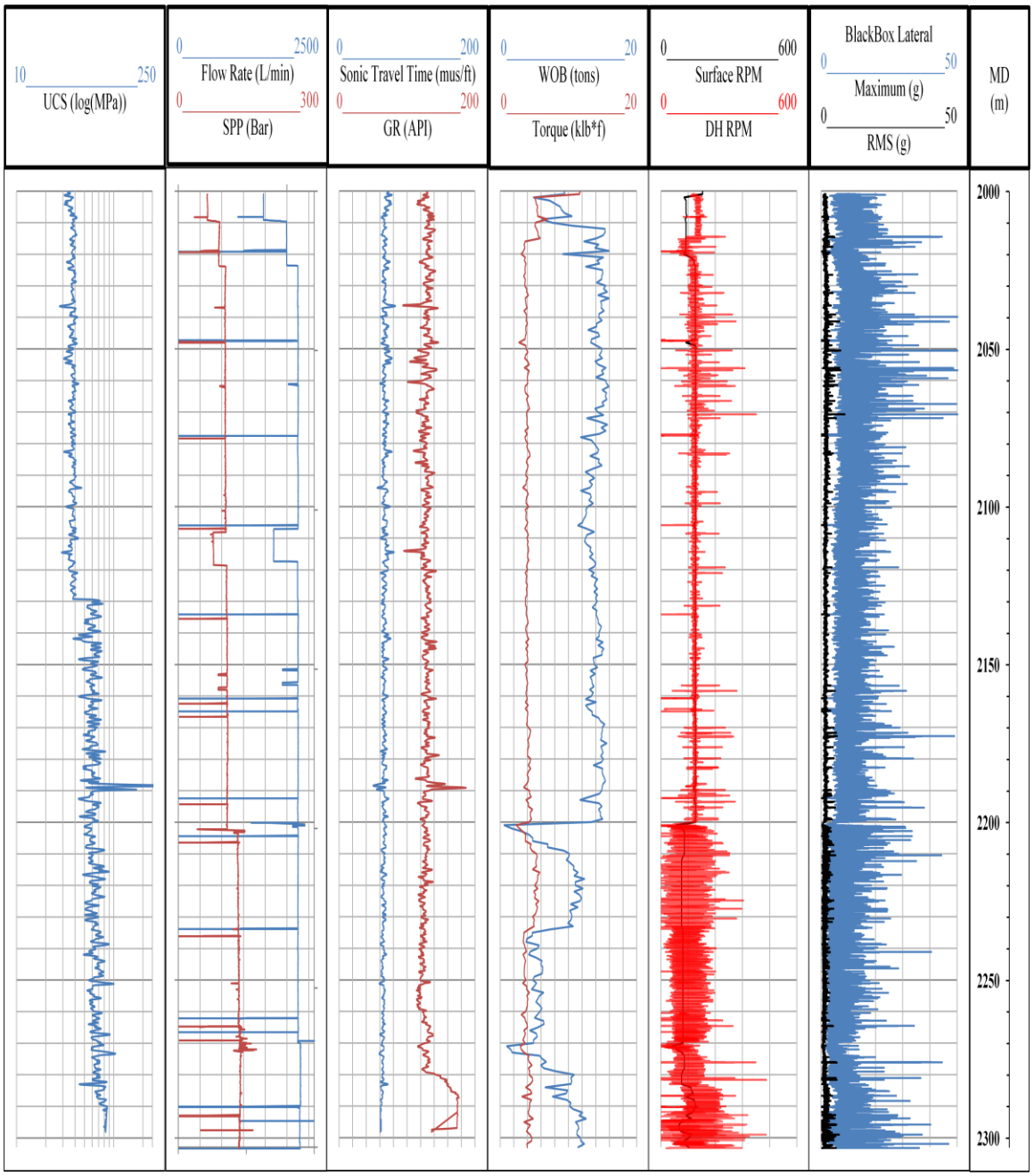

Figure 3.3 Well C Drilling Parameters

3.2. FORMATION TOPS VERSUS LATERAL VIBRATION

Box-plot of maximum near bit lateral acceleration for each lithology was created (Figure 3.4) for Well A to test for any statistical different in lateral acceleration at each formation.

Figure 3.4 shows that maximum near bit lateral acceleration was different for each formation. A significant amount of outliers can be noticed in the graph. The measured lateral vibration measures the whole wave, which generates a significant amount of outliers. Also, maximum near bit RMS acceleration was plotted in a box-plot (Figure 3.5) for each lithology.

The different in lateral RMS acceleration for each formation was plotted in a box plot in Figure 3.5. Both lateral vibration measurmets showed that each formation has different lateral vibration levels, however, lateral RMS has fewer outliers than the lateral acceleration.

The reason between the different amounts of outliers in both figures return to the different between the two measurements of lateral acceleration and lateral RMS acceleration.

A test for equal variances of lateral acceleration at each formation was preformed next. Figure 3.6 shows the variances in lateral acceleration range at each formation.

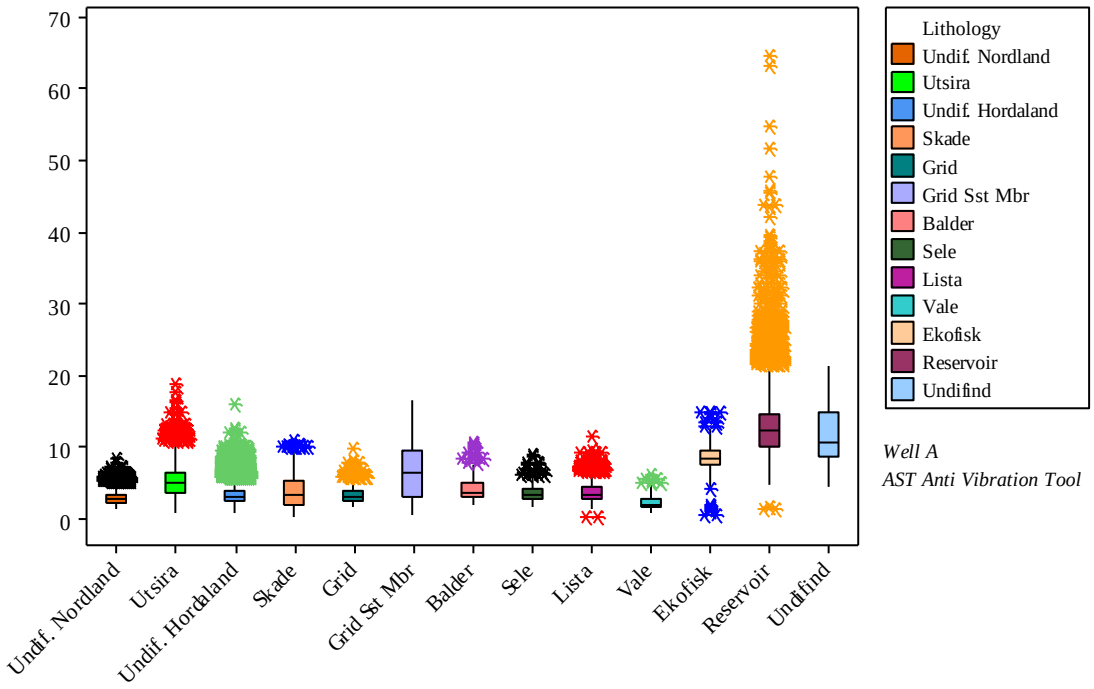

Figure 3.4. Maximum Near Bit Lateral Acceleration (Well A)

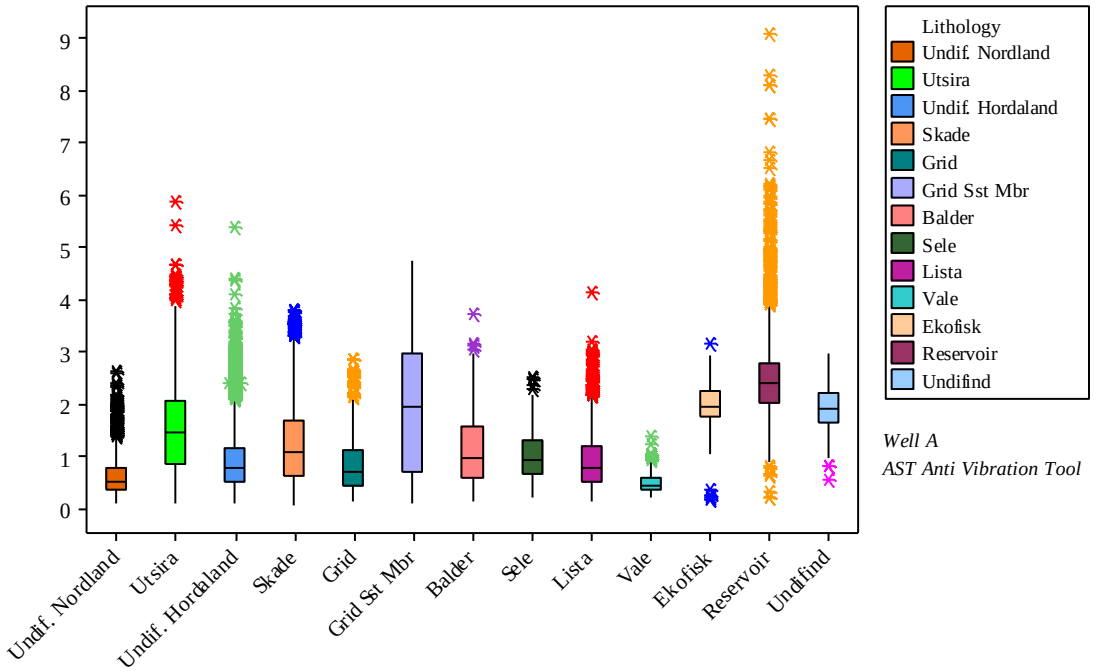

Figure 3.5. Maximum Near Bit Lateral RMS Acceleration (Well A)

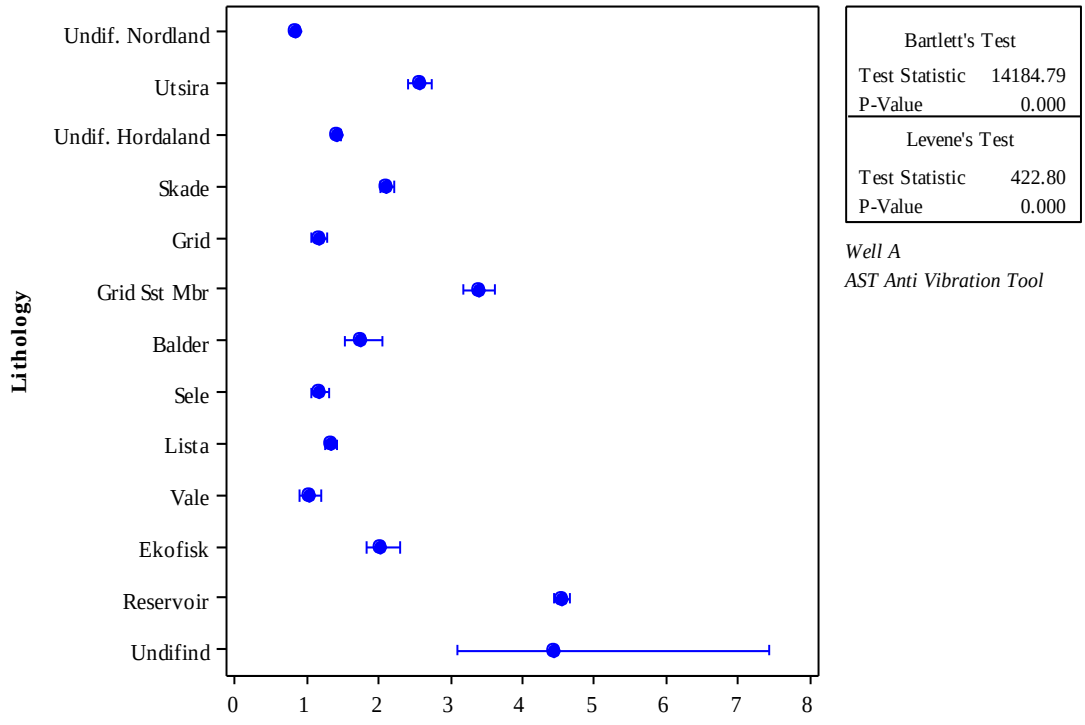

Figure 3.6. Equal Variances Test of Lateral Acceleration (Well A)

The test for equal variances of maximum near bit lateral acceleration at each formation reveals that each formation does not have equal variances. Also, since the calculated P value by using both Bartlett's and Levene's tests were zero, which confirm that each formation has a different levels and ranges of vibrations.

Using the gamma ray and the geolocial report of this well, the sand, shale, lime and granite was identified. Box plot of lateral vibration at each lithology was plotted Figure 3.7.

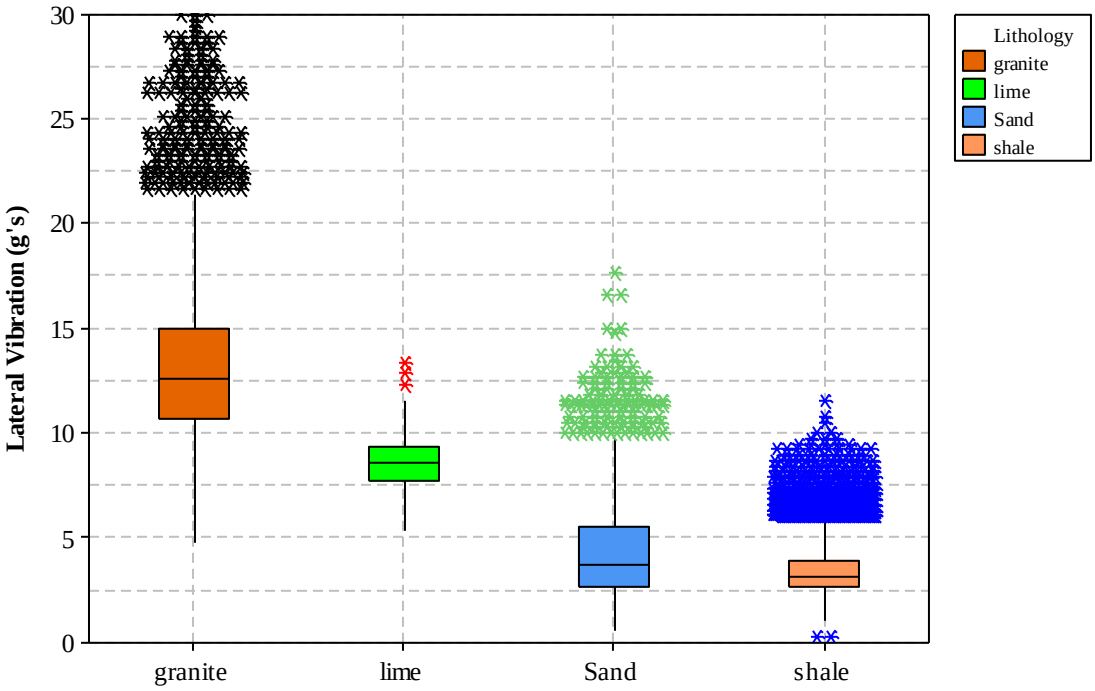

Figure 3.7 Maximum Near Bit Lateral Accelerations for different Lithology of Well A

Figure 3.7 show that the lateral vibration of granite has the higher vibration levels. The shale formation however has the lowest level of lateral vibration.

For Well B, a box-plot of maximum near bit lateral acceleration for each formation came with the same expected results (Figure 3.8).

Figure 3.8 show that each formation has different values of lateral acceleration. Well B lateral vibration at each formation shows the same result as Well A. Another box-plot of maximum near bit Lateral RMS acceleration (Figure 3.9) was created.

The same results from maximum near bit lateral acceleration can be seen in maximum near bit lateral RMS acceleration in Figure 3.9. However, the only different is that the RMS acceleration has fewer outliers. Test for equal variances between maximum near bit lateral acceleration at each formation (Figure 3.10) was analyzed next.

The test for equal variances between each formation shows that the vibration of each formation does not have equal variances. On the other hand, the calculated P-value from both Bartlett's and Levene's tests was zero, which confirm that each formation has a different lateral acceleration range and frequencies.

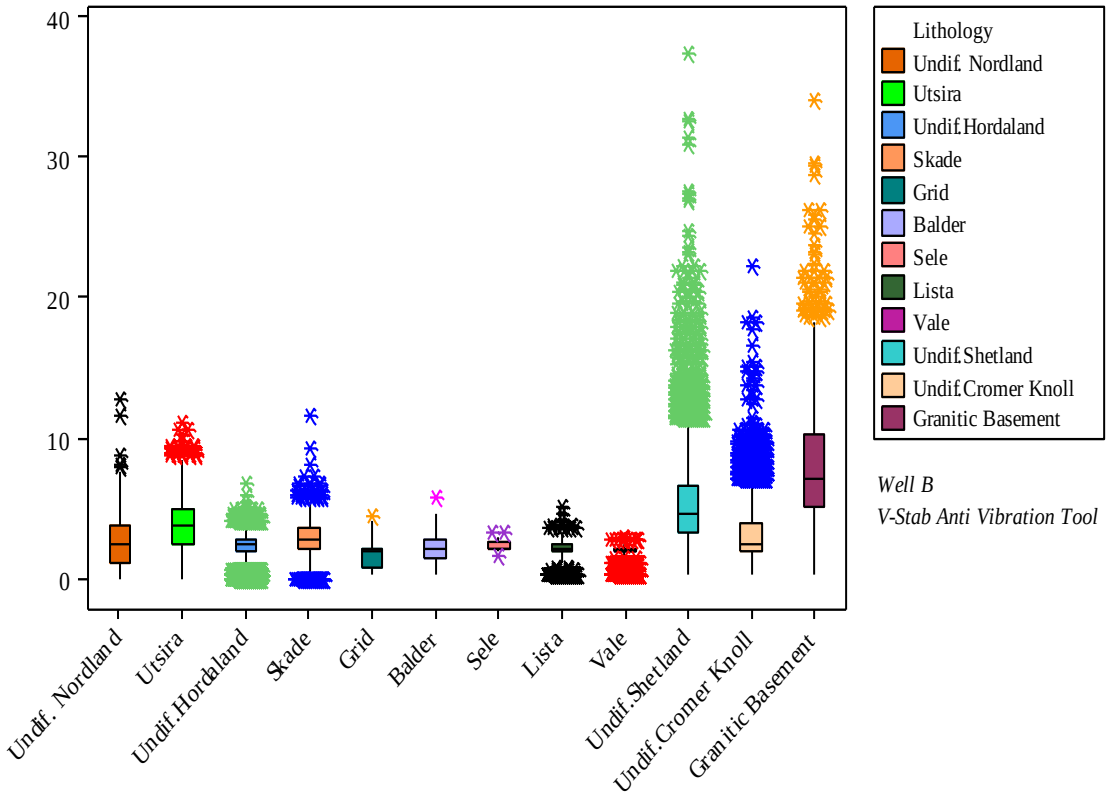

Figure 3.8. Maximum Near Bit lateral Acceleration (Well B)

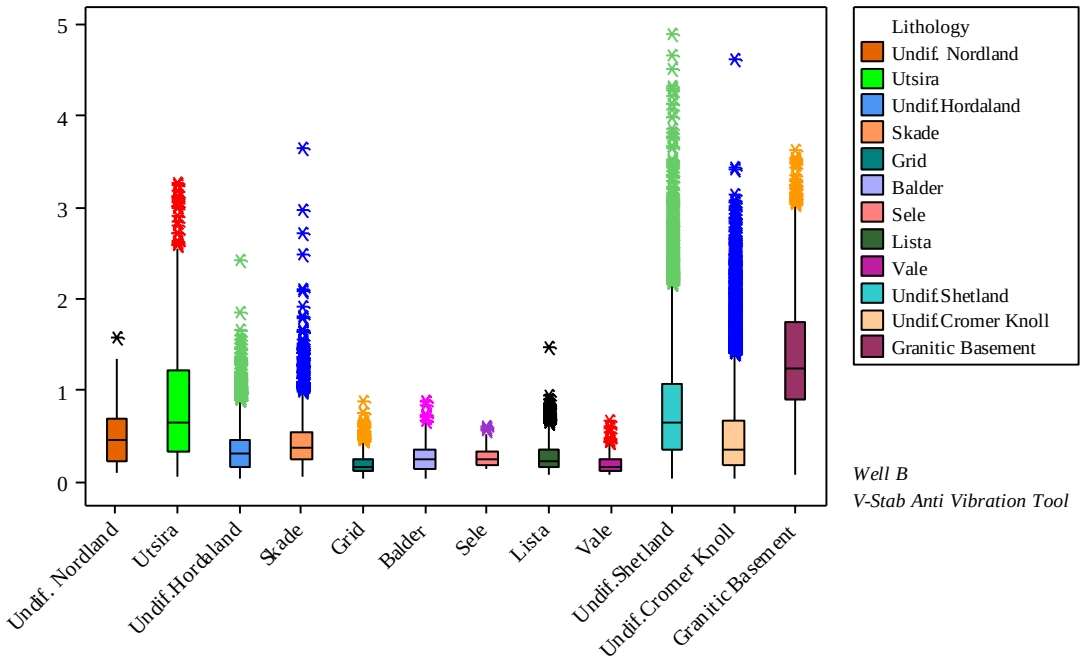

Figure 3.9. Maximum Near Bit Lateral RMS Acceleration (Well B)

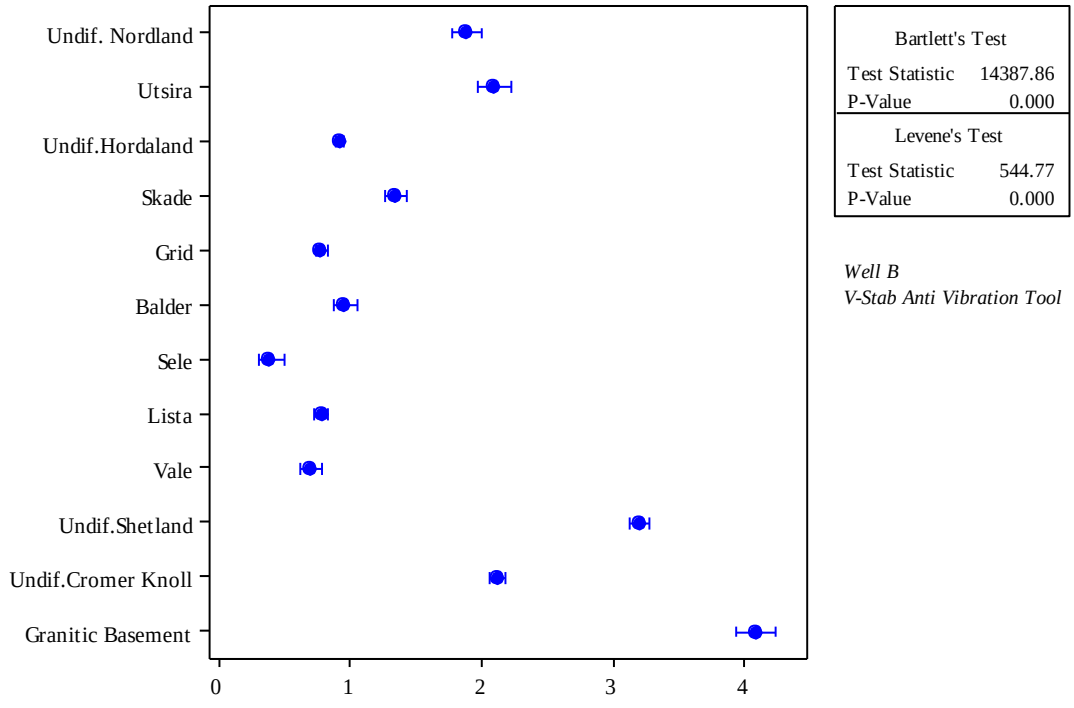

Figure 3.10. Equal Variances Test of Lateral Acceleration (Well B)

3.3. VIBRATION REDUCTION TOOLS EVALUATION

After collecting near bit lateral acceleration from three different wells with different anti vibration tool for each BHA, a log graph was created to compare the amount and frequency of the generated lateral vibration versus depth from each well (Figure 3.11). The AST tool was used in Well A, the V-Stab was used in Well B and Well C did not have any anti vibration tool installed in the BHA.

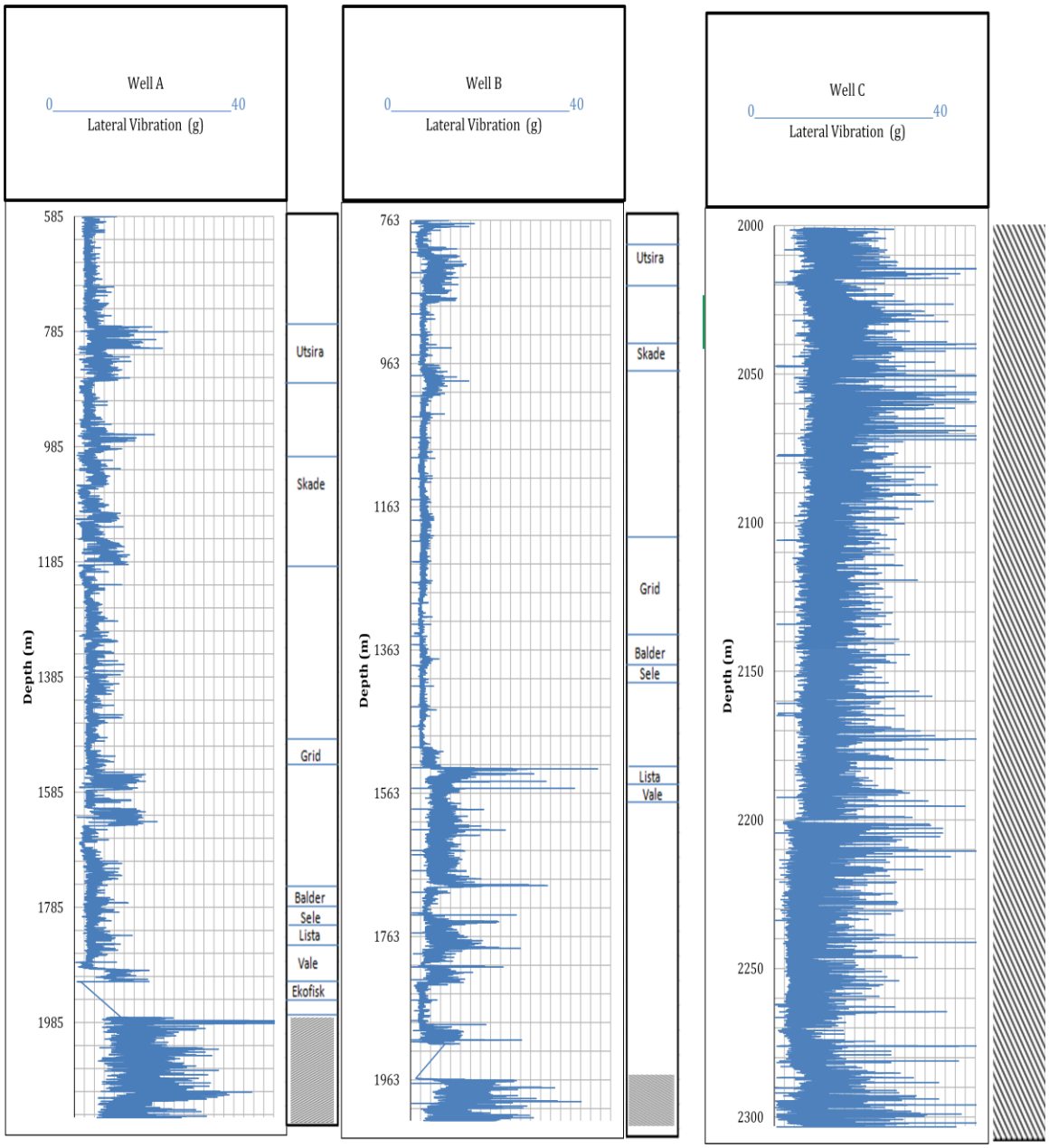

Figure 3.11. Maximum Near Bit Lateral Acceleration for the Three Wells

Maximum near bit lateral acceleration graphed in Figure 3.11 shows that Well C that consists of no anti vibration tool has the highest level of lateral vibration. However, Well B that consisted of the V-stab has lower lateral vibration overall. After removing the V-stab, lateral vibration started to increase; this increase however did not reach the severity level.

Log graph of lateral RMS vibration was plotted against measured depth in Figure 3.12.

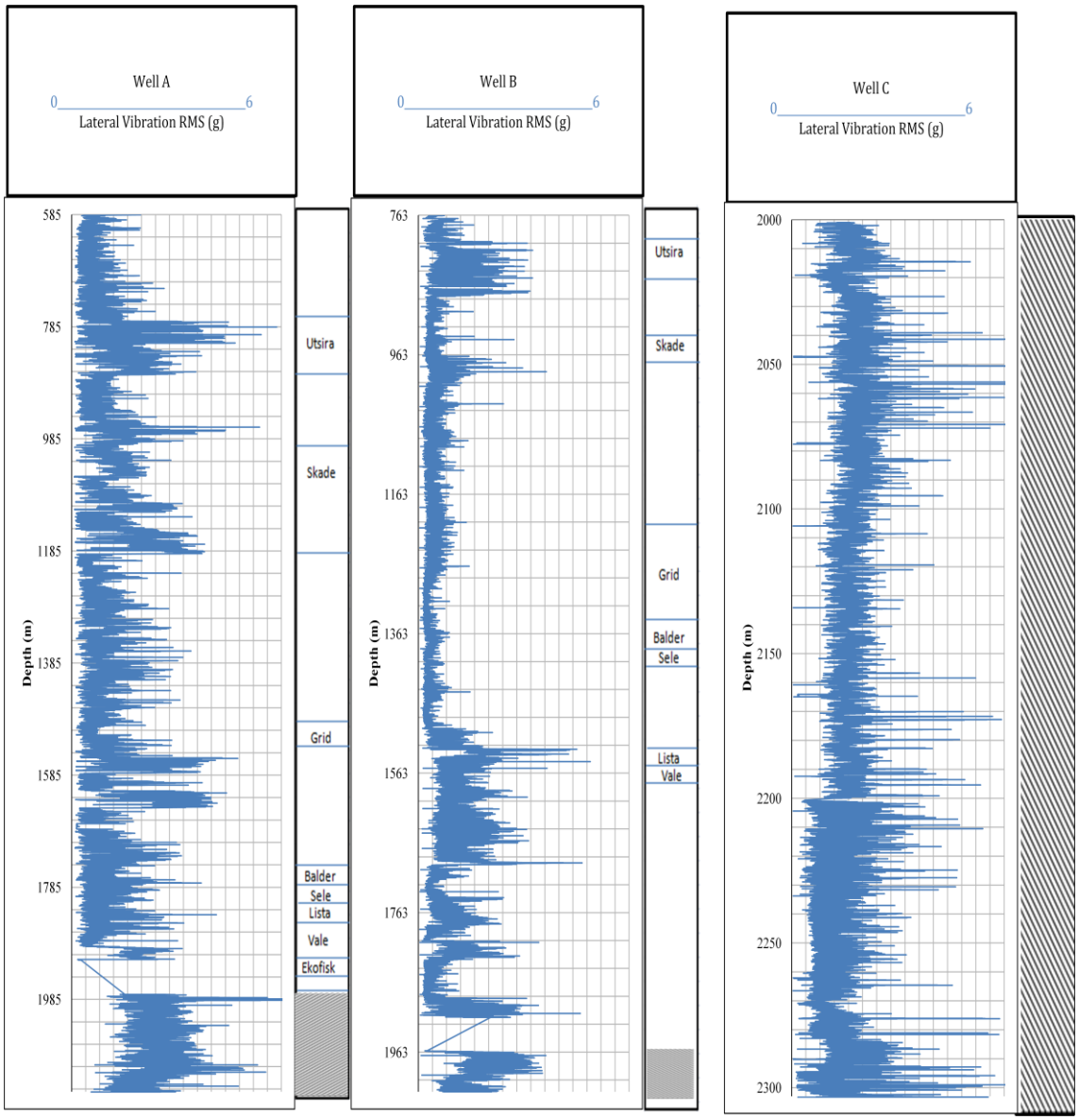

Figure 3.12. Maximum Near Bit Lateral RMS Acceleration For the Three Wells

Maximum lateral RMS acceleration showed the same result as lateral vibration. Well C faced severe lateral RMS vibration.

Another representation of comparing the two different anti vibration tools with the well that does not have anti vibration tool was preformed. A bar graph of each maximum near bit lateral and lateral RMS was created by calculating the median, average and standard deviation of each well individually than a graphed as bars forms. Also a distribution bar graph was created for near bit lateral RMS acceleration of the three well was created in the same graph. (Figure 3.13)

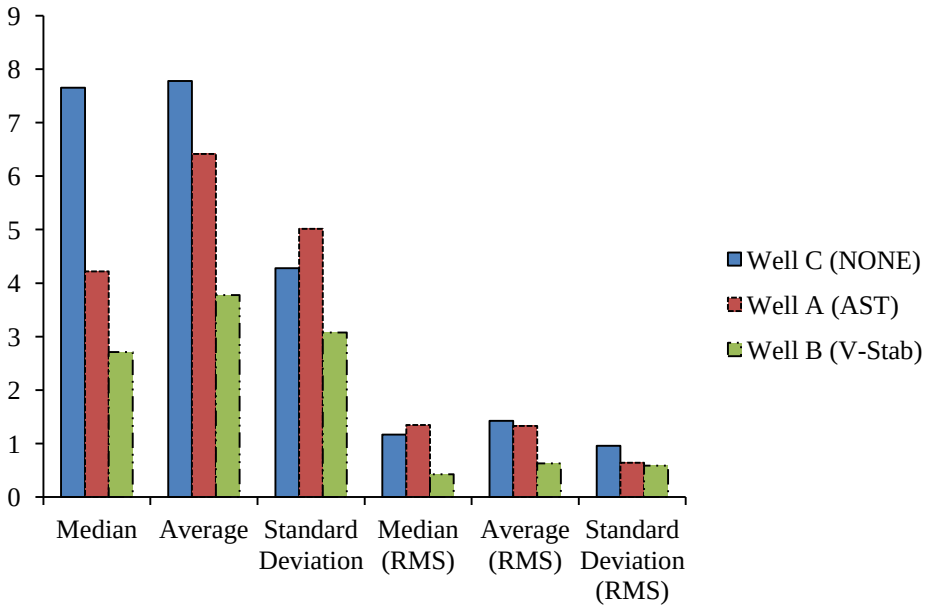

Figure 3.13. Maximum Near bit Lateral Acceleration of the Three wells

Figure 3.12 shows that the median and average of near bit lateral acceleration of Well C are higher than the other fields. However, the standard deviation of Well A is higher. Well B has the lowest lateral acceleration levels of the three wells. For lateral RMS vibration, Well C has the highest lateral RMS vibration. However, the average of

Well A is higher than Well C. The lowest lateral RMS acceleration is Well B which consisted of the V-stab anti vibration tool.

3.4. COMPARING LATERAL VIBRATION OF MATCHING FORMATION AND LITHOLOGY

Lateral vibration of Well A and Well B generated in Utsira formation was graphed in one plot in Figure 3.14. The right y-axis in the figure refer to Well B depth and the left y-axis will refer to Well A depth.

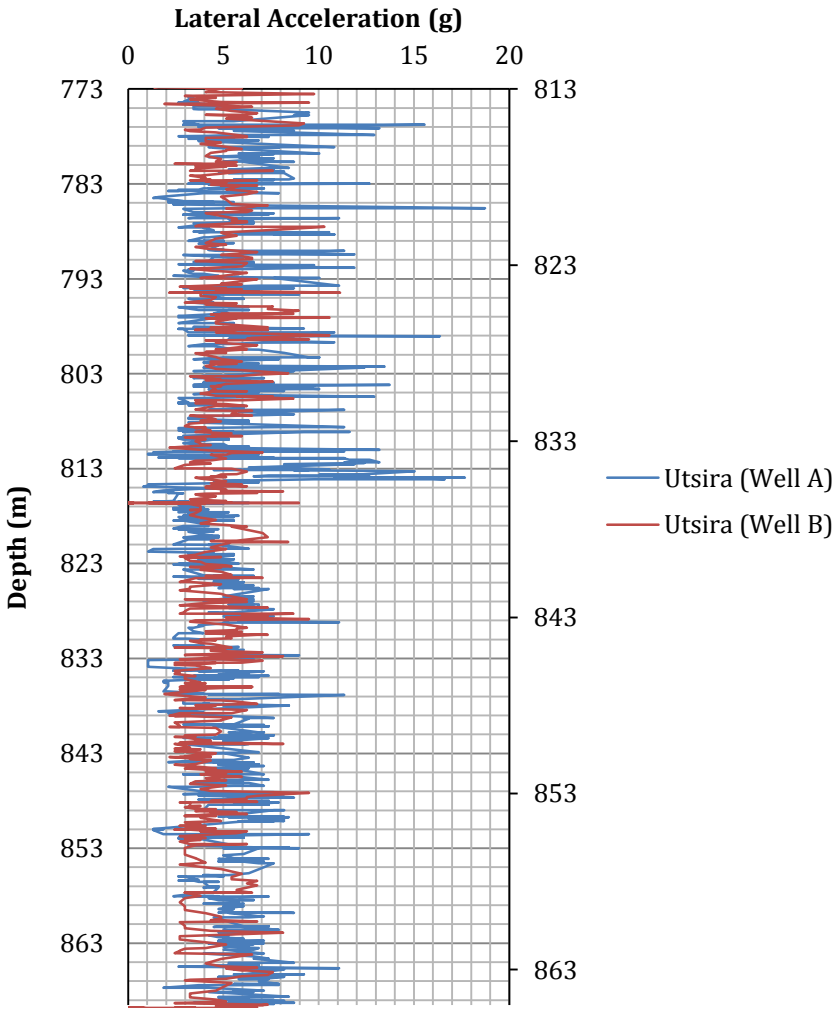

Figure 3.14. Lateral Acceleration of Utsira Formation

Lateral vibration of Well A and Well B in the other six matching formation can be seen in APPENDIX D.

From the generated figures of lateral vibration at matching formation, Well B has lower lateral acceleration in all common formations.

Figure 3.15 shows that the calculated average of lateral vibration of Well B is the lowest at all matching formations.

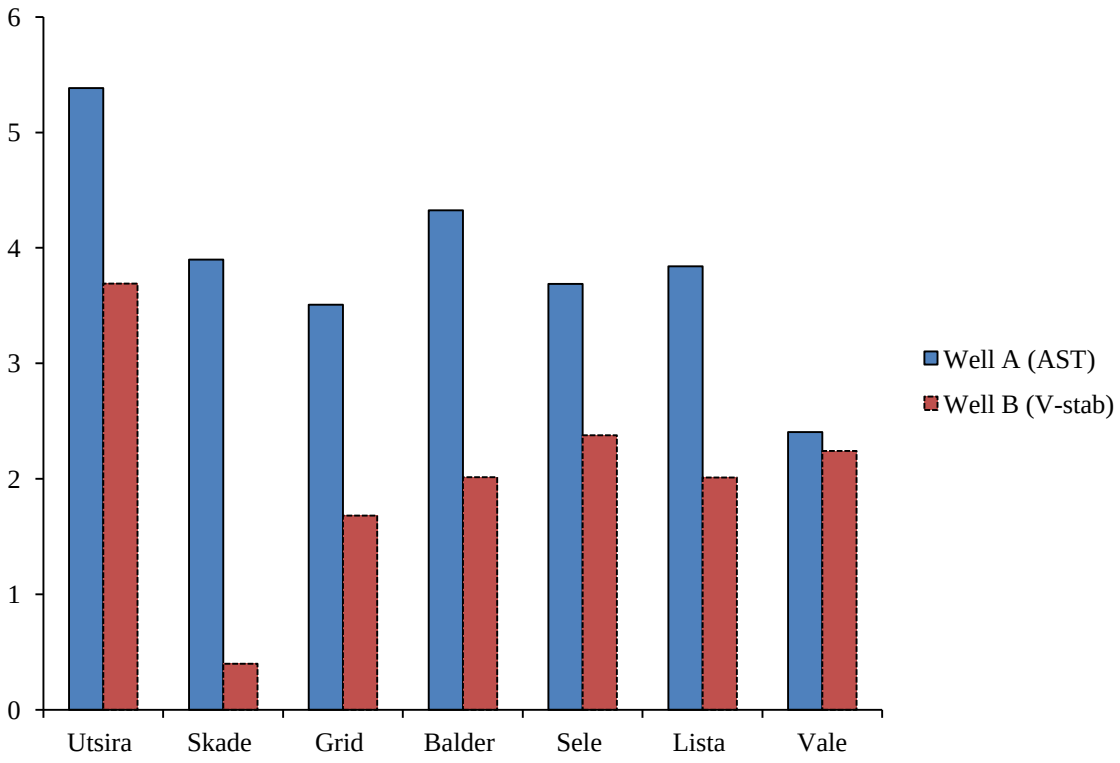

Figure 3.15. Average Lateral Acceleration for Each Formation

Lateral acceleration from both wells are combined to generate box-plots and interval plots of standard deviation to analyze the difference between each well vibration at each formation. For this analysis, the lateral acceleration of matching formation wa analyzed per formation top. Figure 3.16 shows lateral acceleration of Well A and Well B at Utsira formation.

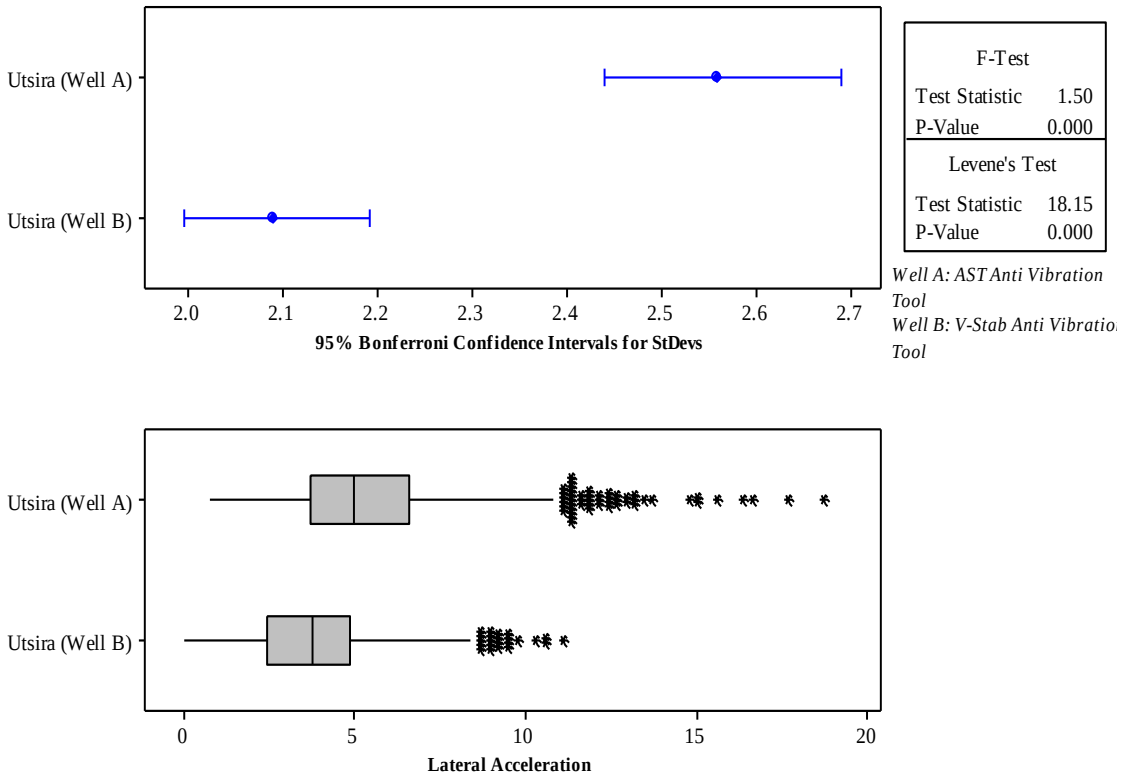

Figure 3.16. Statistical Analysis of Utsira Formation

Statistical analysis of Well A and Well B vibration in the other six matching formation can be seen in APPENDIX E.

The statistical analysis of Utsira, Skade, Grid, Balder, Sele and Lista formations, shows that lateral acceleration from both wells are not equal. The analysis revealed that Well B has lower lateral acceleration in all of these formations.

Interestingly, the statistical analysis of the Vaale formation shows that Well A and Well B have the same mean, however, the standard deviation is different.

3.5. EVALUATING STICK/SLIP

The stick/slip severity was calculated for the three different wells. Figure 3.17 shows stick/slip severity of the three different wells. The stick/slip severity figure include

three line , beside stick/slip severity line, those three lines represent the severity level of stick/slip as indicated in Table 2.4.

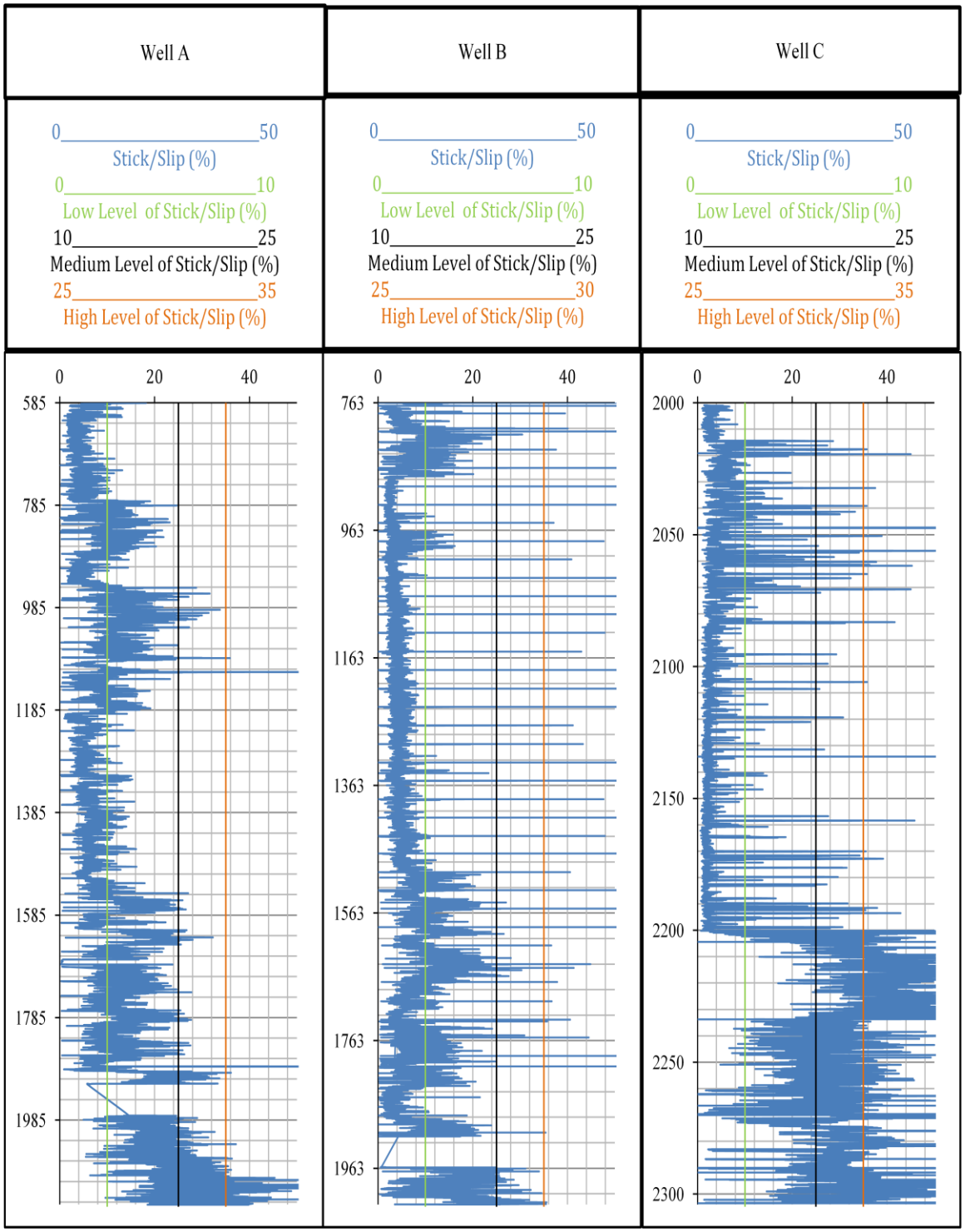

Figure 3.17. Stick/Slip Identification of Well A, B and C

Figure 3.17 shows that the severity of stick/slip of Well A and Well B was not in the severe conditions. For Well A, in most cases the stick/slip severity was in the medium range. And for Well B, in most cases stick/slip severity was in the normal range. However, the stick/slip severity of Well C reached the severe level.

3.6. STATISTICAL ANALYSIS OF SAMPLING RATE

The statistical summary of both data sets for each well was preformed graphically. Figure 3.18 and Figure.3.19 shows statistical summary of lateral acceleration for the original data set and for the 10^{th} data sampling respectively of Well A.

The P-value of both data sets are less than the chosen α value of 0.05, which conclude that the data do not follow a specific disruption.

The statistical analysis and nonparametric distribution for sampling rate of both data sets for Well B and Well C are located in APPENDIX.F.

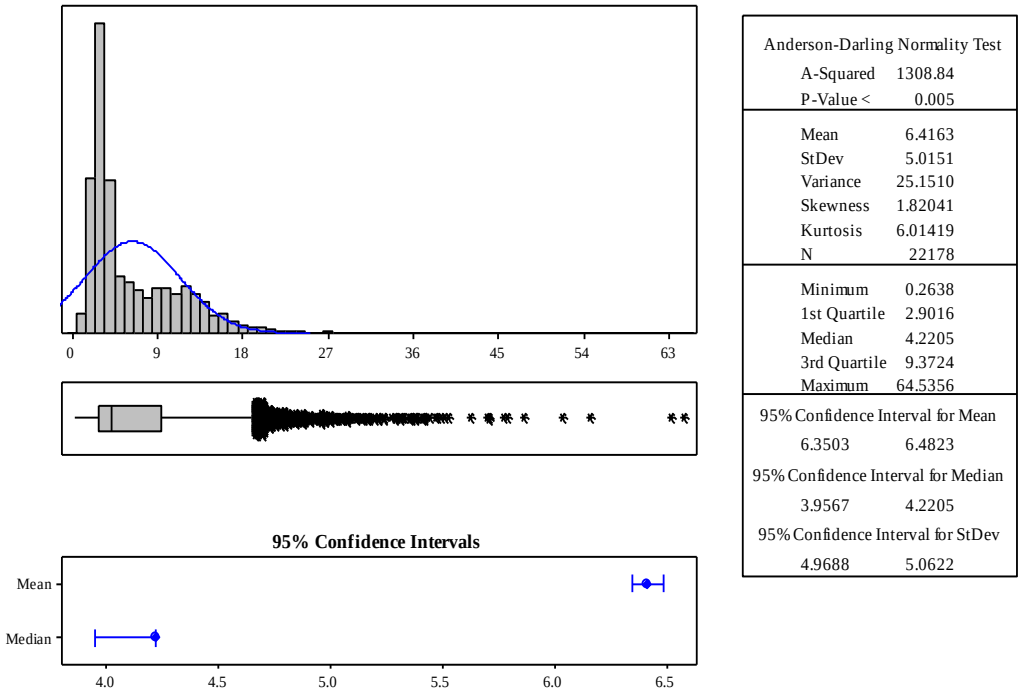

Figure 3.18. Statistical summary of the Original Data of Well A

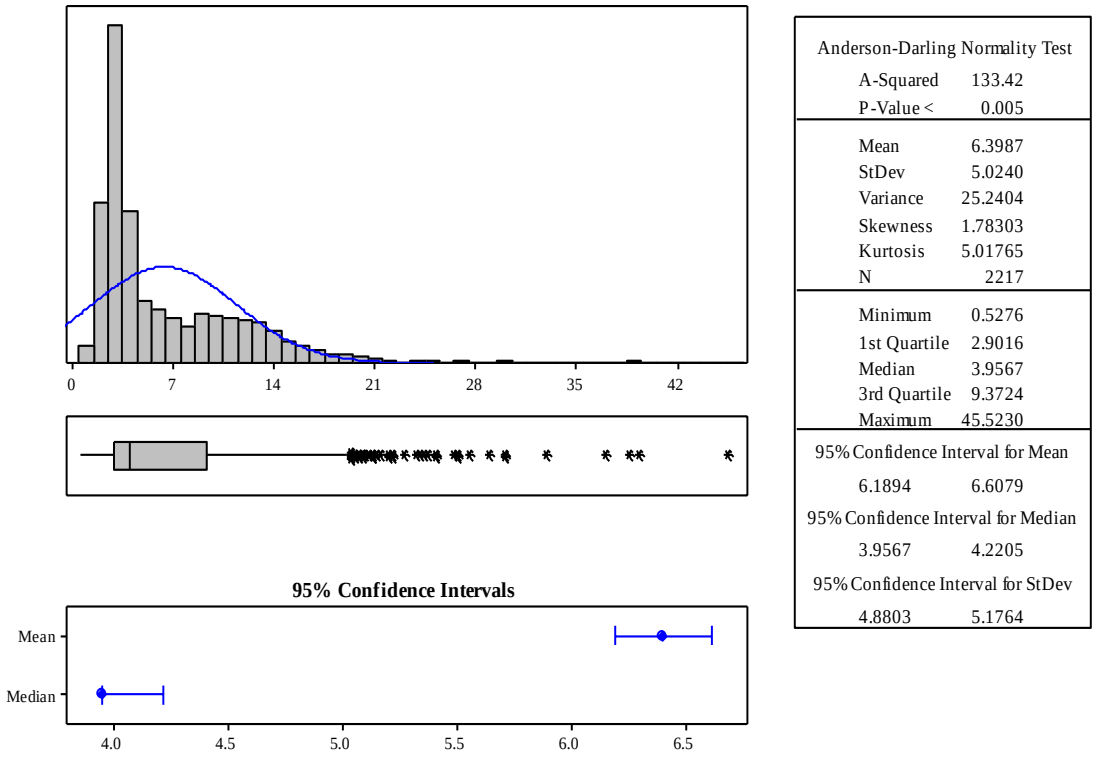

Figure 3.19. Statistical Summary of the 10th Data Sampling of Well A

The Wilcoxon test was used to compare the two data sets. The output of Wilcoxon test was summarized in Table 3.1.

Table 3.1. Wilcoxon test of both data for Well A

	N	Estimated Median	Achieved Confidence	Confidence Interval Lower	Confidence Interval Upper
Actual Data	22178	5.803	95	5.735	5.877
10th Sample	2217	5.803	95	5.539	6.067

Table 3.1 shows that both data have the same estimated median. The confidence intervals for both data however are slightly different. The nonparametric distribution

analysis tests generated a survival graph (Figure 3.20). The survival plot shows both lateral acceleration data versus the probability percentage of survival. The Kaplan Meier test showed that both data sets are statistically equal.

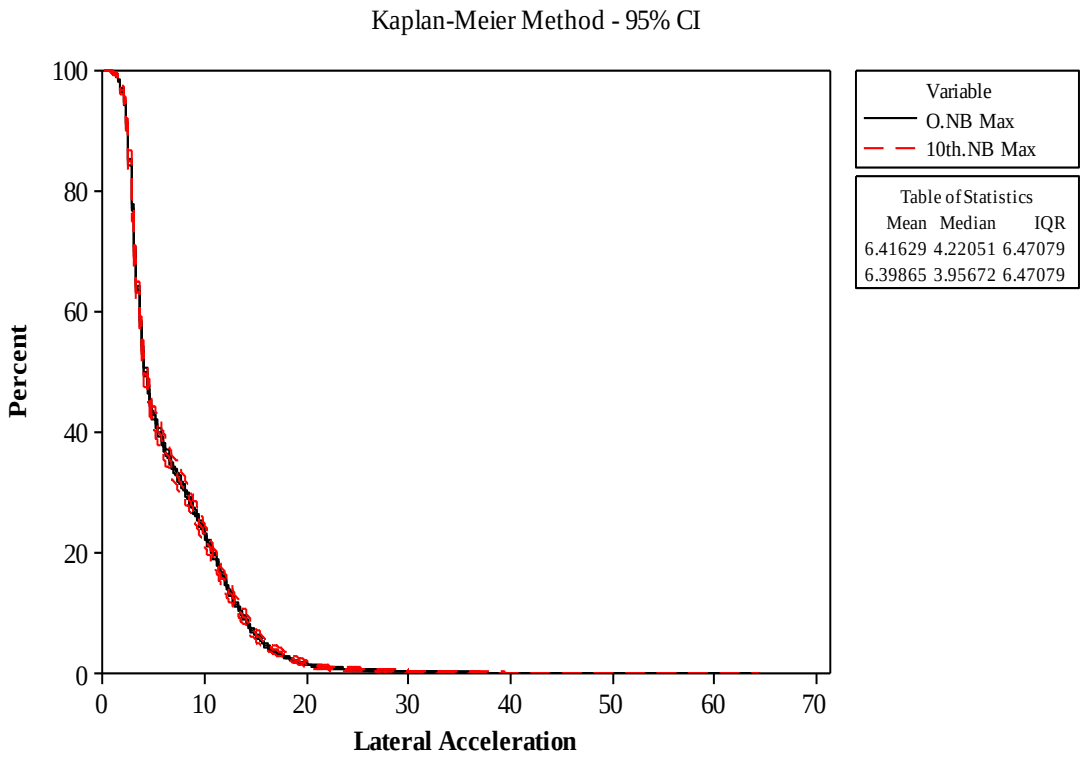

Figure 3.20. Survival test of original and 10th sample data for Well A

The P-value of each set of data was also calculated with two different methods. (Table 3.2)

Table 3.2. Comparison of Survival Curves Well A

Method	Chi-Square	DF	P-Value
Log-Rank	0.024443	1	0.876
Wilcoxon	0.156032	1	0.693

Since α value was set to 0.05 and both tests have a P-Value greater than value of α, the two data sets are equal.

Lateral acceleration was also compared between the different blackboxes in each bit run. Figure 3.21 shows lateral vibration from different blackboxes location for each bit run within the three different wells.

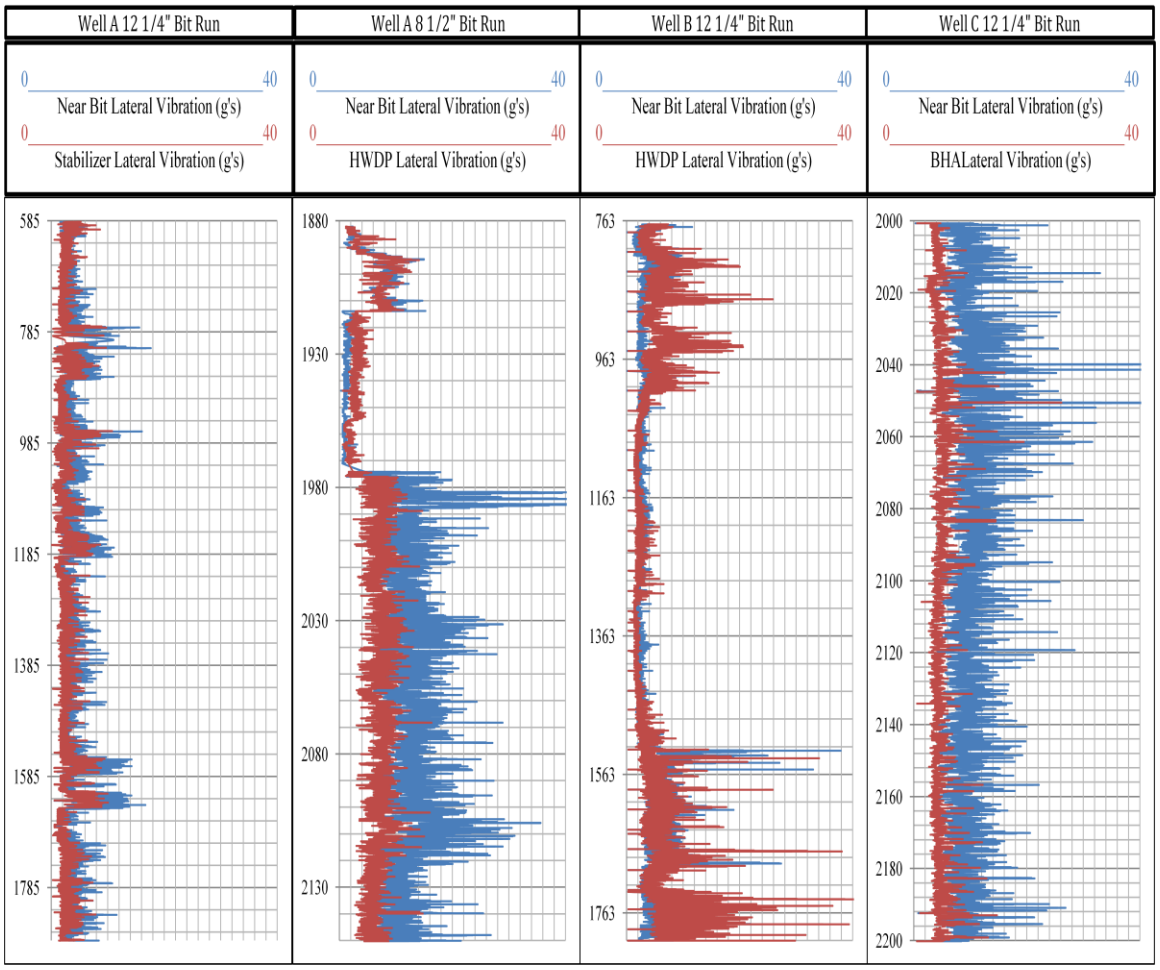

Figure 3.21 Lateral Vibration of Different Blackboxes Locations within the Same Bit Run

For Well A using the AST vibration reduction tool, lateral acceleration located above the bit have higher lateral vibration. For Well C that did not consist of vibration reduction tool, lateral vibration above the bit was higher. Using the V-stab on Well B

lateral vibration within the heavy weight drill pipe (HWDP) was higher than the one located right above the bit.

A statistical comparison between the two blackboxes within the same well was done for the three different wells. Figure 3.22 shows lateral acceleration of both blackboxes measurements within the same wells for the three different wells.

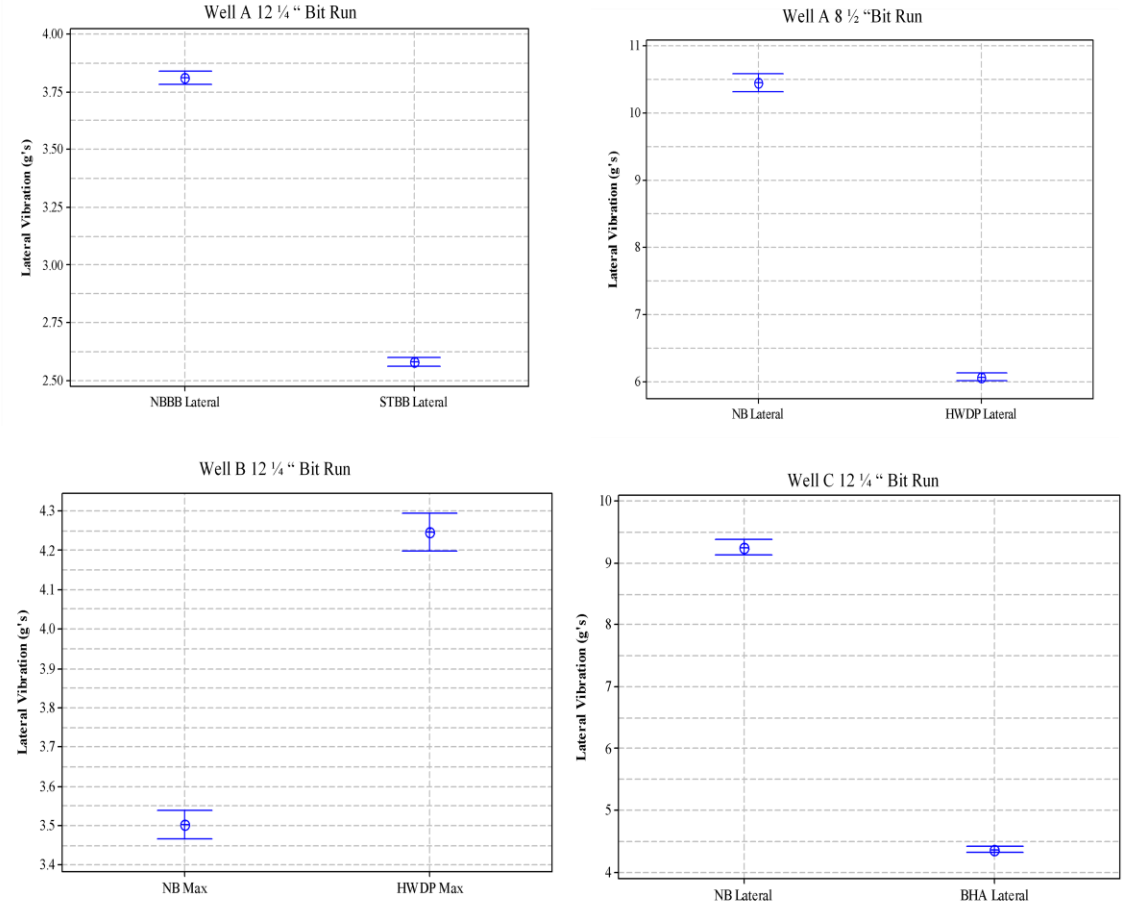

Figure 3.22. Lateral Vibration Within the Same Well for The Three Different Wells

The same result that was predicted using log graphs of lateral vibration was achieved. Near bit lateral vibration using the V-stab of Well B has lower vibration than the vibration of the HWDP.

3.7. MULTI VARIABLES EFFECT ON DRILLSTRING VIBRATION

The effect of WOB, torque, RPM and UCS on lateral vibration was investigated. However, only torque, WOB, and RPM was considered for Well B. Figure 3.23, 3.24 and 3.25 shows the obtained correlations of lateral vibration of Well A and two different bit run of Well B respectively. Parameter distributions of each well can be seen in APPENDIX G.

The cross plot of well A (Figure 3.23) shows that UCS have a good correlation with lateral vibration, torque and WOB. However, UCS does not correlate with surface RPM. For Well B, the UCS and surface RPM was not included. Figure 3.24 shows that lateral vibration does not have a good correlations with WOB and torque. Surface RPM, torque, WOB and lateral vibration does not correlate with UCS; in fact, USC does not have effect on lateral vibration. The effect of each parameter on lateral vibration was modeled with a linear relationship. The effect of each parameter on lateral vibration of each well can be summarized in Figure 3.26.

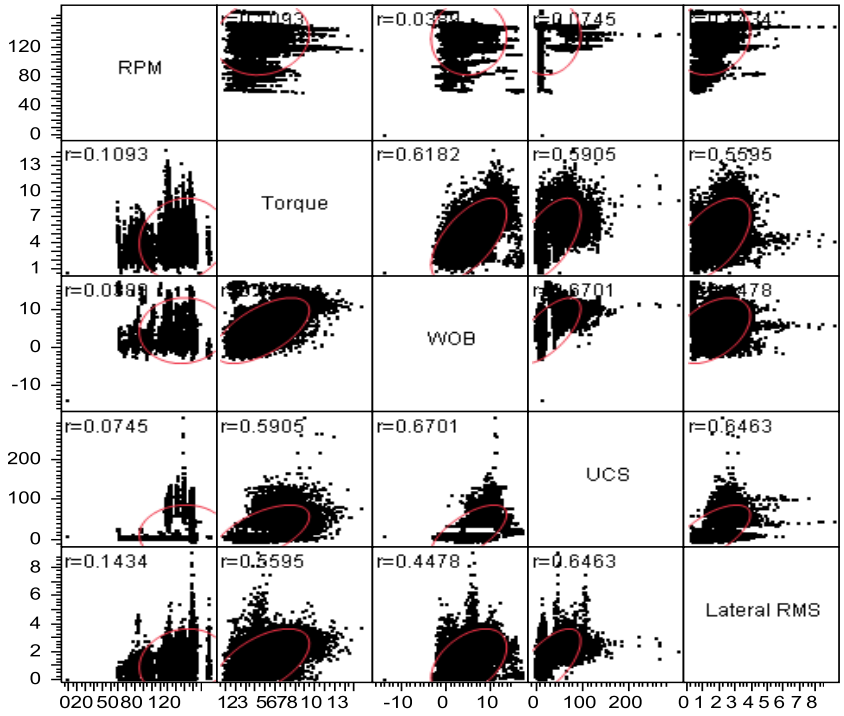

Figure 3.23. Lateral Vibration Correlations of Well A

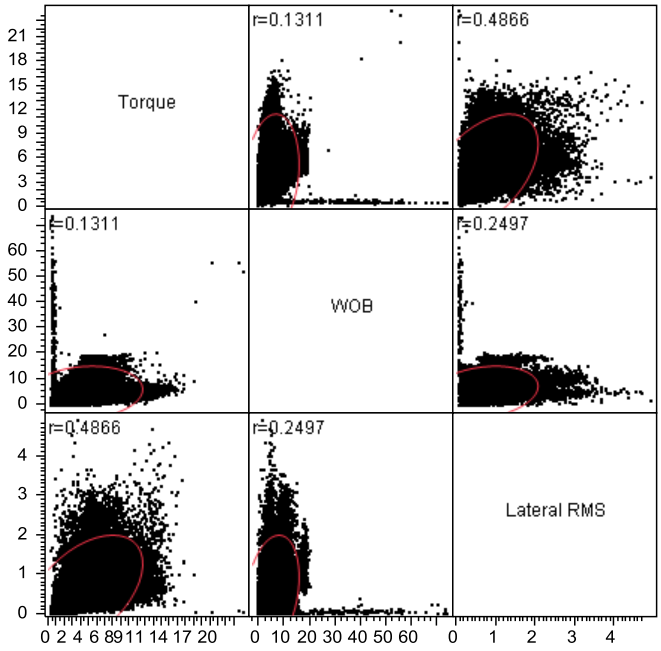

Figure 3.24. Lateral Vibration correlations of Well B

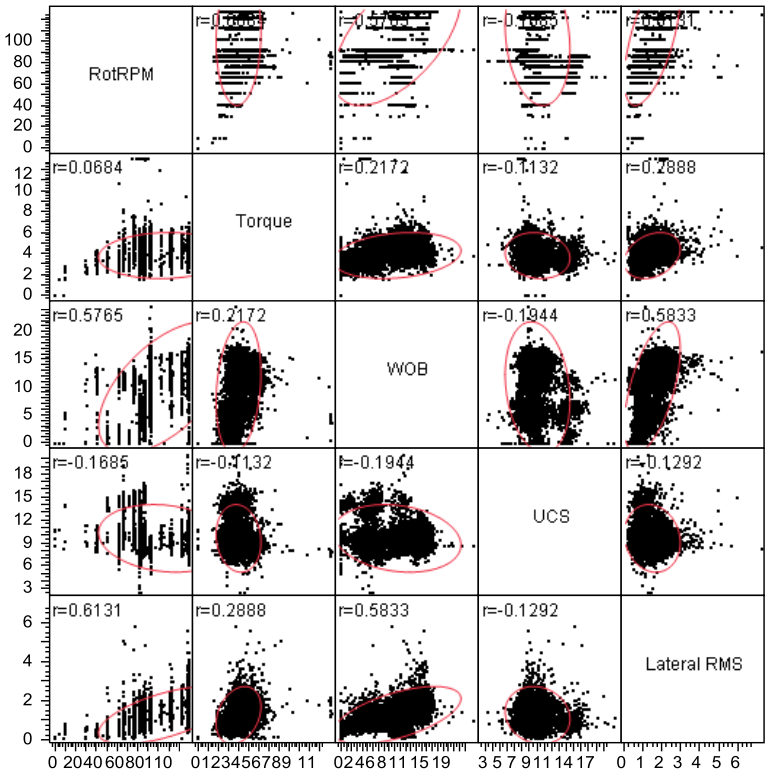

Figure 3.25. Lateral Vibration Correlation of Well C

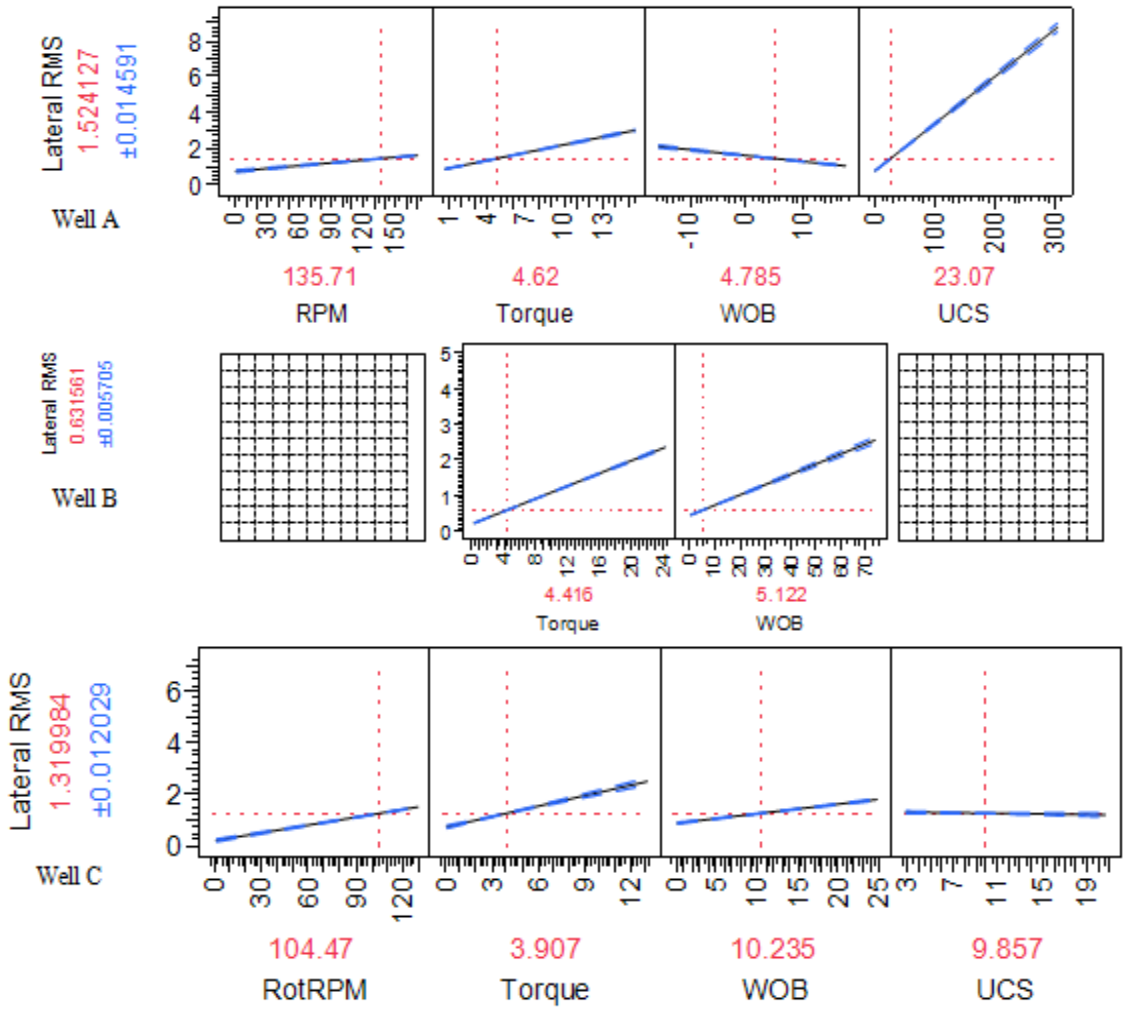

Figure 3.26. Lateral vibration Profile for the three wells

Lateral vibration profile for Well A shows that with the increase of WOB Lateral vibration decrease. The UCS however, has a big impact on lateral vibration on Well A, as the UCS increase Lateral vibration increase. Lateral vibration tends to increase with the increase on surface RPM. For Well B, the obtained relationship for Well B shows that with the increase of WOB and torque lateral vibration increase. Well C correlation shows that there is no effect on lateral vibration caused by UCS.

MSE relationship with drillstring vibration was investigated. The 8 ½" section of Well C using a PDC bit was normalized for constant range of UCS and flow rate. Figure 3.27 shows the correlation obtained for this section.

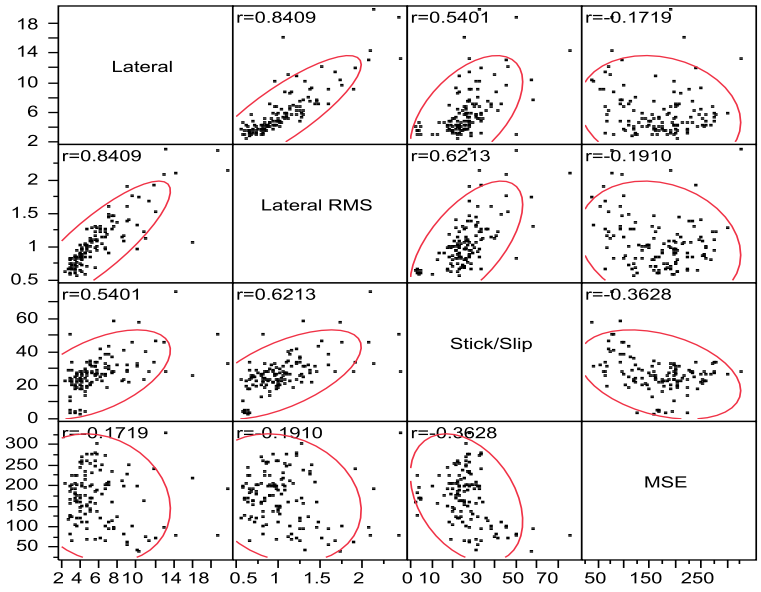

Figure 3.27. Drillstring vibration and MSE correlations of Well C (PDC Bit)

Figure 3.27 shows that there is no relationship between MSE and drillstring vibration. The r square (fit percentage) for MSE and drillstring vibration is low for this section. 12 ¼" section of Well C was also analyzed under the same condition. (Figure 3.28)

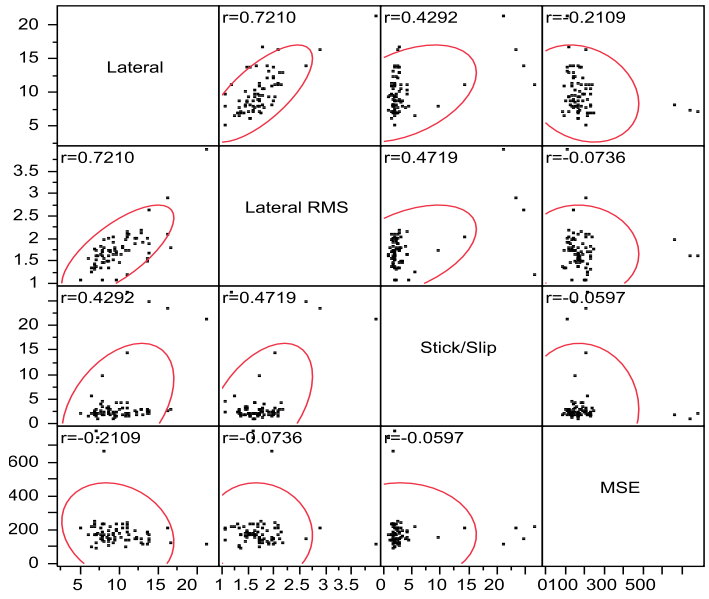

Figure 3.28. Drillstring Vibration and MSE Correlation of Well C (tri cone Bit)

Figure 3.28 shows that there is no evidence that drillstring vibration has an effect on MSE or vice versa, which matches the result obtained from the previous section.

Well A also was subjected to the same study. 12 ¼" of Well A using PDC bit was analyzed for the effect of vibration on MSE. Figure 3.29 shows the MSE and drillstring vibration correlation at this section.

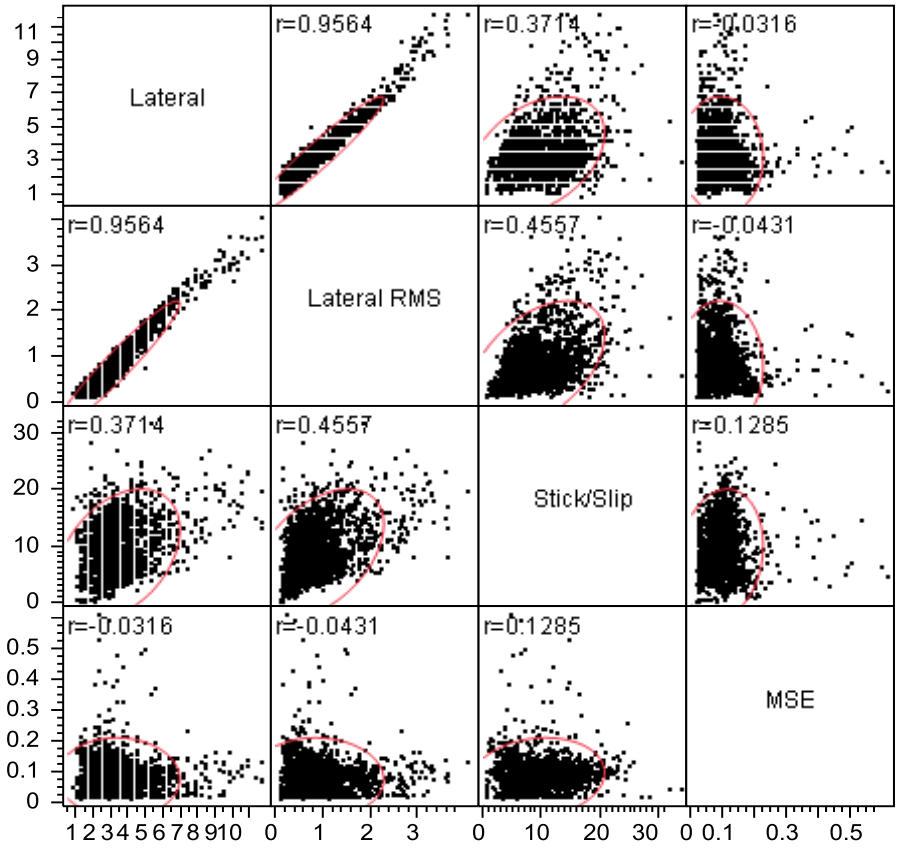

Figure 3.29. Drillstring Vibration and MSE correlations of Well A (12 ½" PDC Bit)

The correlation obtained from Well A, also shows that MSE does not have a good correlation with drillstring vibration.

Drilling parameters and UCS was set constant to analysis the effect of WOB on drillstring vibration for Well C. Figure 3.30 shows the obtained correlation between WOB and drillstring vibrations.

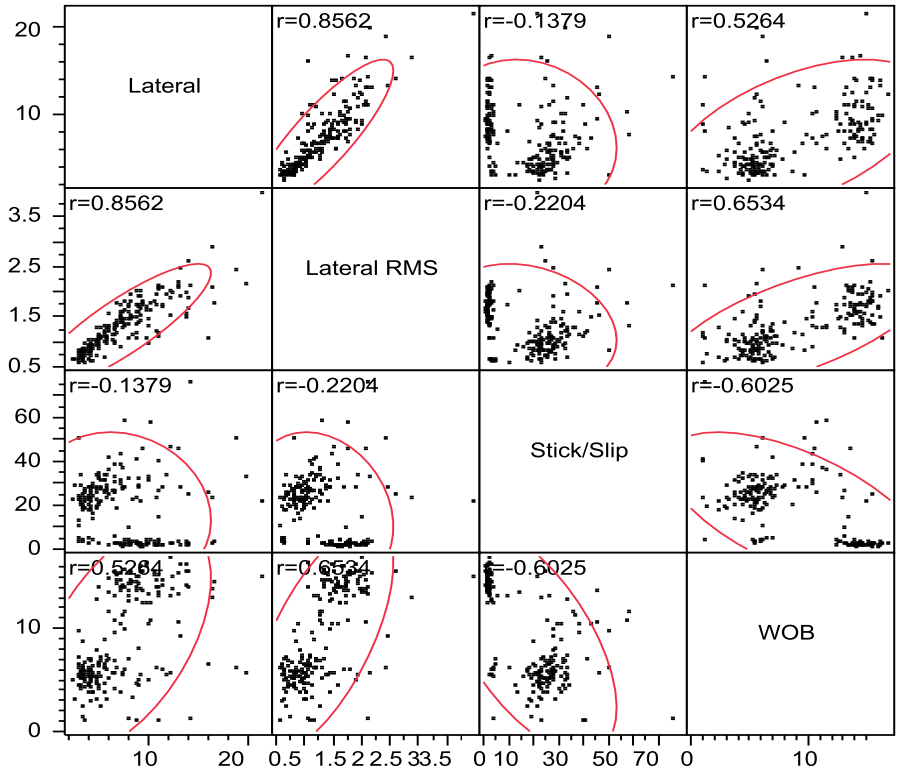

Figure 3.30. Correlation of Drillstring Vibration and WOB for Well C

Figure 3.30 shows that WOB correlates well with stick/slip and lateral RMS vibration. The effect of WOB on the drillstring vibration was modeled as a linear model. The effect of WOB was summarized in Figure 3.31.

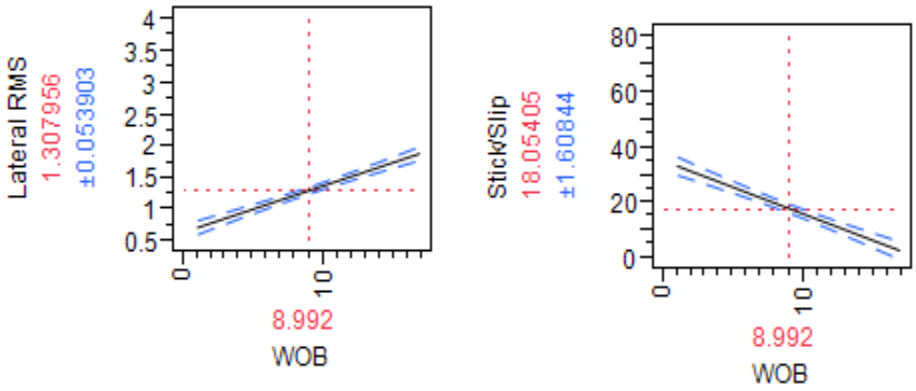

Figure 3.31. Effect of WOB on Lateral RMS and Stick/Slip of Well C

The obtained relationship between WOB and lateral vibration (Figure.3.31) shows that lateral vibration tends to increase with the increase of WOB, however, stick/slip tend to decrease with the increase of WOB.

For Well B, the same procedure was followed to study the effect of WOB on drillstring vibration. Figure.3.32 shows a cross plot that shows the correlation of WOB with drillstring vibrations.

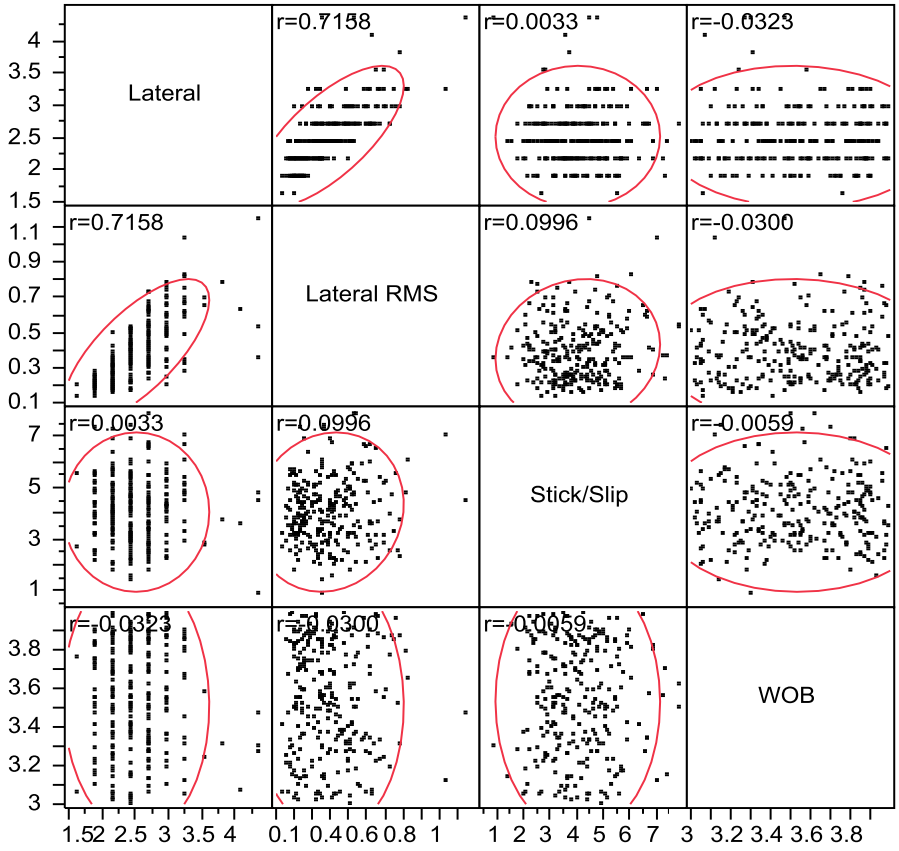

Figure 3.32. Correlation of Drillstring Vibration and WOB for Well B

Figure 3.32 shows that WOB does not correlate well with drillstring vibrations for this well. Same procedure was applied to Well A to study the effect of WOB. The correlation obtained for Well A also did not correlate with drillstring vibration. (Figure.3.33)

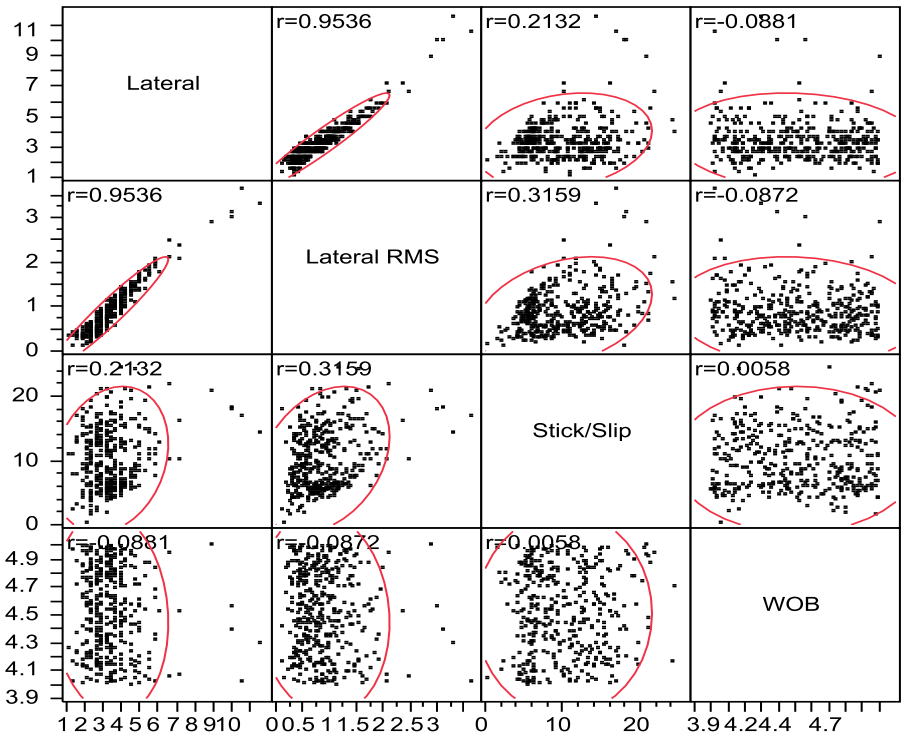

Figure 3.33. Correlation of Drillstring Vibration and WOB for Well A

The study of the effect of stick/slip on lateral vibration was conducted for the three wells. Stick/Slip showed a good correlation with lateral vibration. The effect of stick/slip on lateral vibration for the three wells was modeled as linear model. (Figure 3.34)

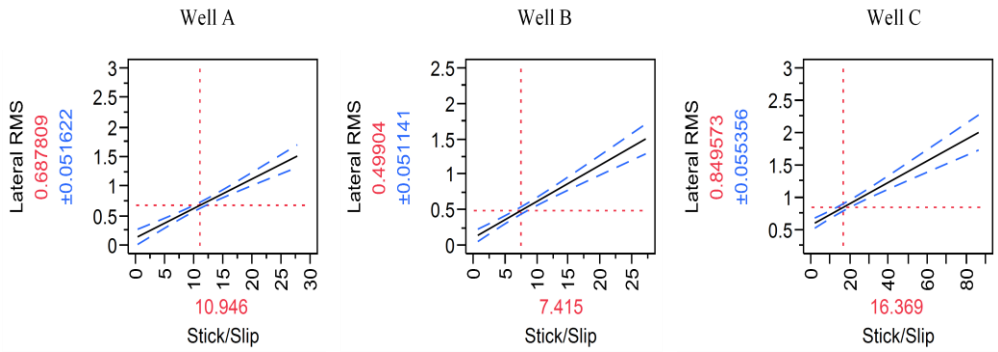

Figure 3.34. Effect of Stick/Slip on Lateral Vibration for the Three Wells

The effect of stick/slip on lateral vibration has the same profile for the three different wells. Lateral vibration tends to increase with the increase of stick/slip.

The comparisons between the V-Stab and AST tool was done statistical. The analysis was done over three different formations. Figure 3.35 shows stick/slip and lateral vibration generated using both reduction tools at the same formation.

Figure 3.36 shows stick/slip and lateral vibration from both tools at common formation. V-stab had lower stick/slip severity and also lower lateral vibration than the AST tool.

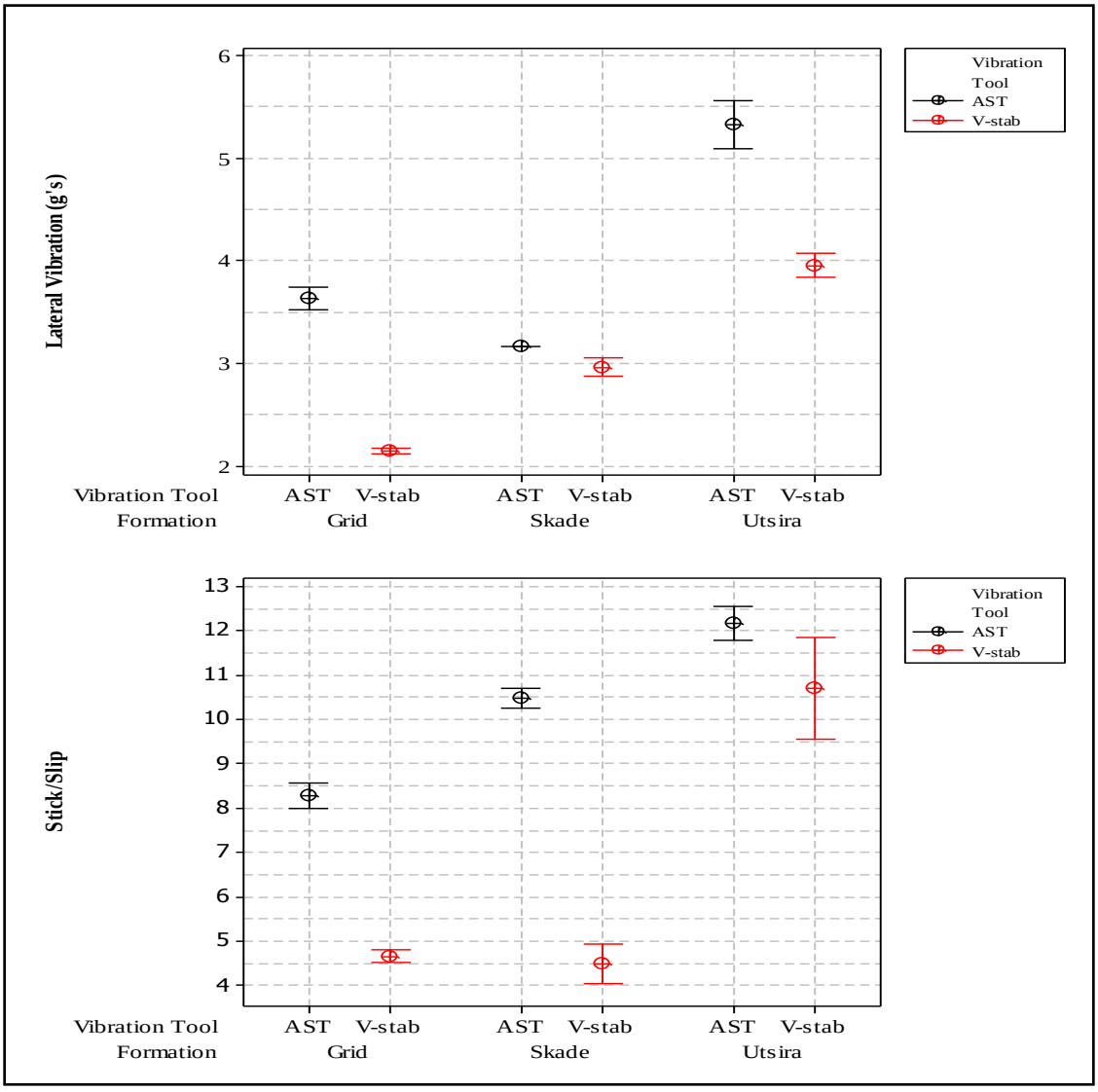

Figure 3.35. Comparison of V-stab and AST Reduction Tools

Stick/Slip severity and lateral vibration generated from roller cone and PDC bit was compared statistically. Figure 3.36 shows stick/slip severity and lateral vibration for the roller cone and the PDC bits.

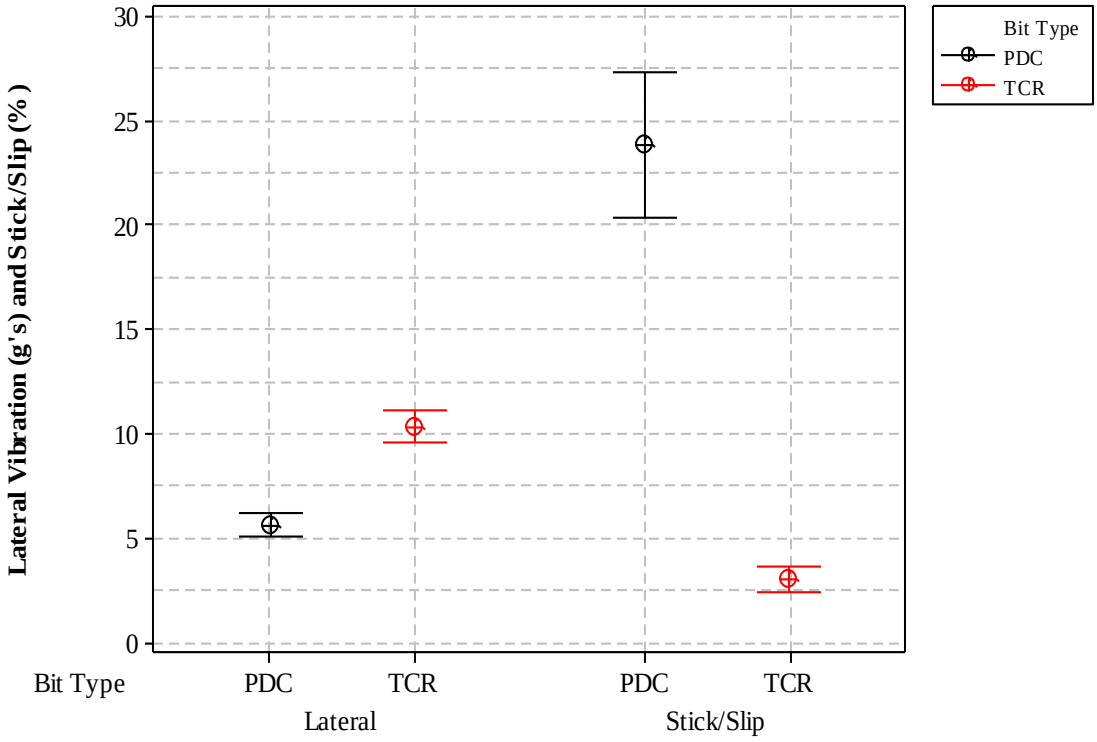

Figure 3.36. Roller cone and PDC Bits Comparison

Figure 3.36 show that roller cone bit has higher lateral vibration than the PDC. However, PDC bit has higher stick/slip than the roller cone bit.

4. DISCUSSION

4.1. FORMATION TOPS VERSUS LATERAL VIBRATION

The statistical analysis of lateral acceleration and formation tops showed that every formation has a specific value and range (Section 3.2). However, lateral acceleration does not increase with depth. Major factors that will cause lateral acceleration to increase were the lithology and drilling parameters.

Lateral vibration analysis of Well A lithology showed that granite basement has the highest levels of lateral vibrations (Figure 3.7). The rock strength within the granite formation is relatively high compare to the other formations, which explain the high vibration level within the granite basement. The lowest levels of lateral vibration were recorded during drilling the shale followed by sand formation. (Figure 3.7)

The calculated UCS for Well A and lateral vibration have approximately the same pattern. Since the graph of the UCS and lateral acceleration was done in log base, the changes between the UCS and lateral acceleration are actually smaller. (Figure 3.1)

For Well C, in most cases, lateral acceleration and the calculated UCS do not have a similar pattern as Well A shows. This is because Well A consisted of an anti vibration tool (AST) where Well C did not have anti vibration tool, which affected the outcome of the comparison. (Figure 3.3)

4.2. VIBRATION REDUCTION TOOLS EVALUATION

The comparison between the three different wells shows that Well B which consists of V-Stab anti-vibration tool has the lowest lateral vibration (Section 3.3). However, at approximately 1500 ft, lateral acceleration started to increase. This increase in lateral acceleration was caused by an increasing the torque without increasing WOB on that section. Even with the increase in the lateral acceleration at that particular section, the overall lateral vibration is still in moderate range which is still lower than the other two wells.

Well A did not face severe lateral vibration levels. Lateral vibration was in moderate range, however the final section (after coring) did encounter some high lateral

vibration. Overall, Well A faced less lateral vibration than well C. The final section started at 1976 m; at that depth a sudden shift in both GR and sonic logs can be noticed. The increase of lateral vibration is caused by change in lithology. (Figure 3.1)

4.3. COMPARING LATERAL VIBRATION OF MATCHING FORMATIONS AND LITHOLOGY

Lateral vibration of Well A and Well B were plotted against their depth. Interestingly, lateral acceleration of both wells have the same pattern in Utsira formation. From the statistical analysis, lateral vibrations from both wells are not the same, but they are close to each other as a value. Since both wells were drilled with different BHA assembly and different vibration reduction tools, the different in lateral vibration was expected. (Section 3.4)

Overall, the lateral vibration generated in Well B has the lowest vibration levels over the entire seven matching formations. The BHA of Well B consisted of V-stab anti vibration tool and Well A BHA consisted of AST anti vibration tool. This test shows the V-stab anti vibration tool minimize lateral acceleration more than the AST tool.

Figure 3.15 shows that drilling into Utsira formation, the highest lateral vibration was recorded both wells (excluding lower section). However, Well B lateral vibration at Utsira formation was lower than Well A. Overall; the lowest lateral vibration was recorded in Well B for all the matching formations. The lowest lateral acceleration recorded in Well A was in the Vaale formation. For Well B, the lowest lateral acceleration was recorded in the Skade formation.

4.4. EVALUATING STICK/SLIP

Well A experienced moderate level of stick/slip during drilling. The BHA of well A consisted of AST anti vibration tool. During drilling the reservoir section of Well A, the stick/slip severity increased to a high level, severity level of stick/slip was recorded for the reservoir section.

Well B experience low level of stick/slip. The BHA of this well consisted of V-stab anti vibration tool. The highest stick/slip severity that Well B reached was high level severity but only for a very small period.

Using roller cone bit on the first bit run of Well C resulted in a very low stick/slip severity. The following two bit runs, PDC bits were used. With Well C not containing a vibration reduction tool, the stick/slip severity for those two sections reached a very high severity level.

Overall, Well B recoded the lowest stick/slip severity using the V-stab. Well A recorded higher stick/slip severity than Well B did. Well C faced the highest stick/slip severity on the last two bit runs over the three wells.

Section 3.3 and 3.4 showed that V-stab and AST vibration reduction tools have a big impact on reducing drillstring vibration with the comparison of not having vibration reduction tool of Well C.

4.5. STATISTICAL ANALYSIS OF SAMPLING RATE

The statistical summary of the three different wells shows that there is no specific distribution of lateral vibration. Lateral vibration is a function of many variables, which makes it very complex; as a result there is no specific distribution of lateral vibration.

Wilcoxon and the nonparametric distribution analysis (survival) tests both showed that there is no different between the original data and the 10^{th} sample of each data. For the three wells, the original data and 10^{th} sample data have approximately the same mean. However, the confident interval for both data is slightly different. (Section 3.6)

The study showed that BlackBox can be used in real time with mud puls and gives the same results.

4.6. MULTI VARIABLES EFFECT ON DRILLSTRING VIBRATION

The effect of RPM, torque, WOB and UCS on lateral vibration for the three wells showed different effect. The different behavior of each parameter is caused by irregularity of the system. Well A drilled into interchangeable formation that made the

UCS values not constant, however, for Well C, one formation was drilled through the whole section which made the UCS constant. For Well B, the UCS and surface RPM were not included in the model, as a result, UCS and RPM effect was not included in the model behavior of Well B. (Section 3.7)

Statistical analysis of MSE on drillstring vibration showed that drillstring vibration did not correlate with MSE. Very low regression value was obtained from the correlation of MSE with lateral and torsional vibration. Which disagrees with the previous claims that drillstring vibration absorbs and reduced drilling efficiency (bit, ROP) (Macpherson et al. 1993).

The effect of WOB on drillstring vibration was analyzed statistical. For Well A and Well B, who's BHA consist of vibration tool reduction, the WOB did not correlate with vibration. However, for Well C, the statistical study showed that with the increase of WOB, stick/slip severity tends to decrease and lateral vibration tends to increase.

Stick/Slip effect on lateral vibration was analyzed, for the three wells. Lateral vibration increases with the increase of stick/slip. (Section 3.7)

Statistical study of stick/slip severity and lateral vibration levels shows that V-stab has lower stick/slip severity and lower lateral vibration.

Statistical analysis of vibration generated from different bit types was analyzed. The study showed that PDC bit has a lower lateral vibration than roller cone bit however; roller cone bit has a lower stick/slip severity than PDC bit. (Section 3.7)

5. CONCLUSIONS

Lateral vibration was analyzed for three different wells. The study of lateral and torsional vibration was performed by considering multiple aspects that was suspected to have an effect on lateral and torsional vibration. The three fields are located in the Norwegian North Sea. The study provided the following conclusions:

Lateral acceleration tends to either increase or decrease with the change of formation. The statistical analysis showed that every formation tends to have a specific range and frequency of lateral vibration. Rock strength (UCS) has a big impact on lateral vibration. Lateral vibration tends to increase with increasing UCS and decrease with the decreasing UCS.

Lateral vibrations generated from two different wells at a matching formation are different. The different in lateral vibration is caused by the different BHA assemblies. Overall, the statistical analysis showed that lateral vibration generated at each formation using V-stab anti-vibration tool are less than the one generated using AST tool.

Statistical study of sampling rate of vibration data measurement showed that the high sampling rate of the device is not required. The statistical analysis revealed that the original data sampling of the measurement device have the same statistical distribution and summary of every 10^{th} of the data sampling. The study shows that there is a possibility of using mud pulse to measure vibration with a smaller sampling rate.

The analysis showed that both of the V-stab and AST vibration reduction tools reduces drillstring vibration. Lateral and torsional vibration was low using the V-Stab vibration reduction tool. The AST tool faced some lateral and torsional vibration. Overall, the V-stab showed better performance on both lateral and torsional vibration than the AST tool did.

Statistical analysis showed that lateral vibration tends to increase with the increase of stick/slip severity.

Torsional vibration is very low using roller cone bit. The severity of torsional vibration increases using PDC bits due to bit geometry. However, lateral vibration using roller cone bit is higher than the one using PDC bit.

Studying the effect of drillstring vibration on MSE showed that drillstring vibration does not have any correlations with MSE. Based on the literature, drillstring vibration absorbs drilling energy and therefore reduces the amount of energy to the bit and make drilling less efficient. However, based on this study, MSE did not have any relationship with drilling efficiency and is not expected to reduce ROP.

APPENDIX A.
MATHEMATICAL DESCRIPTION OF DRILLSTRING VIBRATION

A mathematical representation was developed for the axial vibration behavior; the undamped axial motion $\varepsilon(x,t)$ of a linear elastic bar is a second order partial-differential equation (Dareing 1984; Bradbury and Wilhoit 1963; Craig 1981) which is in the form of

$$\frac{\partial^2 \varepsilon(x,t)}{\partial x^2} = \frac{1}{c^2}\frac{\partial^2 \varepsilon(x,t)}{\partial t^2} \tag{1}$$

This has the general solution of

$$\varepsilon_n(x,t) = \left(C_A \sin\frac{\omega_n}{c}x + C_B \cos\frac{\omega_n}{c}x\right) \times (C_C \sin\omega_n t + C_D \cos\omega_n t),\ n = 1,2,.. \tag{2}$$

Where $C_A, C_B, C_C,$ and C_D are constants, they are determined by applying initial and boundary condition, $\frac{\omega_n}{c}x$ are dimensionless parameters, and finally c is the axial wave velocity $c = \frac{E}{\rho}$ where E is the Young's modulus and ρ is the density of the material.

The equation of motion has been developed for the axial vibrations of drillstring of a cross sectional area of A_s, accounting for damping and subjected to an external forcing function (Sengupta 1993, Bronshtein and Semendyayev 1997, Chin 1994)

$$\rho\frac{\partial^2 \varepsilon}{\partial t^2} + c_a\frac{\partial \varepsilon}{\partial t} - E\frac{\partial^2 \varepsilon}{\partial^2 x^2} + \rho g_z = G_a\left(x, t, \varepsilon, \frac{\partial \varepsilon}{\partial x}, \frac{\partial \varepsilon}{\partial t}\right) \tag{3}$$

Where c_a is a damping factor, g_z is the gravity acceleration, and G_a is the external axial force per unit mass applied in the drillstring.

A bit bounce model is one of the most important phenomena in axial vibration. This model corresponds to the intermittent lift of the drilling assembly off the formation, which mainly relates for roller-cone bits. This is because of the pattern they leave on the rock surface that may generate vibration of the BHA.

In 1995 Spanos presented a model that considers the coupling of axial and torsional vibrations of the BHA submitted to an excitation origination from the rock surface. A quarter-sin radial variation established the continuity of the surface in its center, which is in the form of:

$$L(r,\theta)=\begin{cases}L_0 Sin\left(\frac{r}{\Delta r_b}\frac{\pi}{2}\right)Sin(3\emptyset), 0\le r\le \Delta r_b \; and \;\; 0\le \emptyset \le 2\pi \\ L_0 Sin(3\emptyset), \Delta r_b \le r \le r_b\end{cases} \quad (4)$$

Where r_b is the radius of the borehole, Δr_b is a smaller radius than r_b , and r and $\emptyset$ are the radial and angular coordinates respectively.

During the condition of liftoff, the bit moves in contact with the formation at a certain time. Its axial displacement after the timestep can be calculated from the governing equation of motion (Equation 4) by setting the excitation equal to zero. If the displacement is greater than the corresponding value of the profile elevation, then the drill bit is no longer in contact with the formation.

For torsional vibration, a continuous torsional vibration model is described by the following differential equation:

$$\rho J\frac{\partial^2 \emptyset}{\partial t^2}-JG\frac{\partial^2 \emptyset}{\partial x^2}=G_T(x,\emptyset,t) \quad (5)$$

Where J is the polar moment of inertia of the cross sectional area, $\emptyset$ is the angular displacement, G is the shear modulus of the drilling assembly, and $G_T(x,\emptyset,t)$ is the torsional applied load. Also from equation 5 we notice that the product of JG is the torsional stiffness of the system.

An analytic modeling approach for the stick/slip phenomenon was developed by Dawson et al. (1987). This approach used a single degree of freedom representation of the drillstring in which a massless torsional spring of stiffness k models the entire length of the drilling assembly. The rotary table drives the system at the surface at a constant speed Ω, which makes the equation of motion on the form of:

$$I\ddot{L_\emptyset}+C_r\dot{L_\emptyset}+F\left(\dot{L_\emptyset}\right)+kL_\emptyset=k\Omega t \quad (6)$$

Where $L_\emptyset$ the angular displacement of the BHA, Cr is is the coefficient of viscous damping, k is the torsional stiffness of the drillstring, I is the mass moment of inertia with respect to the rotation axis, and $F(\dot{\emptyset})$ is the friction induced forces.

Furthermore, by normalizing equation 6 by the moment of inertia and getting the following equation:

$$\ddot{\phi} + 2\xi\omega_0\dot{\phi} + f(\dot{\phi}) + \omega_0^2\Omega t \tag{7}$$

Where

$$\omega_0 = \sqrt{\frac{k}{I}} \text{ and } \xi = \frac{c_r}{2\sqrt{KI}} \tag{8}$$

And $f(\dot{\phi})$ is in the form of

$$f(\dot{\phi}) = \begin{cases} F_s - \dfrac{F_s - F_{ss}}{V_0}\dot{\phi}, & 0 \le \dot{\phi} < V_0 \\ F_{ss}, & V_0 \le \dot{\phi} \end{cases} \tag{9}$$

The parameters F_s, F_{ss}, and V_0 in the above equation depend on the physical characteristic of the drilling assembly. Furthermore, this simple system considers the reduction of the friction when the system switches from a static to a kinetic state.

A mathematical expiration was developed for the continuous lateral vibration model. The Euler-Bernoulli beam theory is considered, and the small slopes assumption is adopted. The Euler-Bernoulli equation is:

$$\rho\frac{\partial^2 u}{\partial t^2} + \frac{\partial^2}{\partial x^2}\left(EI_z\frac{\partial^2 u}{\partial x^2}\right) = g(x,t) \tag{10}$$

Where u(x,t) is the lateral displacement, ρ is the mass density, E is the modulus of elasticity, and I_z is the relevant moment of inertia of the cross section of the beam, and finally, g(x,t) is the external loading.

However, if taking the axial force into the consideration the equation becomes:

$$\rho \frac{\partial^2 u}{\partial t^2} + \frac{\partial^2}{\partial x^2}\left(EI_z \frac{\partial^2 u}{\partial x^2}\right) - F_P \frac{\partial^2 u}{\partial x^2} = g(x,t) \tag{11}$$

Where F_P is donated by the axial force.

The most important phenomena in lateral vibrations is whirling, a lot of studies have approached this phenomena in a 2D, single lumped mass representation of the assembly (Vandiver et al 1990; Kotsonis 1994; Jansen 1992). The equation of motion at equal distance between two stabilizers with a constant rotary speed (Lee 1993) is

$$m\ddot{y} + C_w \dot{L_y} + k_w L_y = m\, e_0\, \Omega^2 \cos(\Omega t) \tag{12}$$

$$m\ddot{z} + C_w \dot{L_Z} + k_w L_Z = m\, e_0\, \Omega^2 \cos(\Omega t) \tag{13}$$

Where L_y and L_Z are the lateral coordinates, m is the equivalent mass of the collar, C_w is the damping coefficient, k_w is the equivalent lateral stiffness of the collar, e_0 is the eccentricity of the center of mass, and Ω is the rotational speed of the assembly.

APPENDIX B.

DESCRIPTION OF BOTTOM HOLE ASSEMBLIE

Table B.1 BHA of the 12 1/4" Section of Well A

Equipment	Length (m)	Comment
SWDP	55.9	
Sub	1.23	Black Box
HWDP	55.88	
Sub	1.23	Drift Sub
X-Over	1.1	
8.25in Drill Collars	9.2	
Jar	9.89	
8.25in Drill Collars	36.2	
Anti- Stall Tool	2.35	Vibration Reduction Tool
Float Sub	1.12	
Sub	2.4	Screen Sub
Roller Reamer	2.11	
Sub	1.2	Black Box
BAT Sonic	11.65	
LWD Tools	4.72	
DGR-EWD-PWD-XHCIM	16.86	
Pin Pin Sub	0.57	
Sub	0.31	Black Box
Stab	0.4	
Bit	0.44	PDC Bit with 9-7/8" Pilot nose

Table B.2. BHA of the 8 1/2" Section before Coring of Well A

Equipment	Length (m)	Comment
5in HWDP	55.94	
Sub	1.23	Black Box
5in HWDP	55.88	
Dart Sub	0.6	
6.5in DC	8.96	
Jar	9.56	
6.5in DC	36.2	
Stab	1.86	
Anti-Stall Tool	3.96	Vibration Reduction Tool
Float Sub	0.53	Black Box
Filter Sub	1.75	
Roller Reamer	1.91	
Sub	1.22	
HOC	4.73	
BAT Sonic	6.17	
ILS	0.59	
RLL Nuke String	9.33	
Ils	1.22	
Rll	8.42	
X/O	0.82	
Sub	0.3	Black Box
Bit	0.32	PDC Bit

Table B.3. BHA of the 8 1/2" Section after Coring of Well A

Equipment	Length (m)	Comment
Sub	1.23	Black Box
5in HWDP	55.88	
Dart Sub	0.6	
6.5in DC	8.96	
Jar	9.56	
6.5in DC	36.2	
Stab	1.86	
Anti-Stall Tool	3.96	Vibration Reduction Tool
Float Sub	0.53	Black Box
Filter Sub	1.75	
Roller Reamer	1.91	
Sub	1.22	
HOC	4.73	
BAT Snonic	6.17	
ILS	0.59	
RLL Nuke String	9.33	
ILS	1.22	
RLL	8.42	
X/O	0.82	
Sub	0.3	Black Box
Bit	0.46	6.75" Pilot, 8.5" Reamer

Table B.4. BHA Components of the 12 1/4" Section of Well B

Equipment	Length (m)	Comment
5" X 4.276" - 19.5# 6-5/8" X 2-3/4" NC 50 (XH)	1500	
5" X 3" HWDP # 49.3-NC50(IF)	55.94	
Black Box Sub	1.22	Black Box
5" X 3" HWDP # 49.3-NC50(IF)	55.88	
X-Over Sub	1.09	
8" X Drill Collar	9.44	
Ulti Torq	9.7	
8 1/2" Drill Collar	36.86	
V-Stabilizer	1.83	Vibration Reduction Tool
8 1/2" Drill Collar	73.79	
Float Sub	0.91	
Screen Sub	2.42	
3-Point Roller Reamer	2.7	
Black Box Sub	0.3	Black Box
8" P4M HOC	4.62	
8" Bat Collar	6.82	
8" CTN Comp Therm Neutron	4.72	
12" ALD Collar	4.97	
8" AC Conversion Sub	1.77	
12 13/16 ILS	1.22	
8" HCIM Collar	1.55	
8" PWD	1.27	
8" EWR-P4 Collar	3.71	
8" DGR Collar	1.53	
P-P-X-Over Sub	0.49	
12-1/4" NR400S w/BB	0.4	Black Box
0-7/8" x 12-1/4" PDC	0.43	PDC Bit

Table B.5. BHA Component of the 8 1/2" Section 1st Bit Run of Well B

Equipment	Length (m)	Comment
5" X 4.276" - 19.5# 6-5/8" X 3- 1/2" S-135	9.7	
6 X 5" HWDP # 49.3- NC50(IF)	55.94	
BlackBox Sub	1.22	Black Box
6 X 5" HWDP # 49.3- NC50(IF)	55.88	
Drift Sub	0.6	
1 X 6 1/2" X Drill Collar	9.13	
Jar	9.58	
4 X 6 1/2" Drill Collar	36.97	
Float Sub-non Ported	0.81	
Screen Sub	2.34	
3-Point Reamer	1.69	
BlackBox Sub	1.12	Black Box
6 3/4" P4M HOC/Directional	4.75	
6 3/4" QBAT Collar	6.16	
8.405"ILS	0.56	
6 3/4" ALD/CTN Collar	9.18	
8.405" ILS	1.18	
6 3/4" RLL, DGR-EWR-PWD	8.93	
P-B X-Over Sub	0.9	
BlackBox Sub	0.31	Black Box
8 1/2" PDC	0.46	PDC Bit

Table B.6. BHA Components of the 8 1/2" Section 2nd Bit Run of Well B

Equipment	Length (m)	Comment
5" X 4.276" - 19.5# 6-5/8" X 3- 1/2" S-135	9.7	
6 X 5" HWDP # 49.3- NC50(IF)	55.94	
BlackBox Sub	1.22	Black Box
6 X 5" HWDP # 49.3- NC50(IF)	55.88	
Drift Sub	0.6	
1 X 6 1/2" X Drill Collar	9.13	
Jar	9.58	
4 X 6 1/2" Drill Collar	36.97	
Float Sub-non Ported	0.81	
Screen Sub	2.34	
3-Point Reamer	1.69	
BlackBox Sub	1.12	Black Box
6 3/4" P4M HOC/Directional	4.75	
6 3/4" QBAT Collar	6.16	
8.405"ILS	0.56	
6 3/4" ALD/CTN Collar	9.18	
8.405" ILS	1.18	
6 3/4" RLL, DGR-EWR-PWD	8.93	
P-B X-Over Sub	0.9	
BlackBox Sub	0.31	Black Box
8 1/2" PDC	0.46	PDC Bit

Table B.7. BHA of the 12 ¼” Section Bit Run of Well C

Equipment	Length (m)	Comment
Drill pipe	1924.4	
Heavy Weight Drill Pipe	120.37	
Drill Collar	9.43	
Mechnical Jar	10.26	
Drill Collar	84.52	
Shock Sub	1.22	BlackBox
Non-Mag Drill Collar	18.38	
Logging While Drilling	6.56	
Logging While Drilling	7.18	
Logging While Drilling	0.66	
MWD Tool	7.43	
Logging While Drilling	0.55	
Logging While Drilling	5.72	
Corss Over	0.41	
Integral Blade Stabilizer	2.36	
Bit Sub	0.3	BlackBox
Tri-Cone Bit	0.25	8 1/2" Insert Bit

Table B.8. BHA of the 8 1/2" Section 1nd Bit Run of Well C

Equipment	Length (m)	Comment
Drill Pipe	2108.83	
Heavy Weight Drill Pipe	37.07	
Drill Collar	28.12	
Mechanical jar	10.26	
Drill Collar	28.19	
Shock Sub	1.22	BlackBox
Non-Mag Drill Collar	18.38	
Non-Mag Integral Blabe Stabilizer	2.22	
Cross Over	0.61	
MWD	7.43	
Logging While Drilling	0.55	
Logging While Drilling	5.72	
Cross Over	0.41	
Near Bit Stabilizer	2.36	
Bit Sub	0.3	BlackBox
Polycrystalline Diamond Bit	0.33	8 1/2 PDC Bit

Table B.9. BHA of the 8 1/2" Section 2rd Bit Run of Well C

Equipment	Length (m)	Comment
Drill Pipe	2159.9	
Heavy Weight Drill Pipe	37.07	
Drill Collar	28.12	
Mechanical Jar	10.26	
Drill Collar	28.19	
Shock Sub	1.22	BlackBox
Non-Mag Drill Collar	18.38	
Non-Mag Integral Blabe stabilizer	2.22	
Cross Over	0.61	
MWD	7.43	
Logging While Drilling	0.55	
Logging While Drilling	5.72	
Cross Over	0.41	
Near Bit Stabilizer	2.37	
Bit Sub	0.31	BlackBox w.2 shock sensors
Polycrystalline Diamond Bit	0.24	8 1/2 PDC Bit

APPENDIX C.

LITHOLOGY DESCRIPTION OF WELL A, B AND C

Table C.1 Description of Well A Lithology

Group	Formation	Lithology description	MD (MSL)	TVD (MSL)
Nordland	Undif. Nordland	Mainly clays with some thin water bearing sand intervals	136	136
	Utsira	Massive sandstone with minor siltstone and claystone intervals. The top is characterized by a sharp drop in the Gamma ray and resistivity readings	773.5	773.5
Hordaland	Undif. Hordaland	Interbedded claystones and siltstones with occasional minor sandstones. The top is characterized by a sharp increase in gamma ray, resistivity values together with a decrease in sonic transit time	869.5	869.5
	Skade	Predominantly sandstones with interbedded claystones of variable thickness. The top is defined by a sudden drop in gamma ray . The neutron density logs indicate high porosity. The sandstone is water filled	994	994
	Undif. Hordaland	The intra hordland group between the skade and the grid formation. Predominantly claystone with occasional limestone stringers and occasionally thinly interbedded with sandstones. The top is marked by a rapid increase in Gamma ray.	1188.5	1188.5
	Grid	Sandstone. The top is marked by a sudden drop in the gamma ray and a decrease in sonic transit time. The density neutron log show excellent porosity. The formation is water bearing	1499.5	1474.5
	Grid Sst Mbr	Sandstone	1552.5	1552.5
	Undif. Hordaland	Lowermoat part of the hordaland group. Claystones and scattered limestone stringers	1641.5	1641.5
Rogaland	Balder	Interbedded claystones and Tuffs. The claystones of the balder formation have relatively high gamma ray values than the claystones of the hordaland group	1767.5	1767.4
	Sele	The transition to the Sele formation is marked by a sudden increase in the gamma ray values and the corresponding decrease in the resisitivity values. It consists of claystones.	1778.5	1778.4
	Lista	The transition from Sele to Lista is picked by a slight decrease in the gamma ray and decrease in the sonic interval transit time and also a slight increase in the resistivity values. Consists of claystones with rare Limestone and dolomite stringers.	1800	1799.9
	Vaale	Sudden drop in gamma ray and sonic interval transit time with an increase in the resistivity and density values. Consists of Marl.	1881	1880.9
Shetland	Ekofisk	Drop in gamma ray and resistivity values and sonic interval transit time. Consists of limestone with occasional chert layers.	1892	1891.9

		Limestone	1915	1915
		Limestone and Marl	1918	1918
		Intrelaminated claystone and sandstone	1920	1920
Reservoir		Sandstone	1920.8	1920.8
		Granite wash	1923	1923
Basement		Granitic Fractured basement	1946	1946
TD	Undifind		2150	2149.9

Table C.2 Description of Well B Lithology

Group	**Formation**	**Lithology description**	**MD (m) (MSL)**	**TVD (m) (MSL)**
Nordland	Undif. Nordland	Mainly clays with some thin water bearing sand intervals	142	142
	Utsira	Massive sandstone with minor siltstone and claystone intervals. The top is characterized by a sharp drop in the Gamma ray and resistivity readings	800	799.9
Hordaland	Undif. Hordaland	The transition from Utsira sands to Hordaland clays is marked by a sharp increase in the gamma ray and resistivity values	877	876.9
	Skade	Predominantly sandstones with interbedded claystones of variable thickness. The top is defined by a sudden drop in gamma ray . The neutron density logs indicate high porosity. The sandstone is water filled	940	939.9
	Undif. Hordaland	The intra hordland group between the skade and the grid formation. Predominantly claystone with occasional limestone stringers and occasionally thinly interbedded with sandstones. The top is marked by a rapid increase in Gamma ray.	1007	1006.9
	Grid	Sandstone. The top is marked by a sudden drop in the gamma ray and a decrease in sonic transit time. The density neutron log show excellent porosity. The formation is water bearing	1276	1275.9
Rogaland	Balder	Interbedded claystones and Tuffs. The claystones of the balder formation have relatively high gamma ray values than the claystones of the hordaland group	1350	1349.9
	Sele	The transition to the Sele formation is marked by a sudden increase in the gamma ray values and the corresponding decrease in the resisitivity values. It consists of claystones.	1387.5	1387.4
	Lista	The transition from Sele to Lista is picked by a slight decrease in the gamma ray and decrease in the sonic interval transit time and also a slight increase in the resistivity values. Consists of claystones with rare Limestone and dolomite stringers.	1395.5	1395.4
	Vale	Sudden drop in gamma ray and sonic interval transit time with an increase in the resistivity and density values. Consists of Marl.	1465	1464.9
Shetland		Limestone, Marl and claystone	1485	1484.9

Cromer Knoll	Asgard formation	consists of Marl and limestones	1780	1779.8
Viking	Draupne shale unit	Claystone. Medium grey to medium dark grey and ocassionally olive black	1915	1914.9
	Draupne sand unit	Sandstone. None to very loosely cemented. Grains were mainly medium sized qaurtz. Clear, also greyish , smoky, occasionally with pinkish tint	1927	1926.8
Basement		Granite wash, weathered or fractured granitic material	1941	1940.8
TD			2020	2019.8

Table C.3 Description of Well C Lithology

Group	**Formation**	**Lithology description**	**MD (m) (MSL)**	**TVD (m) (MSL)**
Nordland	Undif. Nordland	Mainly clays with some thin water bearing sand intervals	135	135
	Utsira	Massive sandstone with minor siltstone and claystone intervals. The top is characterized by a sharp drop in the Gamma ray and resistivity readings	766	766
Hordaland	Undif. Hordaland	Interbedded claystones and siltstones with occasional minor sandstones. The top is characterized by a sharp increase in gamma ray, resistivity values together with a decrease in sonic transit time	878	878
	Skade	Predominantly sandstones with interbedded claystones of variable thickness. The top is defined by a sudden drop in gamma ray . The neutron density logs indicate high porosity. The sandstone is water filled	952	952
	Undif. Hordaland	The intra hordland group between the skade and the grid formation. Predominantly claystone with occasional limestone stringers and occasionally thinly interbedded with sandstones. The top is marked by a rapid increase in Gamma ray.	1129	1129
	Grid	Sandstone. The top is marked by a sudden drop in the gamma ray and a decrease in sonic transit time. The density neutron log show excellent porosity. The formation is water bearing	1467	1465.3
	Undif. Hordaland	Lowermost part of the hordaland group. Claystones and scattered limestone stringers	1627	1625.1
Rogaland	Balder	Interbedded claystones and Tuffs. The claystones of the balder formation have relatively high gamma ray values than the claystones of the hordaland group	1764	1762
	Sele	The transition to the Sele formation is marked by a sudden increase in the gamma ray values and the corresponding decrease in the resisitivity values. It consists of claystones.	1771	1769
	Lista	The transition from Sele to Lista is picked by a slight decrease in the gamma ray and decrease in the sonic interval transit time and also a slight increase in the resistivity values. Consists of claystones with rare Limestone and dolomite stringers.	1787	1785

	Vale	Sudden drop in gamma ray and sonic interval transit time with an increase in the resistivity and density values. Consists of Marl.	1877	1875
Shetland	Ekofisk	Drop in gamma ray and resistivity values and sonic interval transit time. Consists of limestone with occasional chert layers.	1888	1886
	Hod formation	ChalkyLimestone	1917	1915
Cromer Knoll	Asgard formation	Upper Asgard is composed of Marl	1917.75	1915.7
	Asgard sand unit	Thin layer of medium to coarse grained sandstone. Identified from biostratigraphic analysis of the cores	1918.1	1916.1
Viking	Draupne sand unit	The sandstones are conglomeratic containing abundant granitic rock fragments	1919.46	1917.4
	Und. Jurassic/Triassic	Cross bedded sandstone sequence of intermediate age. The transition from the Viking group is marked by the decrease in GR and increase in ITT.	1920.25	1918.2
Hegre	Und. Hegre	Conglomerate - sandstone, rounded granitic pebbles and mudstones	1959.8	1957.8
TD			2303	2300.9

APPENDIX D.

LATERAL VIBRATION OF MATCHING LITHOLOGY

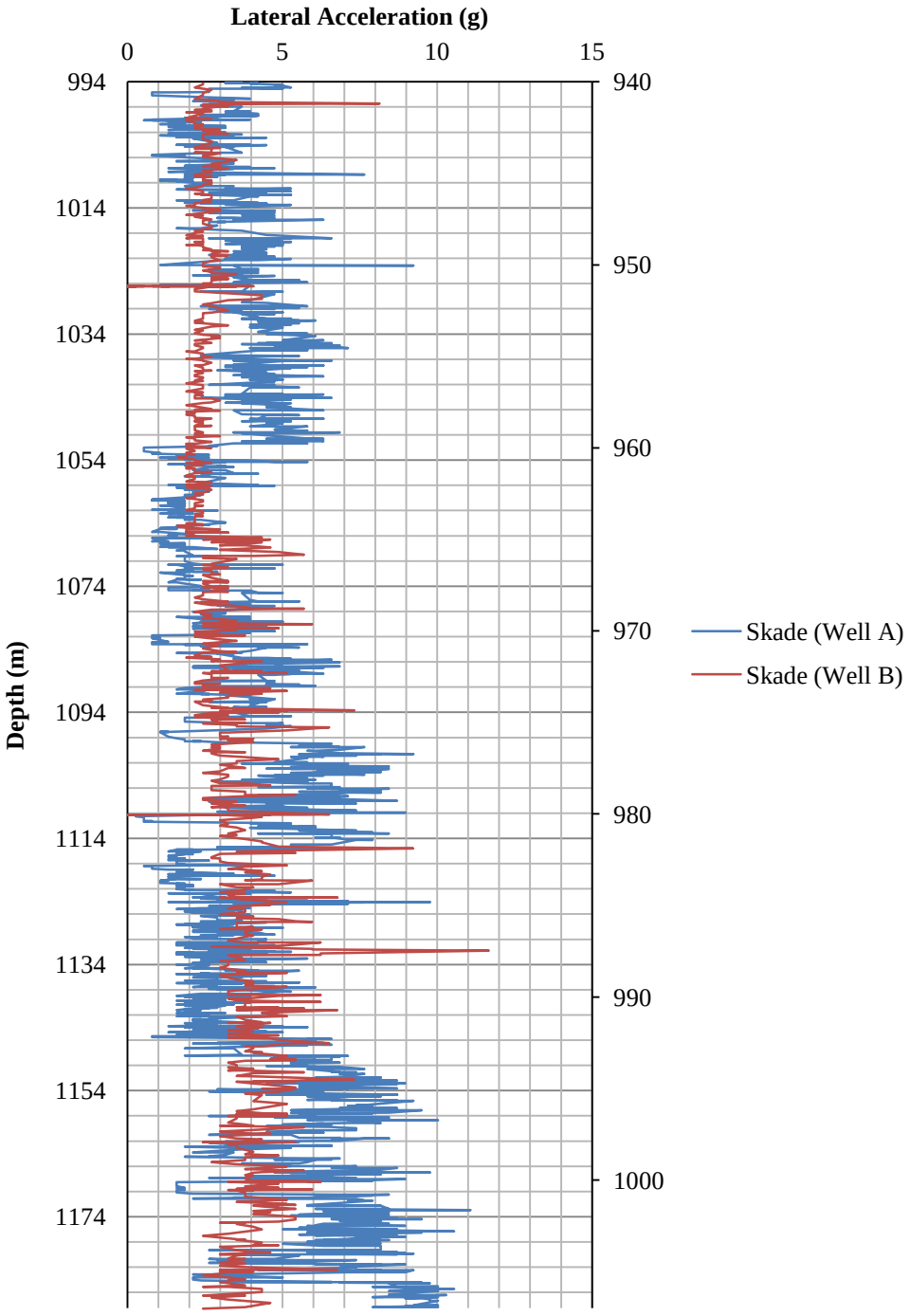

Figure D.1. Lateral Acceleration of Skade Formation

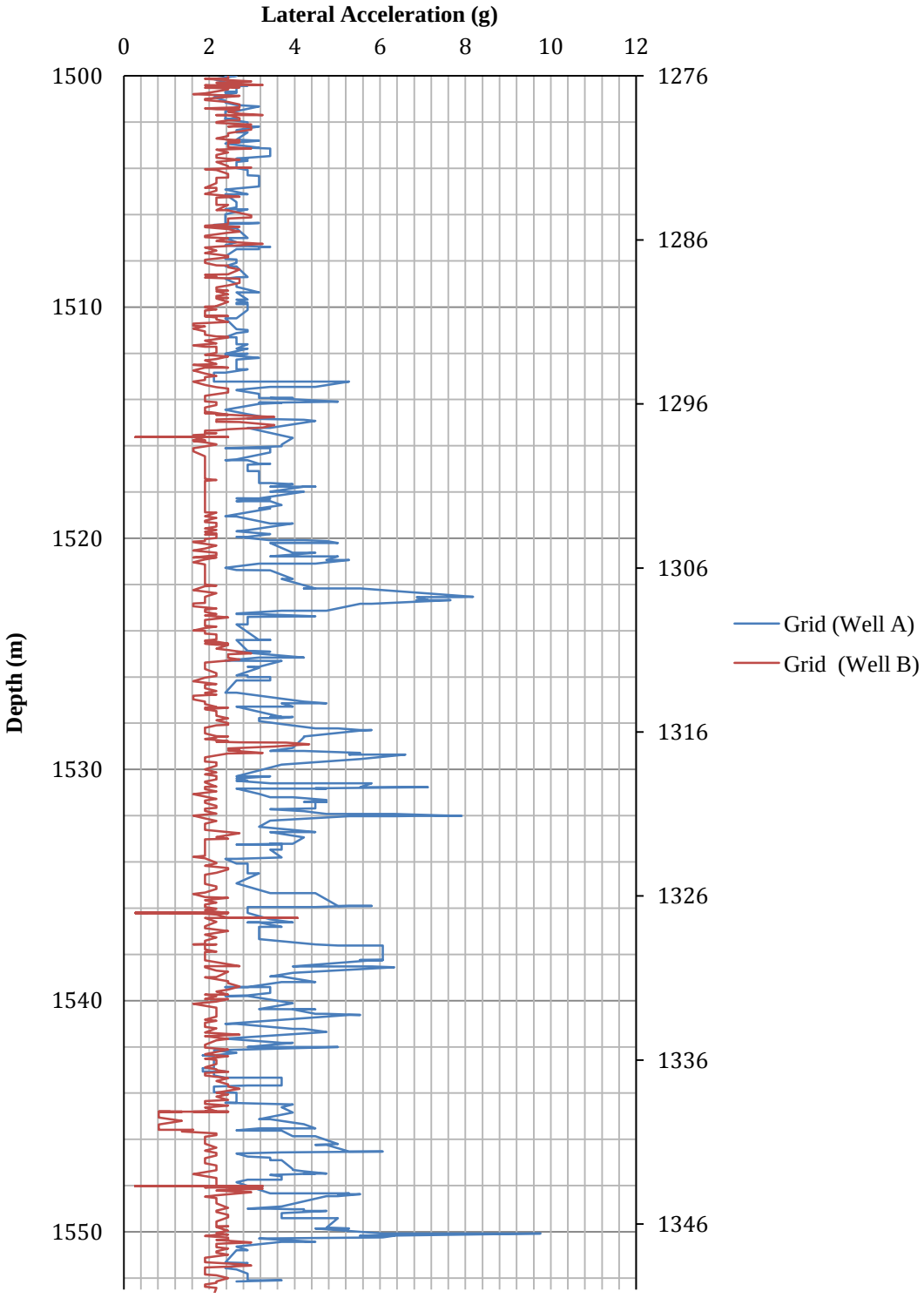

Figure D.2. Lateral Acceleration of Grid Formation

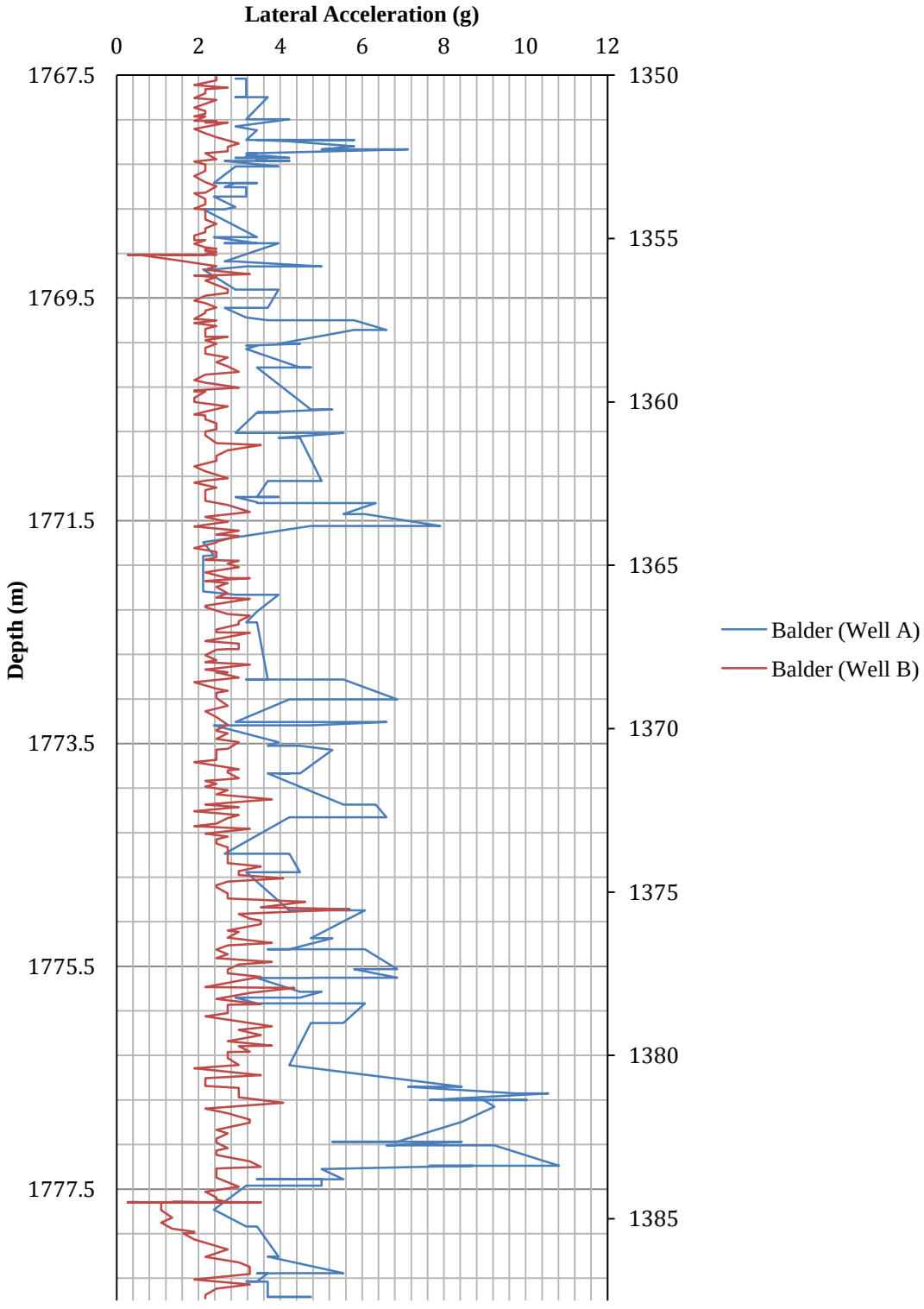

Figure D.3. Lateral Acceleration of Balder Formation

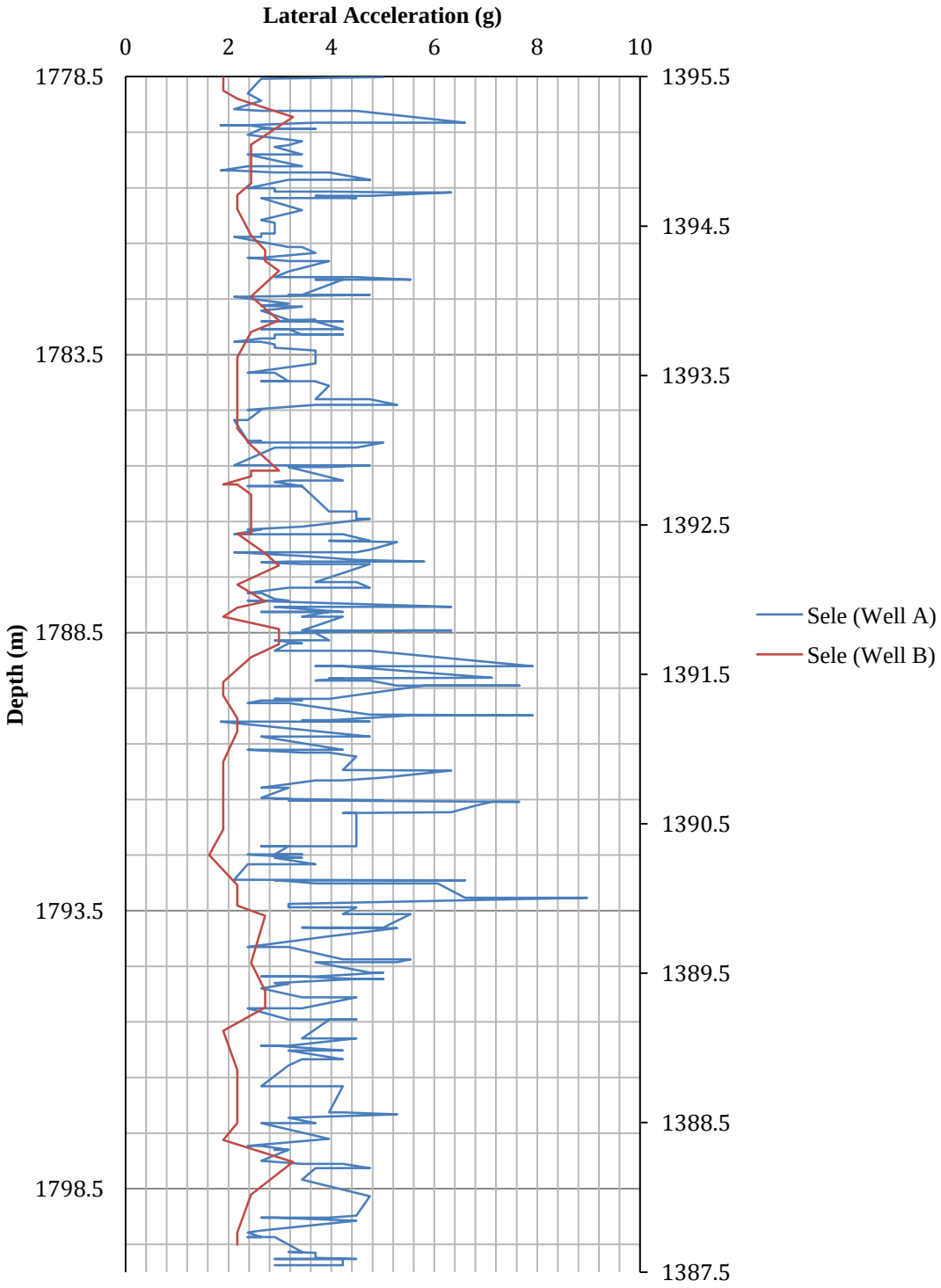

Figure D.4. Lateral Acceleration of Sele Formation

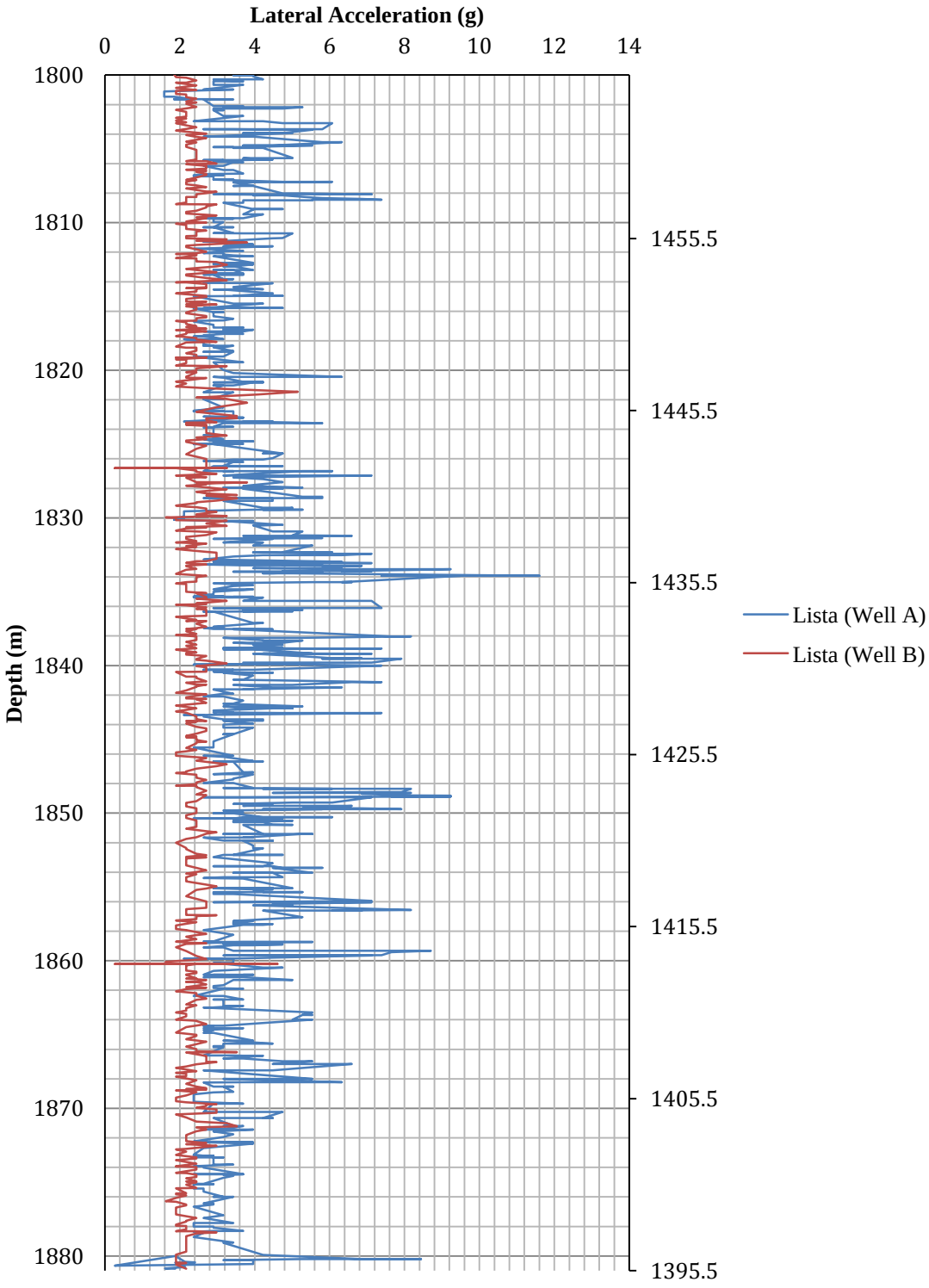

Figure D.5. Lateral Acceleration of Lista Formation

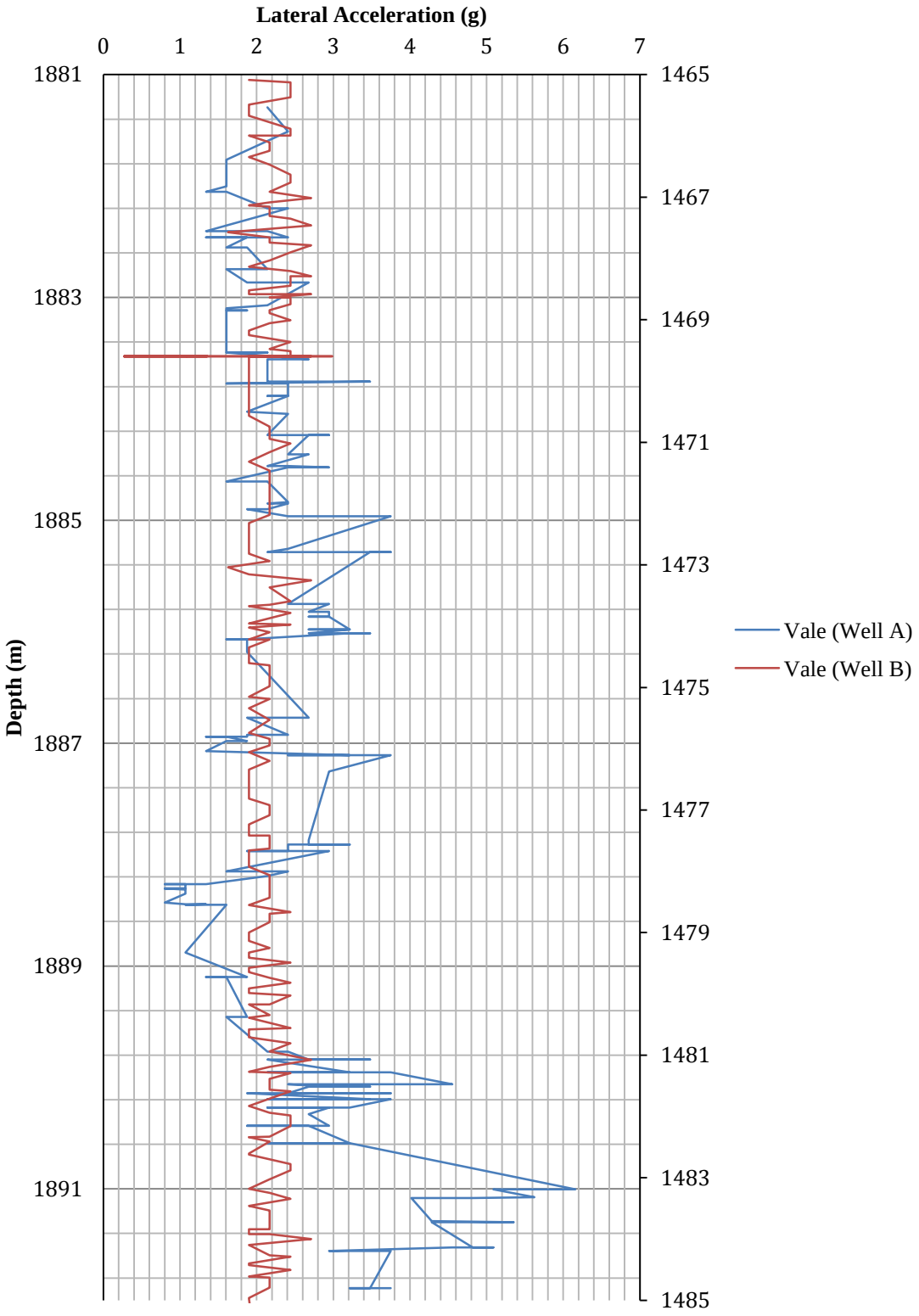

Figure D.6. Lateral Acceleration of Vaale Formation

APPENDIX E.

STATISTICAL ANALYSIS OF MATCHING LITHOLOGY

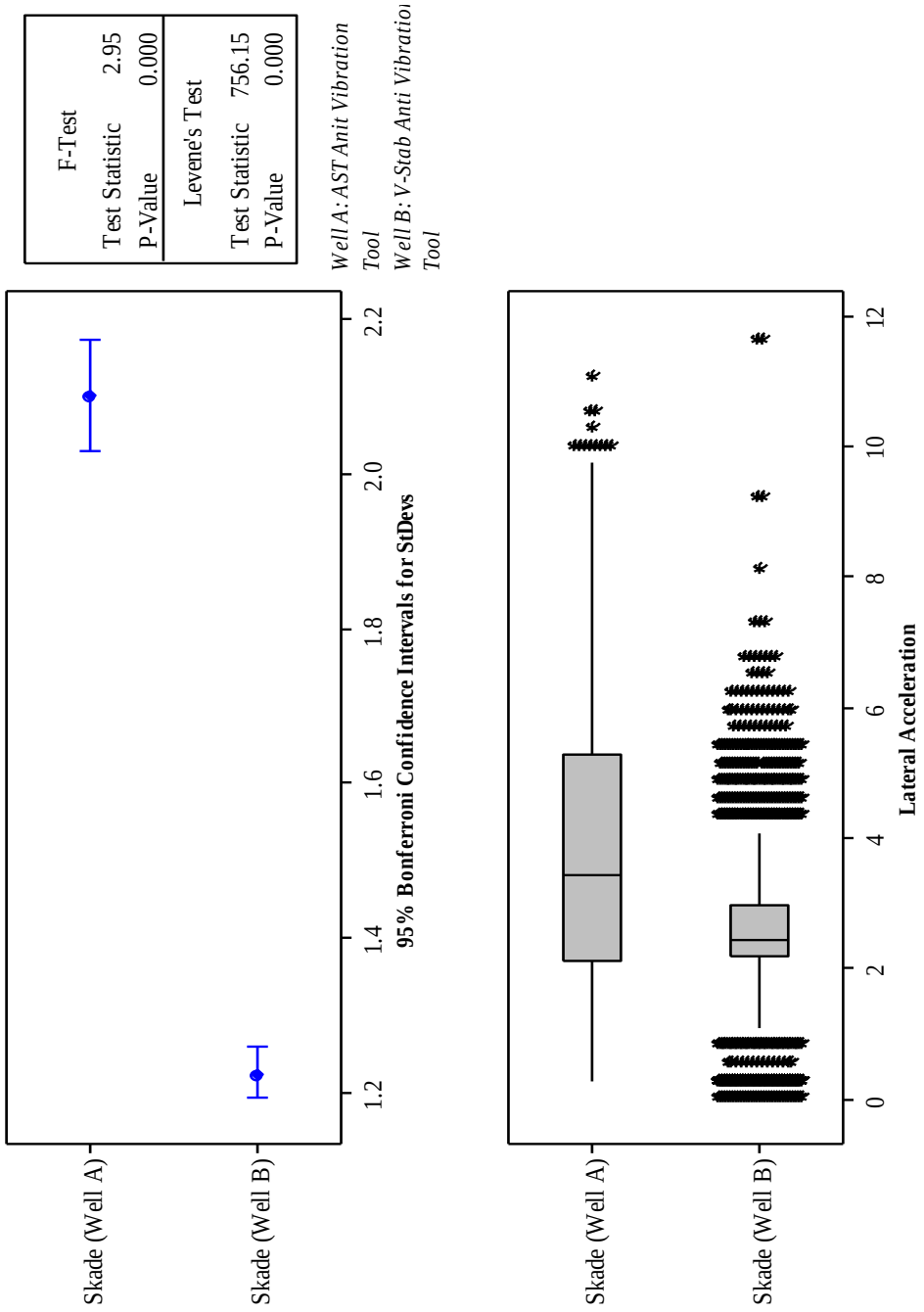

Figure E.1. Statistical Analysis of Skade Formation

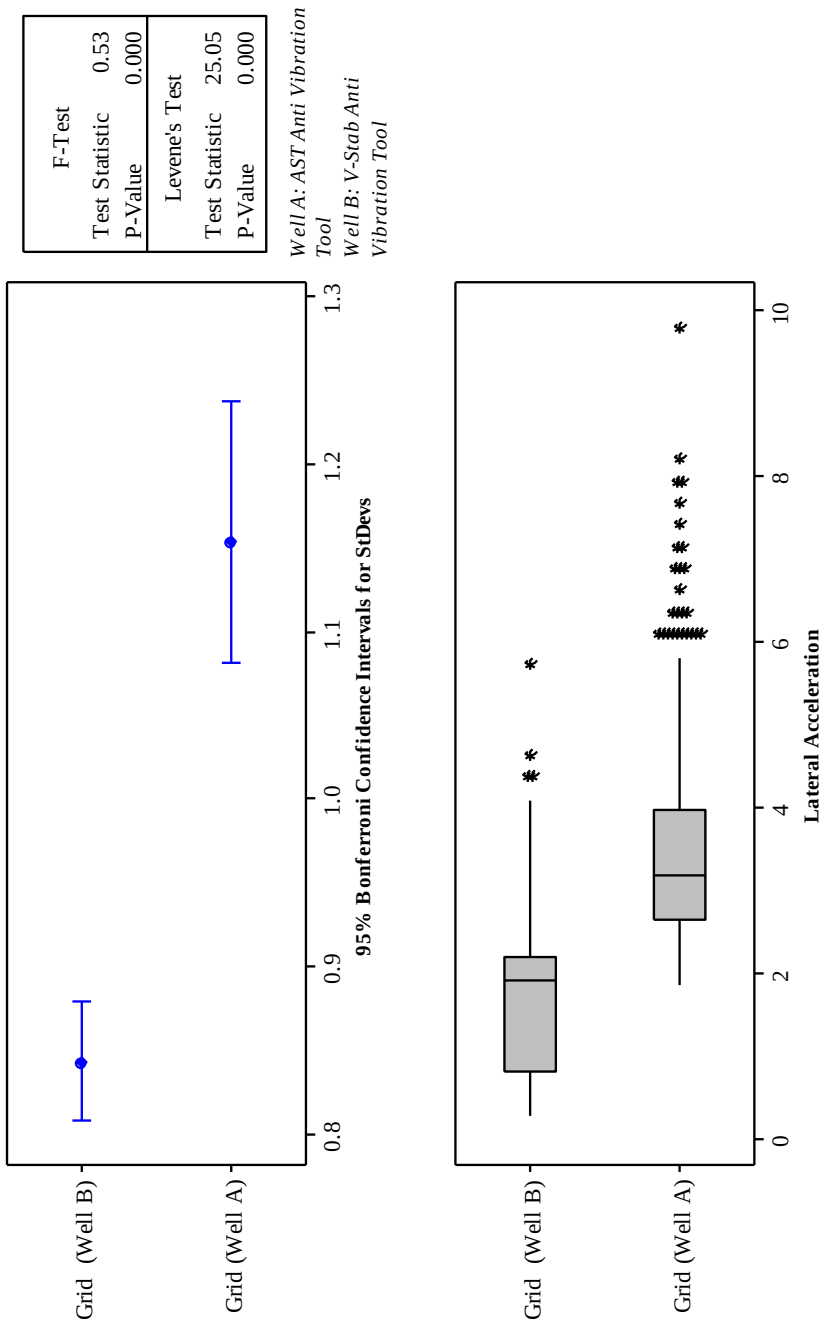

Figure E.2. Statistical Analysis of Grid Formation

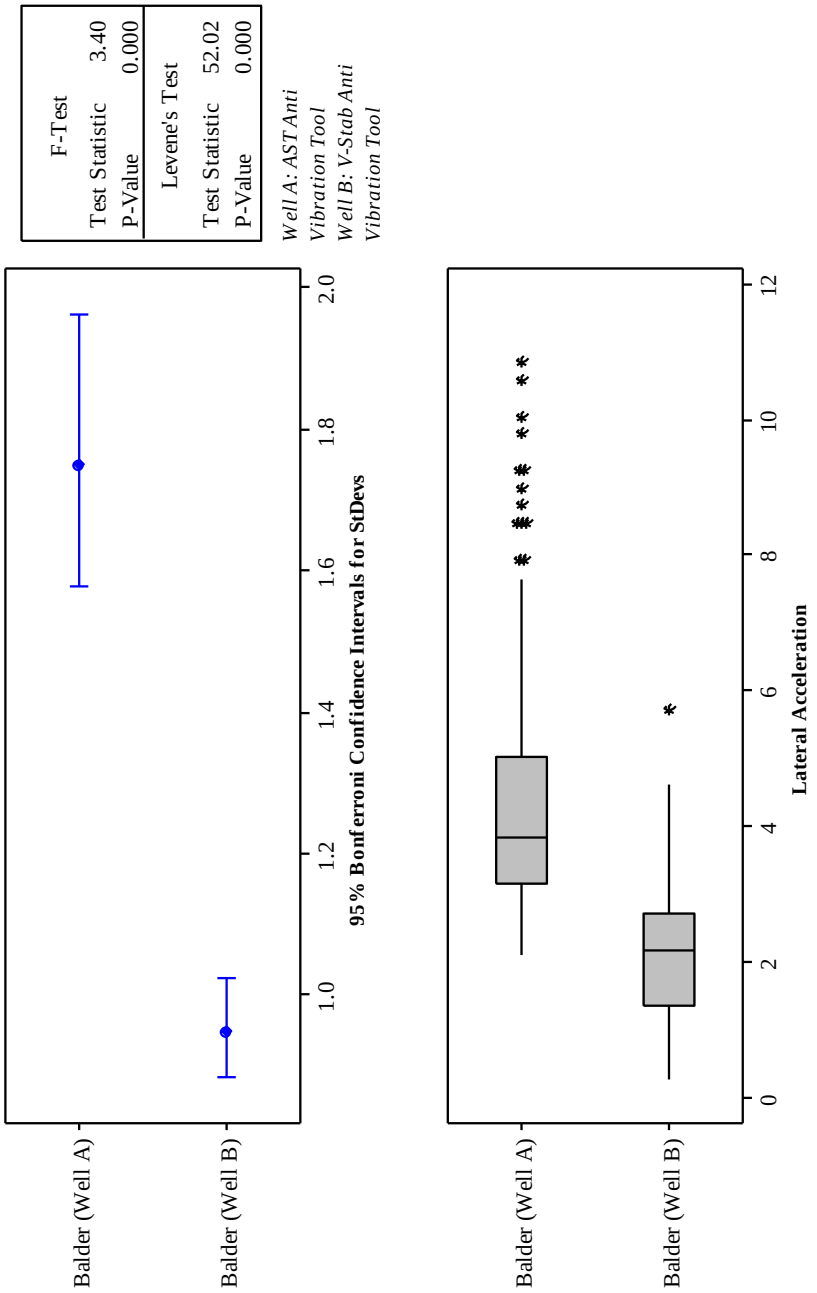

Figure E.3. Statistical Analysis of Balder Formation

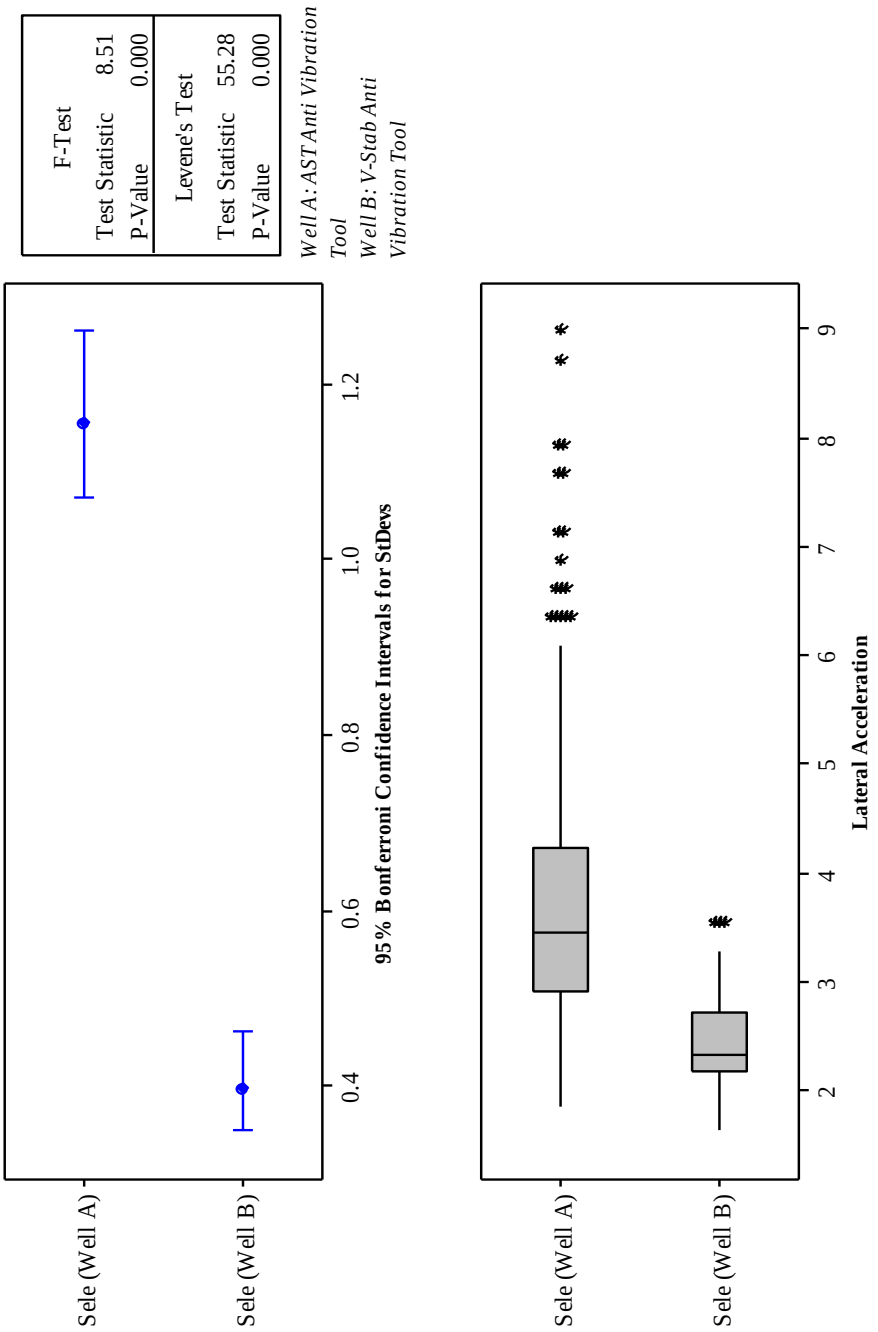

Figure E.4. Statistical Analysis of Sele Formation

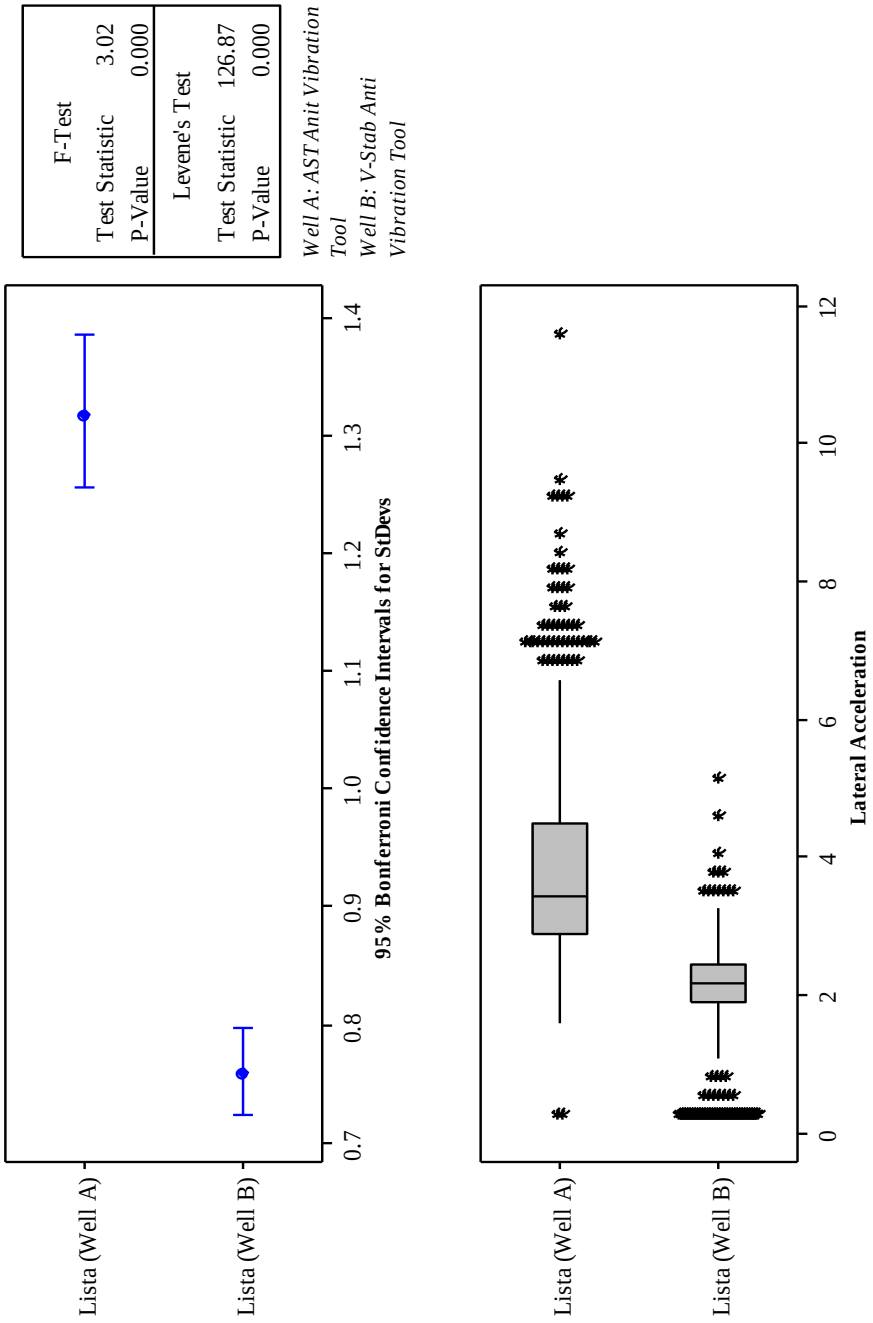

Figure E.5. Statistical Analysis of Lista Formation

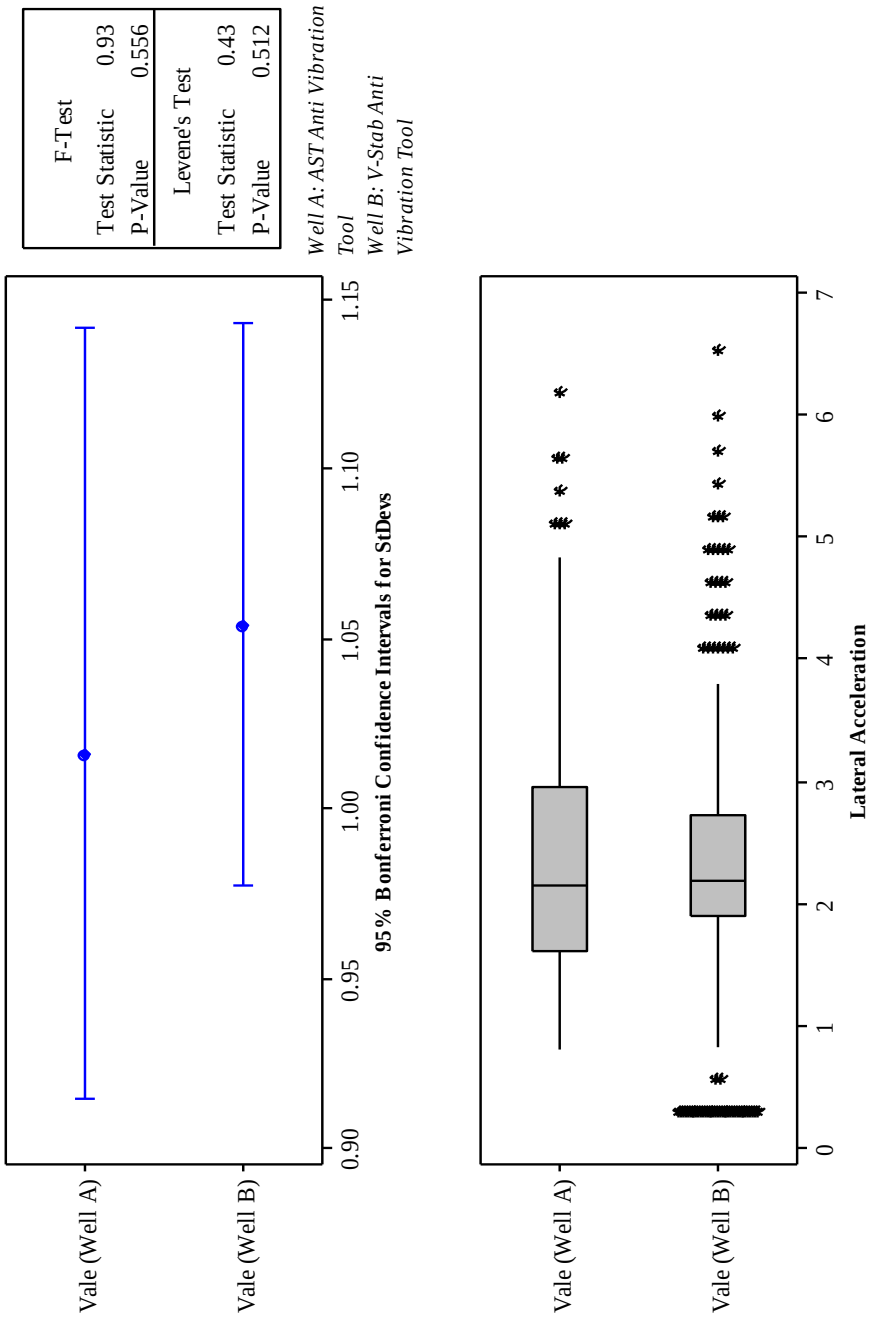

Figure E.6. Statistical Analysis of Vaale Formation

APPENDIX F.

SAMPLING RATE ANALYSIS OF WELL B AND WELL C

For Well B, the statistical summary of both data sets be seen in Figure.F.1 and Figure. F.2

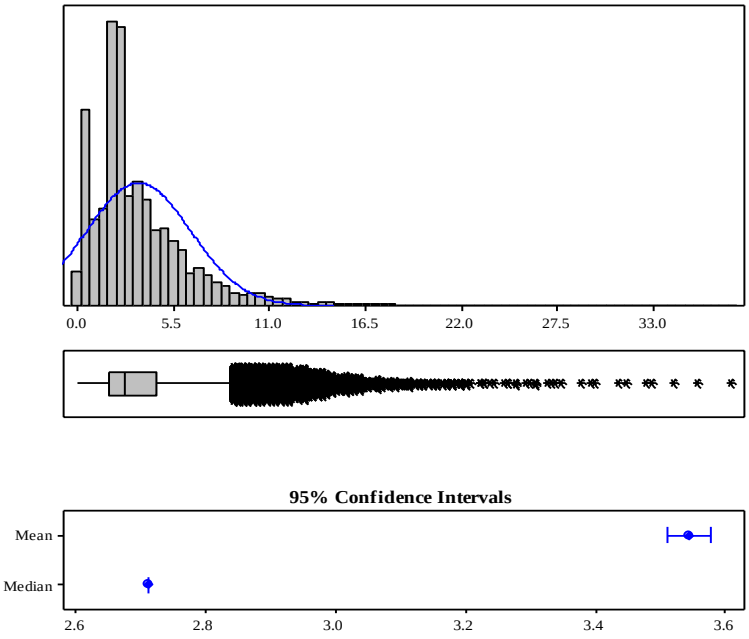

Anderson-Darling Normality Test	
A-Squared	1240.49
P-Value <	0.005
Mean	3.5439
StDev	2.9880
Variance	8.9280
Skewness	2.17142
Kurtosis	8.50598
N	31831
Minimum	0.0000
1st Quartile	1.8512
Median	2.7119
3rd Quartile	4.6102
Maximum	37.4237
95% Confidence Interval for Mean	
3.5111	3.5767
95% Confidence Interval for Median	
2.7119	2.7119
95% Confidence Interval for StDev	
2.9649	3.0114

Figure F.1. Statistical summary of the original data of Well B

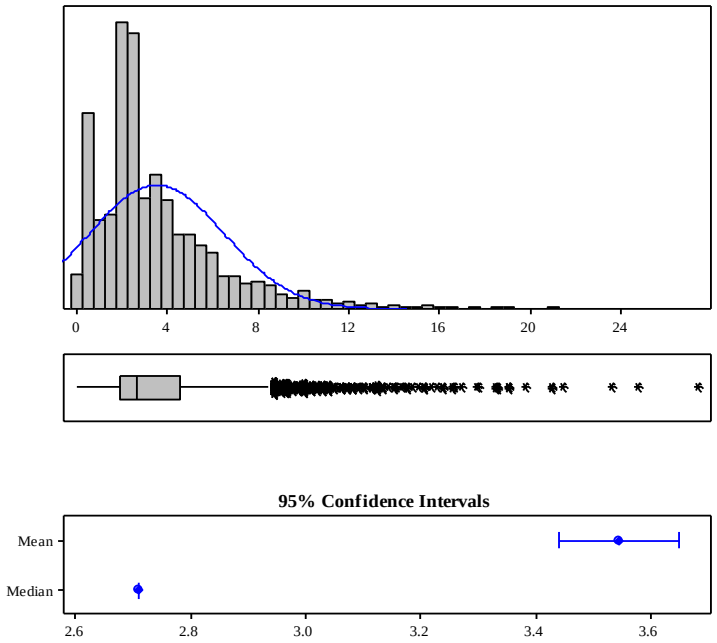

Anderson-Darling Normality Test	
A-Squared	124.79
P-Value <	0.005
Mean	3.5447
StDev	2.9723
Variance	8.8345
Skewness	2.07813
Kurtosis	7.06457
N	3183
Minimum	0.0000
1st Quartile	1.8983
Median	2.7119
3rd Quartile	4.6102
Maximum	27.3898
95% Confidence Interval for Mean	
3.4414	3.6480
95% Confidence Interval for Median	
2.7119	2.7119
95% Confidence Interval for StDev	
2.9010	3.0472

Figure F.2. Statistical Summary of the 10th Sample Data of Well B

Both data sets are approximately equal looking at both data sets statistical summary. However, since both data have a P-Value less than 0.05 (α value), that conclude that both data sets do not follow a specific distribution.

The Wilcoxon test was applied to both data sets. (Table.F.1)

Table F.1. Wilcoxon test of both data for Well B

				Confidence Interval	
	N	Estimated Median	Achieved Confidence	Lower	Upper
Actual Data	31831	3.098	95	3.072	3.119
10th Sample	3183	3.095	95	2.983	3.174

The estimated median of both data sets are approximately equal. A different of 0.003 between the median of both sets can be seen, which is very small. The confidence interval of both data for the lower interval is different by 0.089 and for the upper interval 0.055. The different in the confident interval is still small for both lower and upper interval.

The nonparametric distribution analysis tests generated a survival graph (Figure.F.3). The survival plot shows both lateral acceleration data versus the probability percentage of survival.

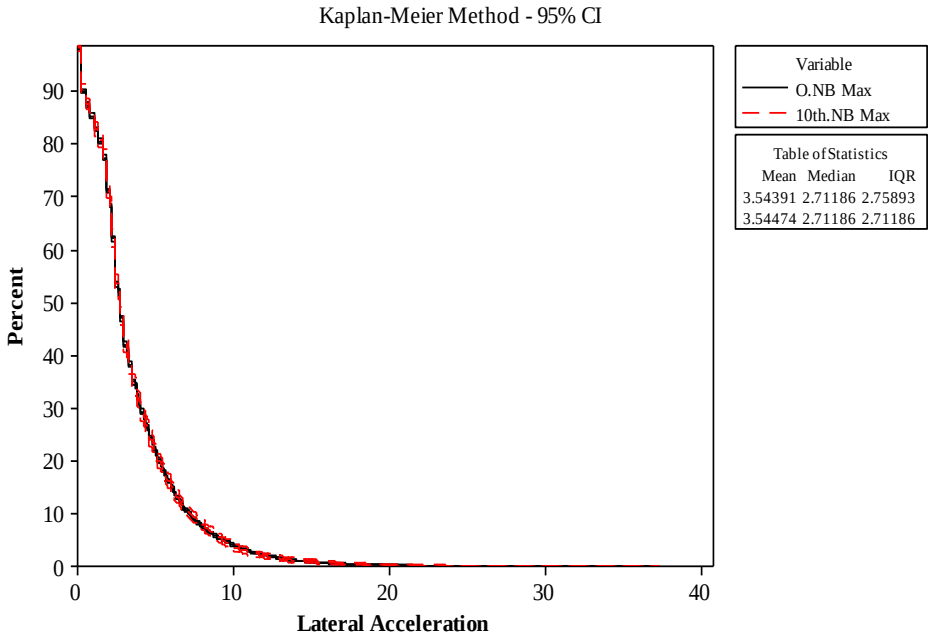

Figure F.3. Survival test of Original and 10th Sample Data for Well B

The P-value of each set of data was also calculated with two different methods. (Table.F.2)

Table F.2. Comparison of Survival Curves Well B

Method	Chi-Square	DF	P-Value
Log-Rank	0.0004086	1	0.984
Wilcoxon	0.013417	1	0.908

Since α value was set to 0.05 and both tests have a P-Value above the value of α, the two data sets are equal.

The statistical summary of both data sets of Well C can be seen in Figure.F.4 and Figure.F.5

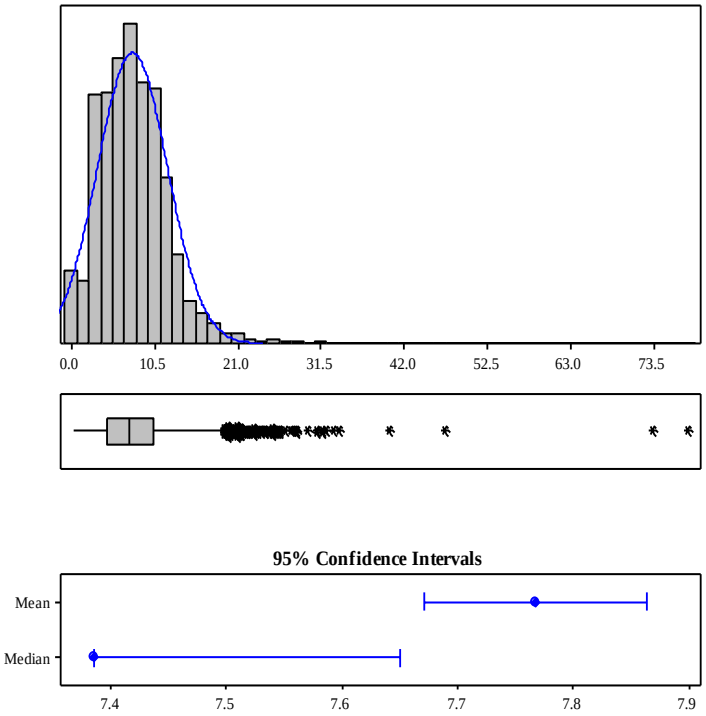

Anderson-Darling Normality Test	
A-Squared	51.53
P-Value <	0.005
Mean	7.7676
StDev	4.4082
Variance	19.4322
Skewness	1.8247
Kurtosis	16.4246
N	8102
Minimum	0.2638
1st Quartile	4.4843
Median	7.3859
3rd Quartile	10.2875
Maximum	77.8156
95% Confidence Interval for Mean	
7.6716	7.8636
95% Confidence Interval for Median	
7.3859	7.6497
95% Confidence Interval for StDev	
4.3414	4.4771

Figure F.4. Statistical Summary of the Original Data of Well C

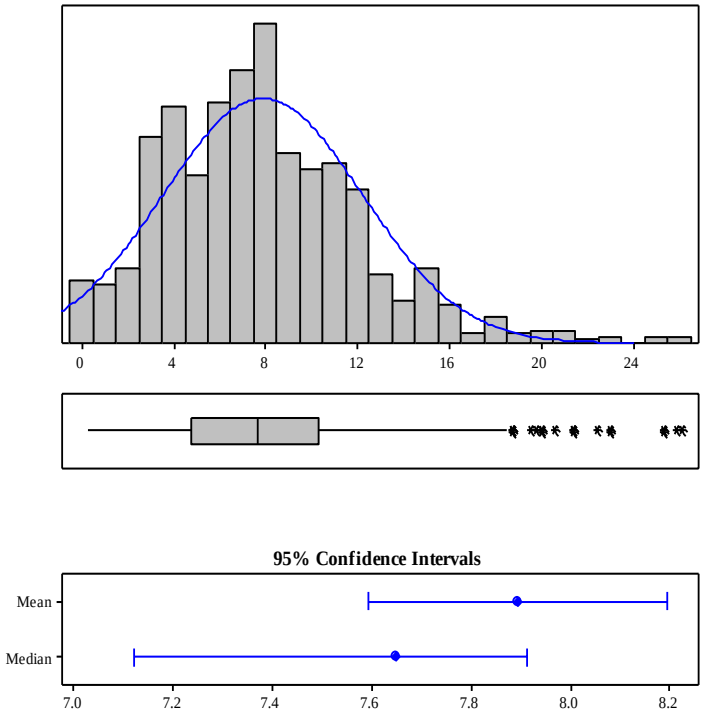

Anderson-Darling Normality Test	
A-Squared	5.09
P-Value <	0.005
Mean	7.8933
StDev	4.3406
Variance	18.8409
Skewness	0.84279
Kurtosis	1.34785
N	810
Minimum	0.2638
1st Quartile	4.7481
Median	7.6497
3rd Quartile	10.2875
Maximum	26.1144
95% Confidence Interval for Mean	
7.5939	8.1926
95% Confidence Interval for Median	
7.1221	7.9134
95% Confidence Interval for StDev	
4.1390	4.5630

Figure F.5. Statistical Summary of the 10th Sample Data of Well C

Both data sets are approximately equal looking at both data sets statistical summary. However, since both data have a P-Value less than 0.05 (α value), that conclude that both data sets do not follow a specific distribution.

The Wilcoxon test was applied to both data sets. (Table.F.3)

Table F.3. Wilcoxon test of both data for Well C

				Confidence Interval	
	N	Estimated Median	Achieved Confidence	Lower	Upper
Actual Data	8102	7.518	95	7.386	7.65
10th Sample	810	7.65	95	7.386	7.913

The estimated median of both data sets are approximately equal. A different of 0.132 between the median of both sets can be seen, which is very small. The confidence interval of both data for the lower interval is different by 0 and for the upper interval 0.263. The different in the confident interval is still small for the upper interval, the lower interval however are exact match.

The nonparametric distribution analysis tests generated a survival graph (Figure.F.6). The survival plot shows both lateral acceleration data versus the probability percentage of survival.

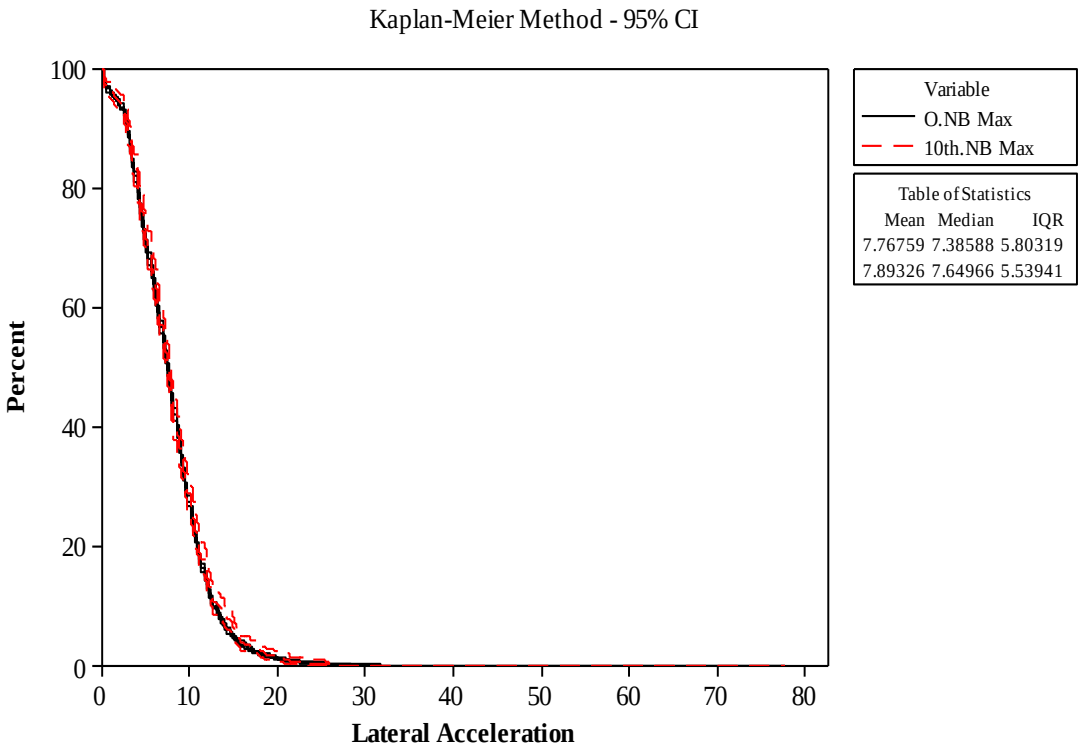

Figure F.6. Survival test of Original and 10th Sample Data for Well C

The P-value of each set of data was also calculated with two different methods. (Table.F.4)

Table F.4. Comparison of Survival Curves Well C

Method	Chi-Square	DF	P-Value
Log-Rank	0.928348	1	0.335
Wilcoxon	0.459495	1	0.498

Since α value was set to 0.05 and both tests have a P-Value above the value of α, the two data sets are equal.

APPENDIX G.

PARAMETER DISTRIBUTIONS OF THE THREE WELLS

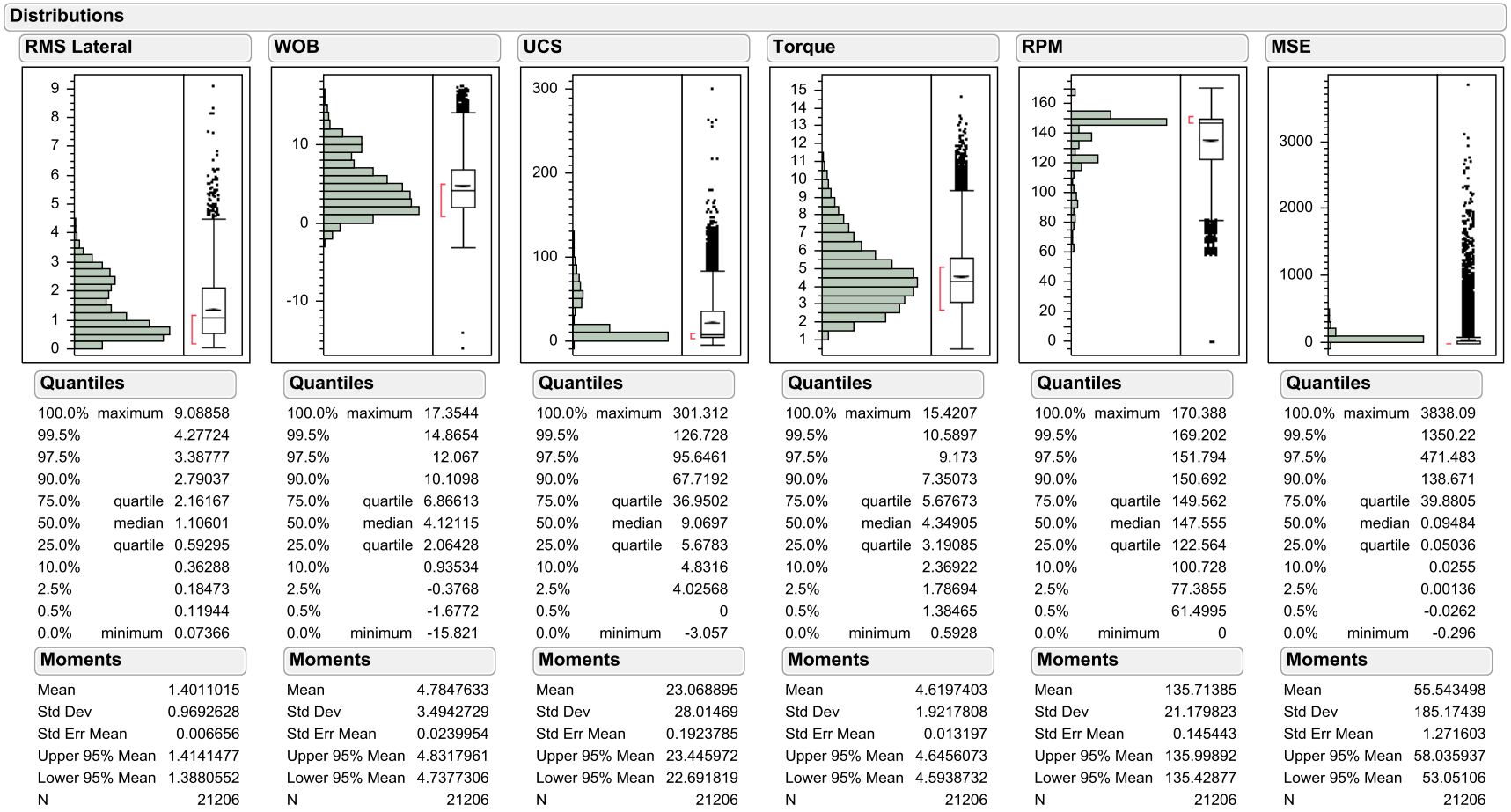

Figure G.1 Parameter Distributions of Well A

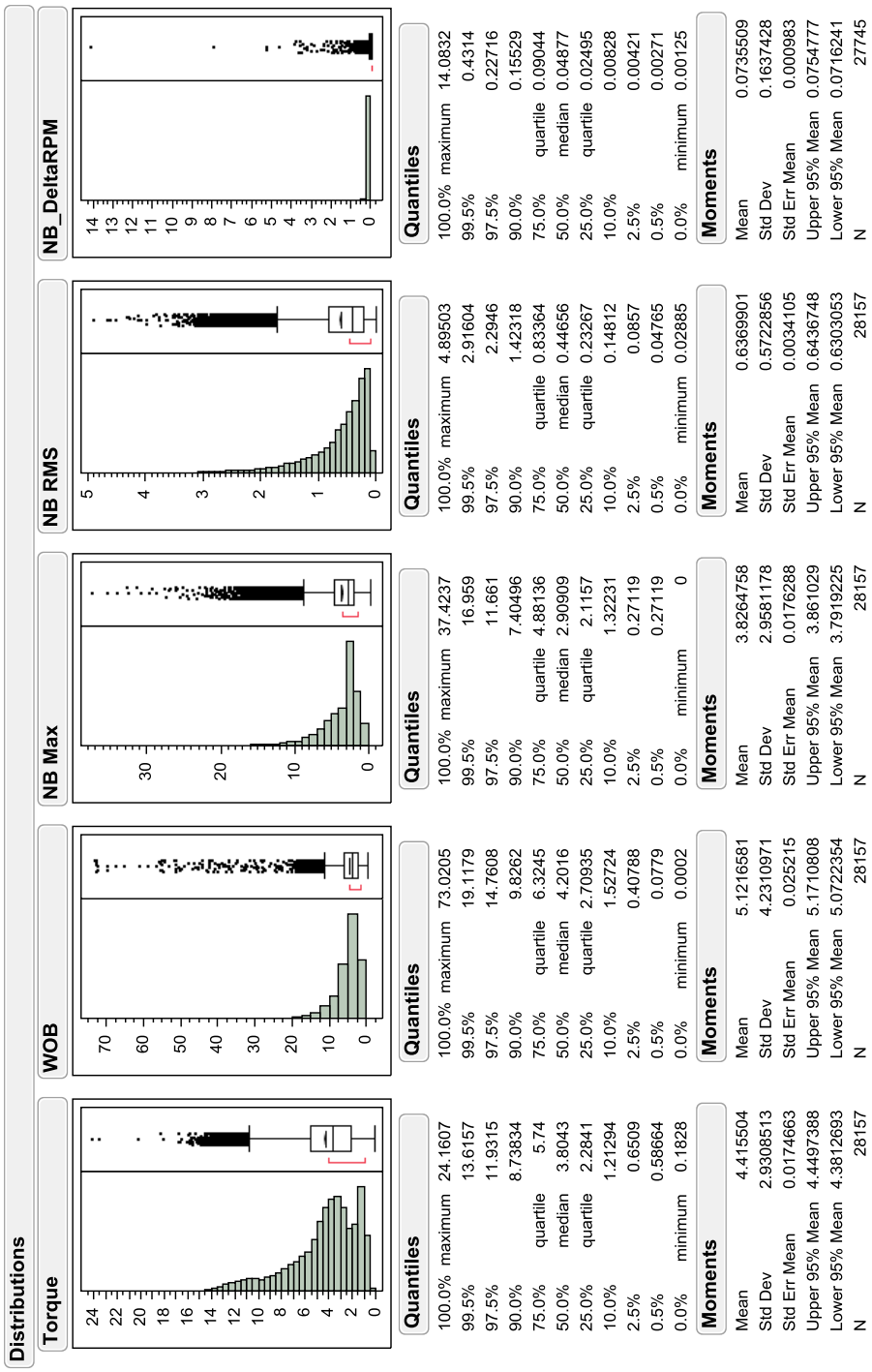

Figure G.2 Parameter Distributions of Well B

Figure G.3 Parameter Distributions of Well C

BIBLIOGRAPHY

Aadnoy, B. S., Cooper, I., Miska, S. Z., Mitchell, R. F. and Payne, M. L. 2009. Advanced Drilling and Well Technology. Society of Petroleum Engineers, TX, USA, p. 876.

Ashely, D. K., McNary, X. M. and Tomlin, J. C. 2001. Extending BHA Life with Multi-Axis Vibration Measurements, Presented at SPE/IADC conference at Netherlands Drilling Conference, 27 February- 1 March, Amsterdam. SPE/IADC 67696.

Bill, L., Ignova, M., Zeineddine, F., Burks, J. and Welch, B. 2011. Testing the Combination of High Frequency Sureface and Downhole Drilling Mechanics and Dynamics Data under a Variety of Drilling Conditions. Presented at The Netherlands Drilling Conference and Exhibition 1-3 March, Amsterdam, The Netherlands. SPE/IADC 140347.

Bradury, R. and Wilhoit, J. 1963. Effect of Tool Joints on Passages of Plane Longitudinal and Torsional Wave Along Drill Pipe. Trans., ASME, Journal of Engineering for Industry 85 (May): 156-162.

Bronshtein, I. N. and Semendyayev, K. A. 1977. Handbook of Mathematics. Berlin: Springer.

Brown, M. B. and Forsythe, A. B. 1974. Robust Tests for the Equality of Variance. Journal of the American Statistical Association, 69, 364-367.

Chi, A., Zhang, J., Ge, W., and Guo, B. 2006. Prediction of Drillstring Fatigue Life under Axial_Torsional_Combined Vibration, Presented at SPE Gas Technology Symposium in Calgray, Alberta, Canada. SPE 99356

Chin, W. C. 1994. Wave Propagation in Petroleum Engineering. Gulf Publishing Company. Houston, TX.

Cobern, M. and Wassel, M. 2005. Laboratory Testing of an Active Drilling Vibration Monitoring and Control system, Presented at AADE 2005, 5-7 April 2005. Houston. TX. AADE-05-NTCE-25.

Craig, A. D., Goodship, R. and Shearer, R. D. 2010. High Frequency Downhole Dynamic Measurements Provide Greater Understand of Drilling Vibration in Performance Motor Assembilies. Presented at IADC/SPE drilling conference, New Orleans, 2-4 February. IADC/SPE 128211.

Craig, R. R. Jr. 1981. Structural Dynamics; An Introduction to Computer Methods. New York; John Wiley and Sons.

Dareing, D. W. 1984. Guidelines for Controlling Drill String Vibration. Journal of Energy Resources Technology 106 (June); 272-277.

Dawson, R. Lin, Y., and Spanos, P. 1987. Drill string Stick-Slip Oscillations. Proc., 1987 SEM Spring Conference on Experimental Mechanics, Houston, TX. 14-19 June, 590-595.

Dufeyte, M- P. and Henneuse, H. 1991. Detection and Monitoring of the Slip-Stick Motion: Field Experiment. Presented at the SPE/IADC Drilling Conference, Amsterdam, The Netherlands 11-14 March. SPE 21945.

Hilgedick, S., Nygaard, R., Hellvik, S., Hoel, E. and Skurtveit, E. 2012. Limitations of Log Based Wellbore Stability Analysis in an Unconventional Conglomerate Rich Reservoir in the Southern North Sea. Presented at ARMA 2012, 24-27 June 2012. Chicago Il. Paper ID No 423.

Janse, J. D. 1991. Nonlinear rotor dynamics as applied to oil well drill string vibrations. Journal of Sound and Vibrations, 147 (1):115-135. DOI: 10.1016/0022-460X(91)90687-F.

Jansen, J. D. 1992. Whirl and Chaotic Motion of Stabilized Drill Collar. SPE 20930.

Jansen, J. D. and Van den Steen, L. 1995. Active Damping of Self-Excited Torsional Vibrations in Oil well Drill strings. Journal of Sound and Vibration 179 (26) 647-668. DOI: 10.1006/jsvi.1995.0042.

JMP® 9. 2010a. SAS Institute Inc., Cary, NC, ISBN 978-1-60764-599-3.

JMP® 9. 2010b. Basic Analysis and Graphing. SAS Institute Inc., Cary, NC, ISBN 978-1-60764-596-2.

JMP® 9. 2010c. Modeling and Multivariate Methods. SAS Institute Inc., Cary, NC, ISBN 978-1-60764-595-5.

Kotsonis, S. J. 1994. Effect of Axial Forces on Drillstring Lateral Vibration. MS thesis, Rice University, Houston, TX.

Kriesels, P. C., Keultjes, W. J., Huneidi, I., Dumont, P., and Hartmann, R. A. 1999. Cost Savings through an Integrated Approach to Drillstring Vibration control, SPE/IADC 57555.

Kyllingstad, A. and Halsey, G.W. 1988. A study of Stick/Slip Motion of the bit. Presented at SPE Annual Technical Conference and Exhibition in Dallas, 27-30 September 1987. SPE 16659.

Lesso, B., Ignova, M. and Zeineddine, F. 2011. Testing the Combination of High Frequency Surface and Downhole Drilling Mechanics and Dynamics Data under a Variety of Drilling Conditions. Presented at SPE/IADC drilling conference and exhibition Amsterdam, The Netherlands 1-3 March 2011. SPE/IADC 140347.

Levene, H. 1960. Contributions to Probability and Statistics. Stanford University Press, CA.

Lin, Y-Q. and Wang, Y-H. 1991. Stick-Slip Vibration of Drill Strings. Trans., ASME, Journal of Engineering for Industry, 113 (February): 38-43.

Lin, Y-Q. and Wang, Y-H.1990. New Mechnism in Drillstring Vibration. Paper OTC 6225 presented at the Offshore technology Conference, Houston, TX. 7-10 May.

Lord, R. 2006. Bit technology keeps pace with operator activity. World Oil(00438790): 1-1, http://search.proquest.com/docview/196671872?accountid=14594 accessed January 10, 2012.

Macpherson, J. D. and Mason, J. S. 1990. Surface Measurment and Analysis of Drillstring Vibrations while Drilling. Presented at SPE/IADE Drilling conference, Amsterdam The Netherlands, 23-25 February. SPE/IDE 25777.

Mason, J and Sprawls, B. 1998. Addressing BHA whirl: the Culprit in Mobile bay 1998. SPE 52887.

Millheim, K.K. and Apostal, M.C. 1981. The effect of Bottomhole Assembly Dynamics on the trajectory of a bit. JPT 33 (12): 2323 -2338. SPE 9222.

Minitab® Statistical Software 2010. StatGuidTM , www.minitab.com

Murdock, A. 2007. Increase Drilling Efficiency Systematically. Exploration & Production Worldwide Coverage. http://www.epmag.com/EP-Magazine/archive/Increase-drlling-efficiency-systematically_257 accessed 23 December 2011.

Narasimhan, S. 1987. A Phenomenological Study of Friction induced torsional vibrations of Drill Strings, MS thesis, Rice University, Houston. TX.

National Oilwell Varco 2011a. BlackBox® HD Downhole Dynamics Recorder. http://www.nov.com accessed 23 December 2011.

National Oilwell Varco 2011b. V-Stab® Vibration Damping Tool. http://www.nov.com/Downhole/Advanced_Drilling_Solutions/V-Stab.aspx accessed 23 December 2011.

New products. 2008. World Oil(00438790): n/a, http://search.proquest.com/docview/196685319?accountid=14594 accessed January 10, 2012.

Reimers, N. 2007. Anti-Stall Improves Coiled Tubing Drilling. Exploration & Production Worldwide Coverage. http://www.epmag.com/EP-Magazine/archive/Anti-stall-tool-improves-coiled-tubing-drilling_297 accessed 23 December 2011.

Samuel. R, and Dongping. Y. 2010. Vibration Analysis and Control with Hole-Enlarging Tools. Paper SPE 134512 presented at the SPE Symposium, Florence, Italy, 19-22 September 2010.

Schlumberger 2011. Shock and vibration Poster, http://www.slb.com/~/media/Files/drilling/posters/shock_vibration_posters.ashx accessed February 8 2012.

Schlumberger. 2007. TeleScope, www.slb.com/~/media/Files/drilling/brochures/lwd/.../telescope.ashx accessed 4 February 2012.

Schlumberger. 2008. EcoScope, http://www.slb.com/~/media/Files/drilling/brochures/lwd/scope/ecoscope.ashx accessed 4 February 2012.

Schlumberger. 2010. Drillstring Vibration and Vibration Modeling, http://www.slb.com/~/media/Files/drilling/brochures/drilling_opt/drillstring_vib_br.ashx downloaded 17 July 2011.

Sengupta, A. 1993. Dynamics Modeling of Roller Cone Bit Life-Off in Rotary Drilling. PHD dissertation, Rice University, Houston, TX.

Shyu, R. J. 1989. Bending vibration of Rotating drill strings. PhD dissertation, MIT department of ocean engineering, Cambridge, Massachussets.

Smit, A. 1995. Using Optimal Control Techniques To Dampen Torsional Drillstring Vibration. PHD dissertation, University of Twente, Enschede, The Netherlands.

Spanos, P. D. Sengupta, A. K., Cunningham, R. A. and Paslay, P. R. 1995. Modeling of Roller Cone Bit Lift-Off Dynamics in Rotary Drilling. Journal of Energy Resources Technoogy 117 (3): 197-207. DOI: 10.1115/1.2835341.

Teale, R. 1965. The Concept of Specific Energy in Rock Drilling, Intl. J. Rock Mech. Mining Sci. 57-73.

Tomax. Anti-Stall Technology. 2010. http://www.tomax.no accessed 23 December 2011.

Van den Steen, L. 1997. Suppressing Stick-Slip induced Drillstring Oscillations: A Hyperstability Approach. PhD dissertation, Universitty of Twente, Ensshede, The Netherlands.

Vandiver, K. J., Nicholson, J. W. and Shyu, R. J. 1990. Case Studies of bending Vibration and Whirling Motion of Drill Collars. Presented at SPE/IADC Drilling conference held in New Orleans 28 February- 3 Match 1989. SPE 18652.

Warren, T. M., Brett, J. F. and Sinor, L. A. 1990. Development of a Whirl –resistant bit. Presented at SPE Annual Technical conference and exhibition held in San Antonio 8-11 October 1989. SPEDE 5 (4): 267-274: Trans., AIME, 289, SPE 19572.

VITA

Mohammed Fayez Al Dushaishi was born on October 24, 1987 in Saudi Arabia. He went to high school in Saudi Arabia and graduated in 2005. He received his Mechanical Engineering Bachelor's degree from Missouri University of Science and Technology in 2010. In August 2010, he started his master degree in Petroleum Engineering at Missouri University of Science and Technology. He earned his Master degree in Petroleum Engineering on the 28th of March of 2012.